UNIVERSITA' DEGLI STUDI DI PADOVA

FACOLTA' DI INGEGNERIA

Corso di Laurea Magistrale in

INGEGNERIA DEI MATERIALI

Tesi di Laurea

SYNTHESIS AND CHARACTERIZATION OF UHTC FROM PRECERAMIC POLYMER.

Relatore: Prof. Paolo Colombo

Correlatore: Dott. Weigang Zhang

Laureando: Francesco Zangrossi

ANNO ACCADEMICO 2012-2013

INDEX

INTRODUCTION. pag. 4

Production and Processing. pag. 7

Polymer Derived Ceramic. pag. 9

THESIS PURPOSE. pag. 10

ZIRCONIUM DIBORIDE. pag. 11

SILICON CARBIDE. pag. 15

1. MATERIALS. pag. 16

1.1 *Zirconium diboride.* pag. 17

1.2 *Silicon carbide.* pag. 18

1.3 *Precursor solutions.* pag. 18

1.4 *Powders.* pag. 19

Powder composition. pag. 19

Foam composition. pag. 22

2. HEAT TREATMENTS. pag. 23

2.1 *Powder treatment.* pag. 23

2.2 *Foam treatment.* pag. 24

2.3 *Work schedule.* pag. 27

3. CHARACTERIZATION AND INSTRUMENTS. pag. 28

3.1 *X-Ray Diffraction (XRD).* pag. 28

3.2 *X-Ray Fluorescence (XRF).* pag. 32

SAMPLES. pag. 34

3.3 *X-ray Photoelectron Spectroscopy (XPS).* pag. 38

SAMPLES. pag. 40

3.4 *Scanning Electron Microscope and Energy Dispersive Spectroscopy.* pag. 42

Scanning Electron Microscope. pag. 42

Energy Dispersive Spectroscopy. pag. 44

SAMPLES. pag. 45

3.5 Compressive Strength. pag. 48

4. RESULTS AND DISCUSSION. pag. 51

4.1 Ceramic Yield. pag. 51

4.2 XRD. pag. 57

4.3 XRF. pag. 68

4.4 XPS. pag. 69

4.5 SEM and EDS. pag. 76

Energy Dispersive Spectroscopy. pag. 76

Scanning Electron Microscope. pag. 77

4.6 Compressive Stregth. pag. 98

5. CONCLUSIONS. pag.102

BIBLIOGRAPHY. pag.103

RINGRAZIAMENTI.

Un sentito ringraziamento ai presenti e a tutte quelle persone che hanno reso tutto questo possibile.

INTRODUCTION.

This dissertation will examine the ultra-high temperature ceramics (UHTCs) produced from preceramic polymer (PP).

UHTCs are refractory ceramics that offer excellent stability at temperatures exceeding 2000 °C[1] and are being investigated as possible Thermal Protection System (TPS) materials, coatings for materials subjected to high temperatures, and bulk materials for heating elements.

Broadly speaking, UHTCs are borides, carbides, nitrides, and oxides of early transition metals, such as Zr, Ta and Hf. These materials possess melting temperature higher than 3000°C making them suitable candidates for structural applications at temperature above 1800°C.

Property	ZrB_2	HfB_2
Crystal system space group prototype structure	Hexagonal[5] *P6/mmm* AlB_2	Hexagonal[6] *P6/mmm* AlB_2
a (Å)	3.17	3.139
c (Å)	3.53	3.473
Density (g/cm^3)	6.119[5]	11.212[6]
Melting temperature (°C)	3245	3380
Young's modulus (GPa)	489[9]	480[11]
Bulk modulus (GPa)	215	212
Hardness (GPa)	23[9]	28[7]
Coefficient of thermal expansion (K^{-1})	5.9×10^{-6} [7]	6.3×10^{-6} [7]
Heat capacity at 25°C ($J \cdot (mol \cdot K)^{-1}$)	48.2[8]	49.5[7]
Electrical conductivity (S/m)	1.0×10^{7} [7]	9.1×10^{6} [7]
Thermal conductivity ($W \cdot (m \cdot K)^{-1}$)	60[7]	104[9]
Enthalpy of formation at 25°C (kJ)	−322.6[8]	−358.1[7]
Free energy of formation at 25°C (kJ)	−318.2[8]	−332.2[7]

Table 1 - ZrB2 and HfB2 characteristic.

Ultra high temperature ceramics have been historically studied and developed since 1960s. These materials are potential candidates for thermal protection materials in both re-entry and hypersonic vehicles because of their excellent and unique combination of high melting points, good thermal-shock resistance and good ablation/oxidation resistance. These properties makes UHTCs attractive

for the design of future hypersonic aerospace vehicles with features like sharp leading edges and sharp nose-cones. Such design features could produce more agile vehicles that would open up a greater range of hypersonic flights paths and re-entry trajectories [2,4], but would requires materials capable of operating in oxidizing atmosphere at temperature above 1700°C.

Improvements in the fields of Ceramic Matric Composites (CMC) for high temperatures structures and thermal protection systems are strongly providing an innovative approach to the design of future Reusable Launch Vehicles (RLV) because of the possibility to combine heat-resistant and load carrying structural external parts. Actual thermal protection systems are made of Reinforced Carbon-Carbon (RCC) materials, coated with silicon carbide against the oxidation and an inside insulation which is needed for protection of primary structure and/or the equipment and payloads inside the vehicle.

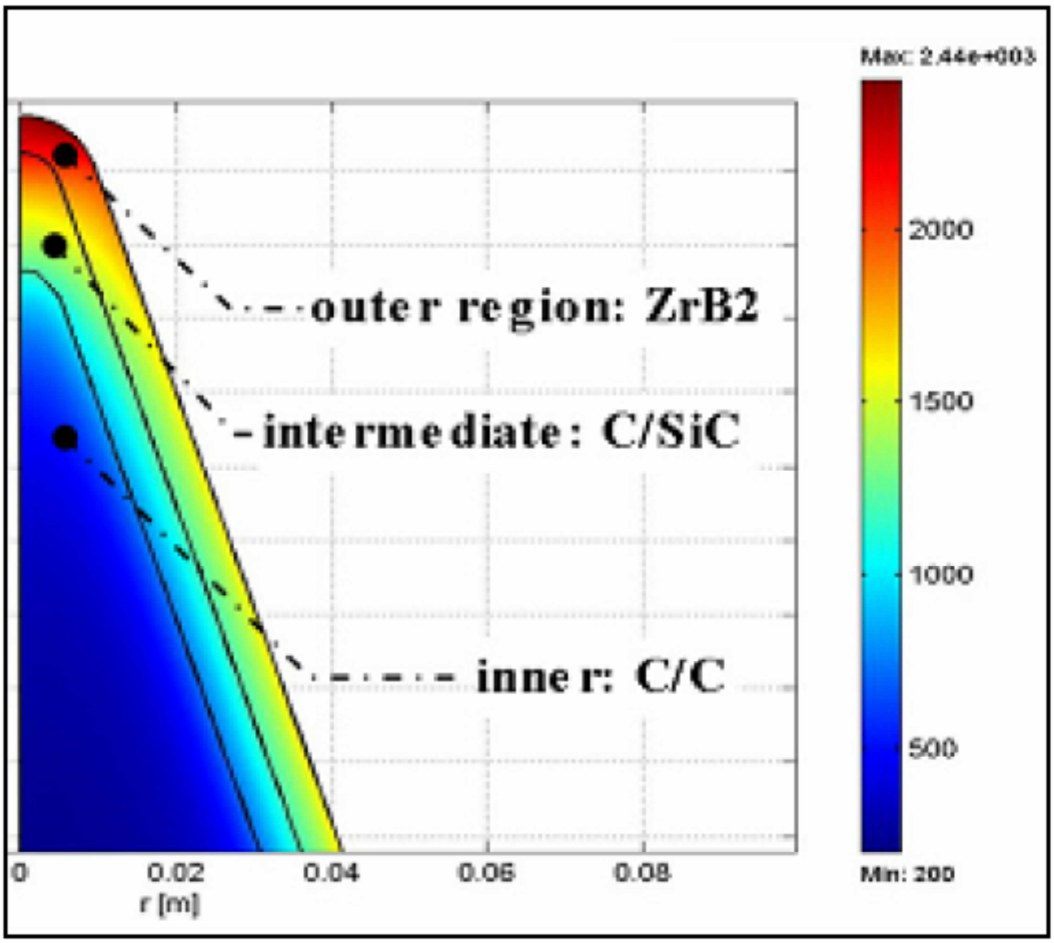

Figure 1 - Nose temperature distribution (source: CIRA, Italian aerospace reserch center). Temperature scale: min =200 K, Max = 2440 K

New hypersonic space plane concepts, characterized by slender bodies with sharp leading edges, are becoming more and more common. The reasons of this new trend of the space industry can be summarized in the following points[19]:

- sharp-body designs reduce weight thus providing consistent saving in the cost per mass expended to put payloads into orbit;
- improved maneuverability;
- sharp leading edges minimize the interferences with radio frequency transmissions during the reentry thus limiting the communications blackout.

UHTCs, specifically Hf and Zr based diboride, are being developed to handle the forces and temperatures experienced by leading vehicle edges in atmospheric reentry and sustained hypersonic flight. The surfaces of hypersonic vehicles experience extreme temperatures in excess of 2400°C while also being exposed to high temperature, high flow rate oxidizing plasma.

Oxidation resistance is a major issue for the use of UHTCs. Great efforts have been devoted to this aspect and much progress has been gained recently[3]. Several studies have shown that the addition of SiC to MB_2 ceramics has beneficial effects not only on sinterability, but also on mechanical properties and resistance to oxidation. These composites exhibit improved resistance to oxidation if compared to the monolithic diboride compacts, thanks to the formation of silica-based glassy product which covers the faces exposed to the air and provides an effective barrier to oxygen transport [5].

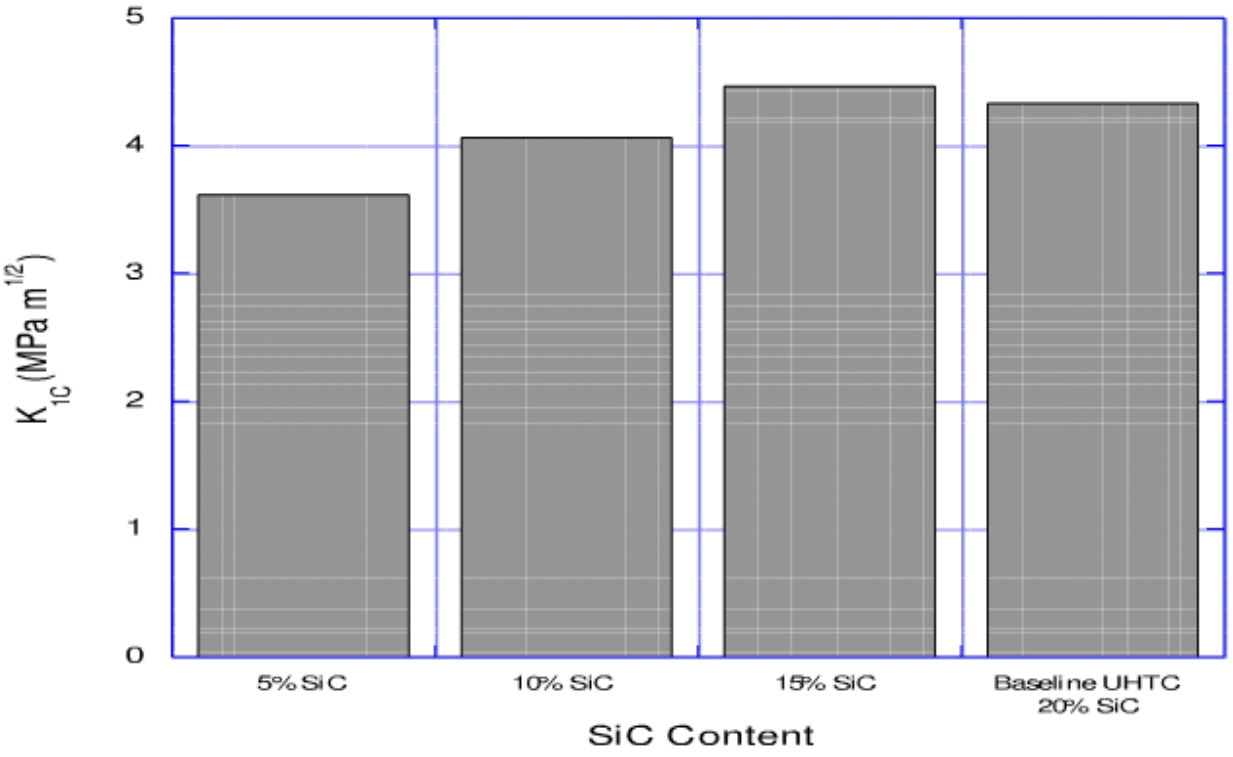

Figure 2 - Fracture toughness vs SiC content (vol%) (source : 10th international conference and exhibition of European ceramic society, 2007).

Production and processing.

About the synthesis of these ceramic materials, UHTCs powder can be prepared by a wide variety of synthetic methods, for example:

- stoichiometric reaction between constituent elements;
- solution-based methods allow for low temperature synthesis of ultrafine UHTC powders;
- preparation from polymeric precursor, also used in this research.

Diboride based UHTCs often require high temperature and pressure processing in order to produce dense, durable materials. The high melting points and strong covalent interactions present in UHTCs make it difficult to achieve uniform densification in these materials. Densification is only achieved at temperatures above 1800 °C once grain boundary diffusion mechanisms become active.[21] Unfortunately, processing of UHTCs at these temperatures results in materials with larger grain sizes and poor mechanical properties including reduced toughness and hardness. To achieve densification at lower temperatures, several techniques can be employed: additives such as SiC can be used in order to form a liquid phase at the sintering temperature, the surface oxide layer can be removed, or the defect concentration can be increased. Silicon carbide can react with the surface oxide layer in order to provide diboride surfaces with higher energy: adding 5-30 vol% SiC has demonstrated improved densification and oxidation resistance of UHTCs.[22] Silicon carbide can be added as a powder or a polymer to diboride UHTCs. The addition of SiC as a polymer has several advantages over the more traditional addition of SiC as a powder because it forms along the grain boundaries when added as a polymer, which increases measures of fracture toughness (by ~24%).[23] In addition to improved mechanical properties, less SiC needs to be added when using this method, which limits the pathways for oxygen to diffuse into the material and react. Although addition of additives such as silicon carbide can improve densification of UHTC materials, it should be noted that these additives lower the maximum temperature at which UHTCs can operate due to the formation of eutectic liquids. The addition of SiC to ZrB_2 lowers the operating temperature of ZrB_2 from 3245°C to 2270 °C.

Hot pressing is a popular method for obtaining densified UHTC materials that relies upon both high temperatures and pressures to produce densified materials. Powder compacts are heated externally and pressure is applied hydraulically. In order to improve densification during hot pressing, diboride powders can undergo milling by attrition to obtain powders of <2μm. Milling also allows for more uniform dispersion of the additive silicon carbide. Hot pressing temperature, pressure, heating rate, reaction atmosphere, and holding times are all factors that affect the density and microstructure of UHTC pellets obtained from this method. In order to achieve >99%

densification from hot pressing, temperatures of 1800-2000 °C and pressures of 30MPa or greater are required. UHTC materials with 20vol.% SiC and toughened with 5% carbon black as additives exhibit increased densification above 1500 °C, but these materials still require temperatures of 1900 °C and a pressure of 30 MPa in order to obtain near theoretical densities.[24] Other additives such as Al_2O_3 and Y_2O_3 have also been used during the hot pressing of ZrB_2-SiC composites at 1800 °C.[25] These additives react with impurities to form a transient liquid phase and promote sintering of the diboride composites. The addition of rare earth oxides such as Y_2O_3, Yb_2O_3, La_2O_3 and Nd_2O_3 can lower densification temperatures and can react with surface oxides to promote densification.[26] Hot pressing may result in improved densities for UHTCs, but it is an expensive technique that relies on high temperatures and pressures in order to provide useful materials.

Pressureless sintering is another method for processing and densifying UHTCs. Pressureless sintering involves heating powdered materials in a mold in order to promote atomic diffusion and create a solid material. Compacts are prepared by uniaxial die compaction, and then the compacts are fired at chosen temperatures in a controlled atmosphere. Exaggerated grain growth that hinders densification occurs during sintering due to the low-intrinsic sinterability and the strong covalent bonds of Ti, Zr, and Hf diborides. Full densification of ZrB_2 by pressureless sintering is very difficult to obtain; Chamberlain et al. have only been able to obtain ~98% densification by heating at 2150 °C for 9 h (Figure 3).[27] Efforts to control grain size and improve densification have focused on adding third phases to the UHTCs, some examples of these phases include the addition of boron and iridium.[28] Addition of Ir in particular has shown an increase in the toughness of HfB_2/20vol.% SiC by 25%. Sintered density has also been shown to increase with the addition of Fe (up to 10% w/w) and Ni (up to 50% w/w) to achieve densifications of up to 88% at 1600°C.[29] More advances in pressureless sintering must be made before it can be considered a viable method for UHTC processing.

Spark plasma sintering is another method for the processing of UHTC materials. Spark plasma sintering often relies on slightly lower temperatures and significantly reduced processing times if compared to hot pressing. During spark plasma sintering, a pulsed direct current passes through graphite punch rods and dies with uniaxial pressure exerted on the sample material. Grain growth is suppressed by rapid heating over the range 1500-1900 °C; this minimizes the time the material has to coarsen. Higher densities, cleaner grain boundaries, and elimination of surface impurities can all be achieved with spark plasma sintering. Spark plasma sintering also uses a pulsed current to generate an electrical discharge that cleans surface oxides of the powder. This enhances grain boundary diffusion and migration as well as densification of the material. The UHTC composite

ZrB_2/20vol%SiC can be prepared with 99% density at 2000 °C in 5 min via spark plasma sintering.[30] ZrB2-SiC composites have also been prepared by spark plasma sintering at 1400 °C over a period of 9 min.[31] Spark plasma sintering has proven to be a useful technique for the synthesis of UHTCs, especially for preparation of UHTCs with smaller grain sizes.

Polymer Derived Ceramics.

Preceramic polymers were proposed over 30 years ago as precursors for the fabrication of mainly Si-based advanced ceramics, generally denoted as polymer-derived ceramics (PDCs). The polymer to ceramic transformation process enabled significant technological breakthroughs in ceramic science and technology, such as the development of ceramic fibers and coatings that are stable at ultrahigh temperatures (up to 2000°C).

The polymer precursors represent inorganic/organometallic systems that provide ceramics with a tailored chemical composition and a closely defined nanostructural organization by proper thermal treatment under a controlled atmosphere. The PDCs route is an emerging chemical process as attested by the increasingly commercial development of preceramic polymers to produce near-net shapes not to be found through other techniques.

In principle, preceramic polymers can be processed or shaped using conventional polymer-forming technique; once formed, objects made from the preceramic polymers can then be converted to ceramic components by heating to temperatures high enough to consolidate the elements contained in the polymer structure to a ceramic.

Initially the research on PDCs was focused mainly on dense bulk materials and fibers for mechanical applications at high temperatures. Nowadays, nanopowders and porous PDCs are gaining increasingly importance. Moreover, the polymer-to-ceramic transformation is a suitable technology to produce a broad spectrum of ceramic based composite materials with adjusted chemical, mechanical, and physical properties. PDCs can also be processed to thin films for optoelectronic applications and to thick films, e.g. for hard coatings, environmental barrier coatings, and others[6]. The great flexibility in terms of processing and forming of preceramic polymers into shaped-ceramic components has also enabled them to play an important role in several other applications.

THESIS PURPOSE.

This work has been conducted at the Institute of Process Engineering (IPE, Chinese academy of science) in Beijing; its target is Polymer-Derived Ceramic system (powders and foams) characterization, made of zirconium diboride (ZrB_2) modified with different quantities of silicon carbide (SiC).

Characterization is provided by:

- X-Ray Diffraction (XRD);
- X-Ray Fluorescence (XRF);
- X-ray Photoelectron Spectroscopy (XPS);
- Scanning Electron Microscope and Energy Dispersive Spectroscopy (SEM+EDS);
- Compressive Strength.

The first four tests have been used for phase morphology and composition analysis.

The mechanical proof results will determine mechanical characteristics of different composition foam prepared with the same thermal treatment.

ZIRCONIUM DIBORIDE (ZrB_2).

Zirconium diboride (ZrB_2) is a highly covalent refractory ceramic material with a hexagonal crystal structure. ZrB_2 is an Ultra High Temperature Ceramic (UHTC) with a melting point of 3246 °C, that can be a leading candidate material for use in critical external surfaces of future aerospace re-entry crafts, such hypersonic aircraft or reusable launch vehicles, and also for other employment like furnace elements, plasma-arc electrodes and rocket engines . This is primarily because it has an excellent combination of mechanical, physical, thermal-shock and oxidation-resistance properties [14, 18].

In contrast to other ceramics, its electrical conductivity (resistivity = $\sim 10^{-5}$ Ω cm) permits the production of complex shaped parts by electrical discharge machining [17].

The development of ZrB_2 with improved properties using low-cost processes is essential to increase the performance and to reduce the cost of products, such as hypersonic aerospace vehicles.

ZrB_2 can be prepared by several techniques. Metal diborides can be synthesized by:

- stoichiometric reaction between constituent elements: the reaction between elemental boron and zirconium can have excellent control on the stoichiometry of the resultant ZrB_2 . This method gives pure ZrB_2 but cannot be considered for commercial production as it involves expensive charge materials. This route can give dense bodies by hot pressing of mixed powder if the reaction with die is avoided. To avoid such reaction, the graphite die is coated with boron nitride. As the formation of ZrB_2 ceramic from elemental powders is thermodynamically favorable (ΔG_{2000K} = -279,6 kJ mol^{-1}), this route can also be used to produce ZrB_2 by self-propagating high temperature synthesis (SHS). Self-propagating high temperature synthesis is a technique that takes advantage of the high exothermic energy of chemical reactions to generate high temperature and fast combustion reactions. Some of the advantages of SHS, when compared to many traditional solid state synthetic routes, are the short process times (typically in the order of few seconds or less), the high purity of the products, the low energy consumption (limited to the ignition step), as well as the low cost of the experimental apparatus. ZrB_2 powders formed using SHS have exhibited increased sinterability, which has been attributed to the presence of lattice defects. These defects were attributed to the rapid heating and cooling rates (200 000 K min^{-1}) associated with SHS. However, rapid heating rates can also result in incomplete reactions, the formation of non-equilibrium phases, the formation of stable oxides or the retention of large amounts of porosity (50%). It is predicted that, due to the high rate of heating and cooling, the SHS process will introduce higher concentration of defect structures in the raw powder. These

defects play an important role in various physical and chemical phenomena, particularly at high temperatures. For example, the high defect concentration in the SHS produced powders is expected to enhance the mass transfer processes during sintering, which may lower the sintering temperatures.

- Reaction between a metal oxide and boron: borothermic reduction of ZrO_2 gives pure ZrB_2 at temperature higher than 1600°C. This method is not economical for commercial production as it involves the loss of expensive boron in the form of boron oxide.

$$ZrO_2(s) + 4B(s) \longrightarrow ZrB_2(s) + 2BO(g) \quad \{1\}$$

- Reaction between metal oxide and boron carbide via carbothermal reduction: this is the most popular method for the synthesis of ZrB_2, as it involves relatively less expensive charge material. ZrB_2 powder is prepared by the following reaction at a temperature higher than 1800°C and holding time of more than 1 h:

$$ZrO_2(s) + 0{,}5\ B_4C(s) + 1{,}5C(s) \longrightarrow ZrB_2(s) + 2CO(g) \quad \{2\}$$

The process results in some loss of boron in the form of boron oxide which causes the formation of nonstoichiometric boride and the presence of residual carbon in the product. In this route a following intermediate reaction takes place that results in boron loss in the form of B_2O_3. Thus excess boron is required to be added for getting pure ZrB_2.

- Metallothermic reduction of ZrO_2 and B_2O_3: this involves cheap raw material and it is self-sustainable due to their exothermic reaction. Mostly magnesium is used as reducing agent and ZrB_2 powder is prepared by the following reaction:

$$ZrO_2 + B_2O_3 + 5\ Mg \longrightarrow ZrB_2 + MgO \quad \{3\}$$

The use of magnesium as the reactant instead of aluminum allowed acid leaching of the unwanted oxide product leaving behind a pure boride phase. In any process for the formation of ZrB_2, it would be necessary to ensure that all of the ZrO_2 is consumed by reaction as ZrO_2 is difficult to remove by dissolution. This could be achieved by using a stoichiometric excess of both Mg and B_2O_3. Mechanical alloying technique can be exploited in this route to reduce the reaction temperature and time.

- Chemical solution processing: one or all components (metal-bearing, boron-bearing and carbon-bearing) are solubilized in a liquid processing medium (more intimate mixing can be achieved)[16]. The solution based methods are effective for low temperature synthesis of ultrafine powders because of the formation of amorphous phases and the intimate contact of the reactants. However, very limited studies were conducted on the synthesis of metal borides using solution phase reactions. Ultrafine ZrB_2 powders have been synthesized using inorganic–organic hybrid precursors of zirconium oxychloride ($ZrOCl_2*8H_2O$), boric acid and phenolic resin as sources of zirconia, boron oxide and carbon respectively. The reactions were substantially completed at a relatively low temperature (1500°C). The synthesized powders had a smaller average crystallite size (~200 nm), a larger specific surface area (32 m^2/g) and a lower oxygen content (~1,0 wt-%), which were superior to some commercially available ZrB_2 powders[20].
- Chemical vapor deposition gives coating of ZrB_2 by vapor phase reaction of zirconium and boron containing gaseous precursors. $ZrCl_4$ and BCl_3 are the most commonly used precursors and hydrogen is generally used as reducing agent. This is a low temperature route and gives good purity. This technique is more suitable for thin films and involves complex set-up. In general, researchers have used the following reaction:

$$ZrCl_4 + 2BCl_3 + 5H_2 \longrightarrow ZrB_2 + 10HCl \quad \{4\}$$

  Temperature, pressure and flow rate of reactants are the major processing parameters, which influence the composition and structure of the product. Deposition rate generally increases with increasing temperature and hydrogen concentration. The deposition rate is more influenced by hydrogen concentration in the gas mixture than by temperature.
- Synthesis by polymer precursor route: a processable precursor to ZrB_2 can be obtained by dispersing a ZrO_2 in a boron carbide polymeric precursor. Heating the mixture then results in either the in situ generation of boron carbide and carbon followed by reaction to produce the boride or in direct reaction of the polymer with the ZrO_2 to give the final boride product. The key requirements of the polymer component are the following: it should be stable, processable and should contain both the boron needed to form the metal boride and carbon to aid in the removal of the oxygen[20].

Densification of monolithic ZrB_2 by any technique requires very high temperature. Hot pressing or Spark Plasma Sintering is necessary to obtain dense shapes. These techniques are limited to simple geometry and complex shapes cannot be made. Metallic additives (Fe, Ni and Co) have been used

to promote liquid phase formation that enhances densification by facilitating particle rearrangement and mass transport. However, the addition of low melting temperature additives results in complete loss of strength by 1200°C, therefore it limits their use in high temperature applications. Ceramic additions that include silicon carbide, silicon nitride, boron carbide, metal silicides and oxides have also been used to improve the densification of ZrB_2. These additives enhance the densification of ZrB_2 ceramics between 1700 and 1900°C. Densification of ZrB_2 at these moderate temperatures can result in fine grain microstructures (2–3 mm) that can exhibit strengths in excess of 1000 MPa. However, the addition of ceramic additives can also significantly decrease the maximum operating temperature due to the formation of eutectic liquids. The most common additive to ZrB_2 is silicon carbide (SiC). The ZrB_2–SiC eutectic temperature is 2270°C, which limits the use of these ceramics to temperatures below this value[20].

In the way of improving the oxidation and ablation resistance of single-phase ZrB_2, the composite approach has been successfully adopted. For example the addition of silicon carbide as second phase, results in a new material with improved strength, better oxidation, thermal shock and ablation resistance. Oxidation improvement and ablation resistance arise from the formation of a coherent passivating oxide scale on the surface[18].

SILICON CARBIDE (SiC).

Silicon carbide (SiC), is a compound of silicon and carbon with chemical formula SiC. It occurs in nature as the extremely rare mineral moissanite. Silicon carbide powder has been mass-produced since 1893 for use as an abrasive. Grains of silicon carbide can be bonded together by sintering to form very hard ceramics which are widely used in applications requiring high endurance, such as car brakes, car clutches and ceramic plates in bulletproof vests. Electronic applications of silicon carbide as light emitting diodes (LEDs) and detectors in early radios were first demonstrated around 1907, and today SiC is widely used in high-temperature/high-voltage semiconductor electronics.

Figure 3- Things made of SiC, in order: cutting tools, trauma plates in ballistic vest, disc brake, ultraviolet LED.

Because of the rarity of natural moissanite, most silicon carbide is synthetic. It is used as an abrasive, and more recently as a semiconductor and diamond simulant of gem quality. The simplest manufacturing process is to combine silica sand and carbon in a graphite electric resistance furnace (Acheson process) at a high temperature, between 1600 and 2500 °C. Fine SiO_2 particles in plant material (e.g. rice husks) can be converted to SiC by heating in the excess carbon from the organic material.[7]

Cubic SiC is usually obtained by the more expensive process of chemical vapor deposition (CVD).[8][9]

Pure silicon carbide can also be prepared by the thermal decomposition of a polyorganocarbosilanes, under an inert atmosphere at low temperatures. With reference to the CVD process, the pyrolysis method is advantageous because the polymer can be formed into various shapes prior to thermalization into the ceramic[10][11][12][13].

Depending on the structure of the carbosilane chain, different ceramic yields are obtained.

In Figure 4[6] different types of polyorganocarbosilanes (PCS) that can be used as precursor for SiC-related ceramics are shown.

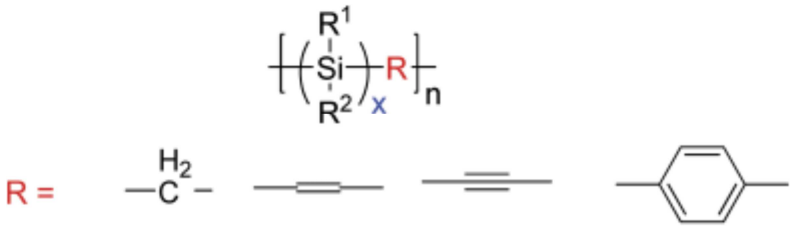

Figure 4 - General types of polyorganocarbosilanes

1. MATERIALS.

Experimental activity has started preparing the polymeric powder of ZrB_2 with different additions of SiC.

1.1 *Zirconium diboride.*

It was synthesized by pyrolysis of a novel Zr-polymeric precursor. The starting Zr-containing and B-containing precursors were both synthesized in the IPE's laboratory. The first one is $[(C_4H_8O)Zr(acac)_2]_n$ with molecular weight about 64870 and a softening point of 170°C. The second precursor was 2,4,6-(trimethylamino)borazine (Figure 5) with the chemical formula $(NHCH_3)_3B_3N_3H_3$ and molecular weight ~600. The component contents of these precursor are shown in *Table 2* [15].

Component	Zr (%)	O (%)	N (%)	C (%)	B(%)	H (%)
Zr-containing	29.82	26.40	-	37.90	-	5.88
B-containing	-	-	34.41	29.89	27.25	8.45

Table 2 - Component contents (wt%) of ZrB_2 prrecursors.

The Zr-precursor is a dark powder and B-precursor looks like a yellow very viscous liquid (Figure 6).

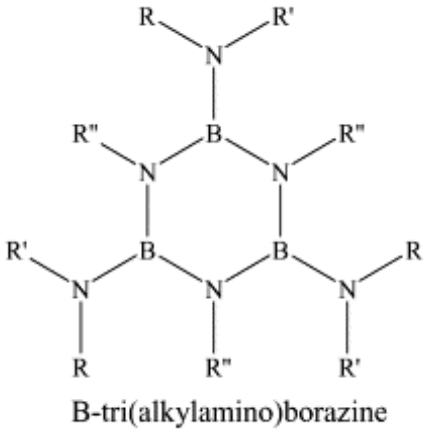

R, R" = H

R' = CH_3

B = 2,4,6

Figure 5 - 2,4,6-(trimethylamino)borazine

Figure 6 - From left: Zr-containing and B-containing precursors.

1.2 *Silicon carbide*.

In this work an ordinary poly(methylsilyne) has been used (Figure 7) and it's presented like a dark yellow solid.

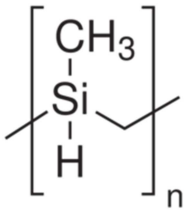

Figure 7 - Poly(methylsilyne)

1.3 *Precursors Solutions.*

To start off with, a ZrB_2-precursor solution has been prepared. To obtain a solution with X grams of ZrB_2, this formula has been followed:

$$A + C = X \quad (1)$$

where A is Zr-containing precursor's grams and C is B-containing precursor's grams. The procedure to prepare ZrB_2-precursor solution was as follows:

- C grams has been put in a flask;

- A = 1,87*C ;
- hereinafter A grams of grinded powder has been added together;
- toluene was added to solubilize the precursor in the same solution; quantity must be enough to dissolve all the polymer.

An examples of quantities that has been used are described in the Table 3 .

A (g)	C (g)	Toluene (g)	Total (g)	ZrB_2-precursor wt%
155,77	83,3	141,2	380,2	62%

Table 3 - Example of precursors and toluene weights.

About SiC-precursor solution, some poly(methylsilyne) has been grinded and dissolved in toluene. Quantities are described in Table 4 .

SiC-precursors (g)	Toluene (g)	Total (g)	SiC-precursor wt%
174	121	295	59%

Table 4 – SiC-precursor and toluene weights.

Many solutions have been prepared during the experiments, all with the same precursors wt%.

1.4 *Powders.*

In this work two classes of powders, called powder and foam composition, have been prepared.

Powder composition.

This class is divided into six different compositions (Table 5).

Name	Ceramic Volume Ratio (ZrB_2/SiC)
1-1	1
2-1	2
3-1	3
4-1	4
1-4	0,25
ZrB_2	Only ZrB_2 precursor

Table 5 - Compositions name.

For each sample the precursor quantities has been calculated respecting the corresponding Ceramic Volume Ratio.

Example:

$$V_{cZrB_2} : V_{cSiC} = 1 : 1$$

$$m_{cZrB_2} : m_{cSiC} = \rho_{cZrB_2} : \rho_{cSiC}$$

where V_{cZrB_2} is volume of ZrB_2 in the sample, V_{cSiC} is volume of SiC in the sample, densities $\rho_{cZrB_2} = 6{,}09\ g/cm^3$, $\rho_{cSiC} = 3{,}22\ g/cm^3$ and m_{cZrB_2} , m_{cSiC} are respectively the masses.

To pass from ceramic to polymeric precursor:

$$m_{cZrB_2} = m_{pZrB_2} * \eta_{ZrB_2} \quad (2)$$

$$m_{cSiC} = m_{pSiC} * \eta_{SiC} \quad (3)$$

where m_{pZrB_2} and m_{pSiC} are respectively the masses of ZrB_2 and SiC polymeric precursor,

$\eta_{ZrB_2} = 32\%$ and $\eta_{SiC} = 50\%$ are ZrB_2 and SiC ceramic yields.

Going ahead:

$$m_{pZrB_2} : m_{pSiC} = (\rho_{cZrB_2} / \eta_{ZrB_2}) : (\rho_{cSiC} / \eta_{SiC})$$

$$m_{pZrB_2} : m_{pSiC} = 19{,}03\ g/cm^3 : 6{,}44\ g/cm^3$$

$$m_{pZrB_2} / m_{pSiC} = 19{,}03 / 6{,}44 = 2{,}96$$

$$\chi_{1:1} = m_{pZrB_2} / m_{pSiC} = 2{,}96$$

Following the same method $\chi_{2:1}$, $\chi_{3:1}$, $\chi_{4:1}$ and $\chi_{1:4}$ have been calculated (Table 6).

$\chi_{1:1}$	2,96
$\chi_{2:1}$	5,92
$\chi_{3:1}$	8,88
$\chi_{4:1}$	11,84
$\chi_{1:4}$	0,74

Table 6 - $\chi_{i:i}$ values.

The precursor solutions have been mixed together in a flask, remembering that:

$$m_{p\text{-}sol\text{-}ZrB_2} = m_{pZrB_2} / 62\% \quad (5)$$

$$m_{p\text{-}sol\text{-}SiC} = m_{pSiC} / 59\% \quad (6)$$

Examples of quantities that have been used are described in the Table 7 .

Name	**$\chi_{i:i}$**	**m_{pZrB_2} (g)**	**$m_{p\text{-}sol\text{-}ZrB_2}$ (g)**	**m_{pSiC} (g)**	**$m_{p\text{-}sol\text{-}SiC}$ (g)**
1-1	4,11	62	100	20,95	35,50
2-1	8,22	62	100	10,47	17,75
3-1	12,33	62	100	6,98	11,83
4-1	16,44	62	100	5,24	8,88
1-4	1,03	62	100	83,78	142,01

Table 7 – Precursors quantities for "powder composition" samples.

The polymeric precursor solutions have been transformed in powder removing the solvent (toluene) by the reduced pressure distillation technology at vacuum of 0,1MPa and temperature 80°C for 2h (Figure 8).

In Table 5, ZrB_2 means that a certain quantity pure zirconium diboride precursor solution have been transformed in powder and then hat treated.

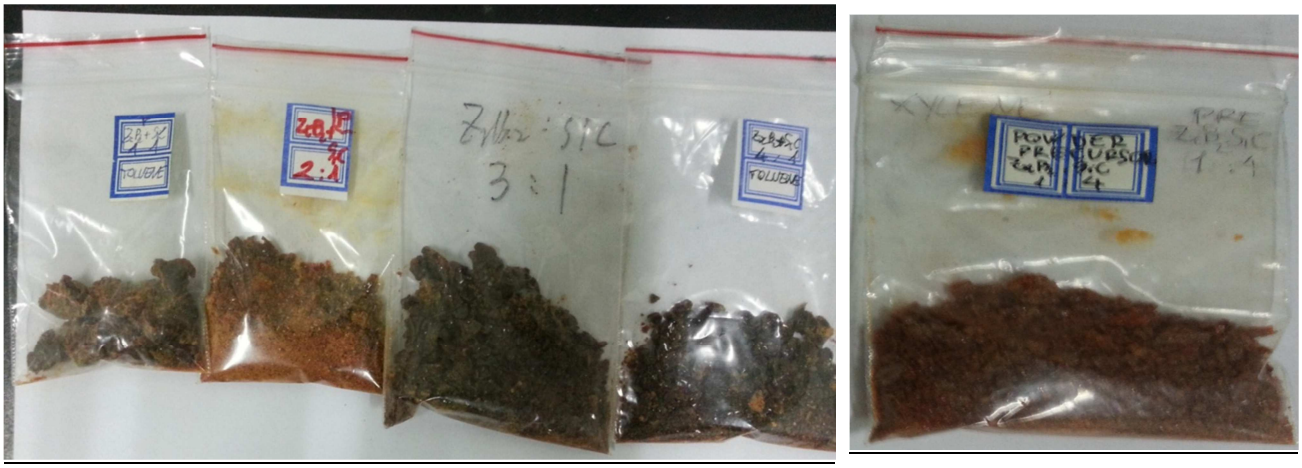

Figure 8 - Precursor powders.

Foam composition.

This class is divided into four different compositions (Table 8).

Name	Precursor Weight Ratio (SiC/ZrB_2)
1_1	1
1_2	2
1_3	3
1_4	4

Table 8 - Compositions name.

For each sample the precursor quantities has been calculated respecting the corresponding Precursor Weight Ratio.
Quantities are described in Table 9.

Name	m_{pZrB2} (g)	$*m_{p\text{-}sol\text{-}ZrB2}$ (g)	m_{pSiC} (g)	$**m_{p\text{-}sol\text{-}SiC}$ (g)
1_1	15	24,19	15	25,42
1_2	10	16,12	20	33,90
1_3	9	14,52	27	45,76
1_4	8	12,9	32	54,24

Table 9 - Precursors quantities for "powder composition" samples.

$$*m_{p\text{-}sol\text{-}ZrB2} = m_{pZrB2} / 62\% \quad (5)$$

$$**m_{p\text{-}sol\text{-}SiC} = m_{pSiC} / 59\% \quad (6)$$

The polymeric precursor solutions have been mixed together in a flask and then they have been transformed in powder removing the solvent (toluene) by the reduced pressure distillation technology at vacuum of 0,1MPa and temperature 80°C °C for 2h.

2. HEAT TREATMENTS.

Polymer precursor powders have undergone two different heat treatments to be transformed in ceramic powder or foam.

2.1 *Powder treatment*.

The subsequent heat treatment was performed at a heating rate of 2°C/min to desired temperature of 1500°C and then held for 2 h in the furnace under flowing argon atmosphere. In this case Composite Ceramic Powders have been obtained by polymer pyrolysis.

Each sample (Table 10) has been hand grinded and then put in a graphite crucible to be heat treated in the furnace.

The mechanism of pyrolysis is generally complex: structural rearrangements and radical reactions lead to the breaking of bonds (like Si-H, Si-C and C-H), release of functional groups (example CH_4, C_6H_6, CH_3NH_2) and formation of an inorganic network.

The ceramic yield of a polymer is an important PDCs parameter to consider: it's the ratio between the mass of ceramic residue after pyrolysis and the one of the starting polymer. The transformation from organic to inorganic ends at 800-1000° C and it is associated with a weight loss of 10-30%. The nature of the precursor determines the ceramic yield: low molecular weight polymers and oligomers drastically lower the yield because of volatilization. Typical yields ceramics are placed in the range of 70-90% but it is possible to reach higher values working in reactive atmospheres.

At the end of conversion, the ceramics obtained show an amorphous structure, typical of PDCs that is a mixture of covalent bonds. With the rising of temperature (1000-1800 ° C) more rearrangements occur, which generate a phase separation and crystallization of the different phases.

Number	Samples name
1	1-1
2	2-1
3	3-1
4	4-1
5	1-4
6	1_1
7	1_2
8	1_3
9	1_4
10	ZrB_2
11	1-1fs

Table 10 – Samples with Foam and Powder composition and others.

In Table 10, 1-1fs means that a certain quantity of 1-1 precursor solution has been spilled in a graphite crucible and then heat treated (fs: powder from solution).

2.2 *Foam treatment*.

In this heat treatment, powders with Foam composition have been heated in different steps:

A - heating rate of 2°C/min to 500°C and held for 1 h, under 1MPa argon or nitrogen atmosphere (product: Precursor Foam);

B - heating rate of 2°C/min to 1000°C and held for 2 h, under flowing argon atmosphere (product: Low T Ceramized Foam);

C - heating rate of 2°C/min to 1500°C and held for 2 h, under flowing argon atmosphere (product: Composite Ceramic Foam) to obtain the complete ceramization by polymer pyrolysis.

The A step allows foaming molding, using gasses originated by polymer decomposition as foaming agents. During treatment the pressure increases, it has been checked that it was no higher than 2MPa, using an appropriate valve installed on the furnace.

The other purpose of the heating treatment is to permit cross-linking of polymer chains to obtain a thermosetting solid; this avoids the collapse of precursor foam due to softening during heating.

The crosslinking can be obtained easily if in the polymer there are functional groups (like –OH, -H or –vinyl) that allow the mechanisms of polyaddition and polycondensation; in this case cross-linking is achieved at a temperature range between 150 ° C and 250 ° C.

Depending on the type of the mechanism, byproducts are released (generally gasses). The gas release causes bubbles which may remain trapped in the polymer: this phenomenon can be exploited for self-foaming porous ceramic production, the same used in this heat treatment.

It must be specified that two different furnaces have been used: a small one for SEM samples and microstructural analysis; a big one for mechanical proof samples, because of high powders amounts that have been used.

Differences between two furnaces are:

- in the small one nitrogen (N_2) atmosphere has been used, while in the big one argon (Ar) has;
- the big furnace was half filled with silica sand.

The Foam composition powder has been put in a becker and then it has undergone different heating treatment depending on the kind of analysis carried out, as it is shown in the following models (Figure 13) :

MODEL 1:

Treatment A small furnace → Treatment B → SEM and microstructural analysis

Treatment C → SEM and microstructural analysis

MODEL 2:

Treatment A big furnace → Treatment C → Mechanical Proof (compressive strength)

Figure 9 - From top: small furnace and big one.

Samples	Weight (g)
1_1	20,90
1_2	23,30
1_3	23,40
1_4	23,30

Table 11 - Samples for Model 1- Treatment A.

Samples	Weight (g)
Low T Ceramized Foam 1_1	0,62
Low T Ceramized Foam 1_2	2,26
Low T Ceramized Foam 1_3	1,86
Low T Ceramized Foam 1_4	1,50

Table 12 - Samples for Model 1 - Treatment B.

Samples	Weight (g)
Composite Ceramic Foam (1) 1_1	17,20
Composite Ceramic Foam (1) 1_2	6,17
Composite Ceramic Foam (1) 1_3	5,80
Composite Ceramic Foam (1) 1_4	8,00

Table 13 - Samples for Model 1 - Treatment C.

Samples	Average Weight (g)
Composite Ceramic Foam (2) 1_1	200,00
Composite Ceramic Foam (2) 1_2	126,50
Composite Ceramic Foam (2) 1_3	150,00
Composite Ceramic Foam (2) 1_4	161,30

Table 14 - Samples for Model 2.

Before A treating, all the powders have been weighed to evaluate the weight loss in the different furnaces; the output products have been called Precursor Foams.

After Treatment A:

- Samples treated in Model 1 have been weighed before and after the heat treatment in the furnace, to calculate the ceramic yield of products: Low T Ceramized Foam, after Treatment B; Composite Ceramic Foam (1), after Treatment C.
- Samples treated in Model 2 have been cut to obtain regular shape ceramic foams, that have been used later for mechanical proof; the output products have been called: Composite Ceramic Foams(2).

2.3 *Work schedule.*

Figure 10 - Powders production model.

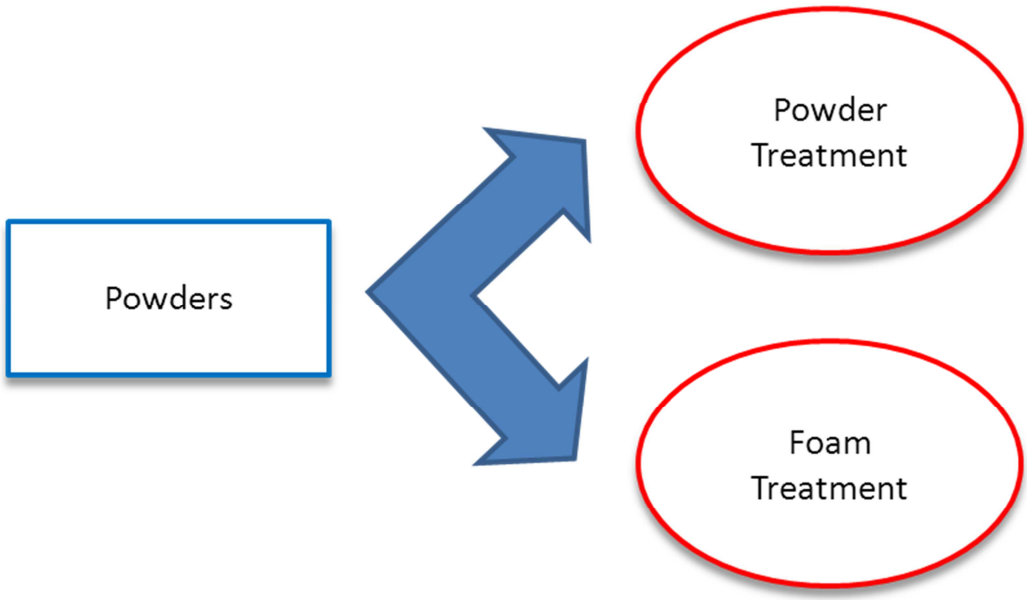

Figure 11 - Heat treatment distinction.

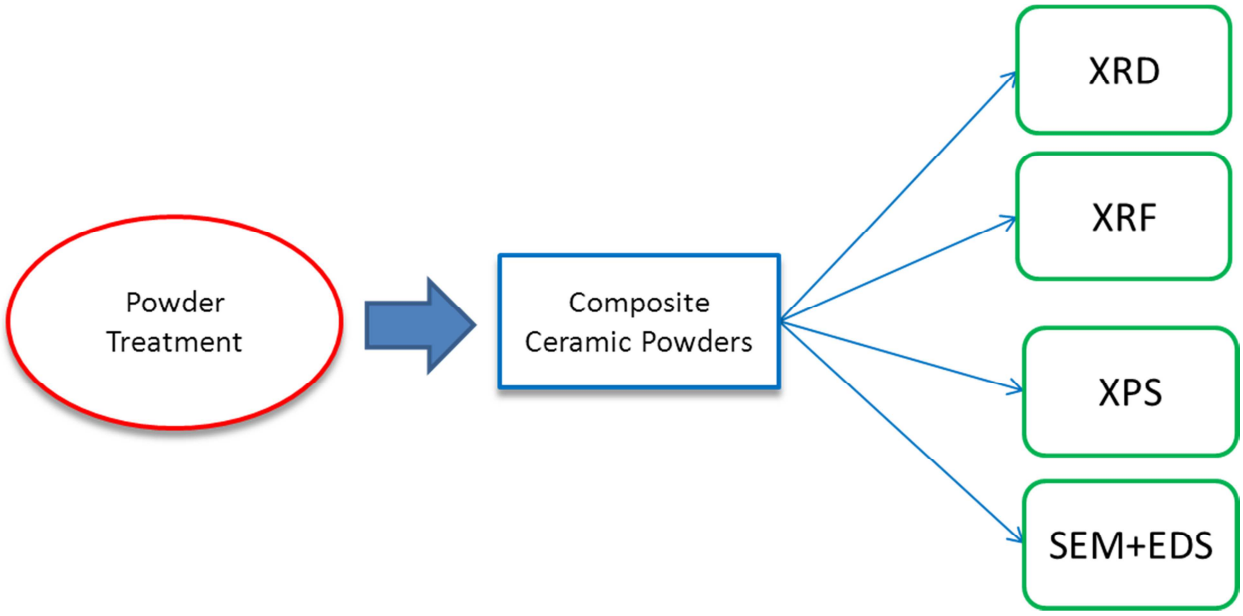

Figure 12 - Powders characterization.

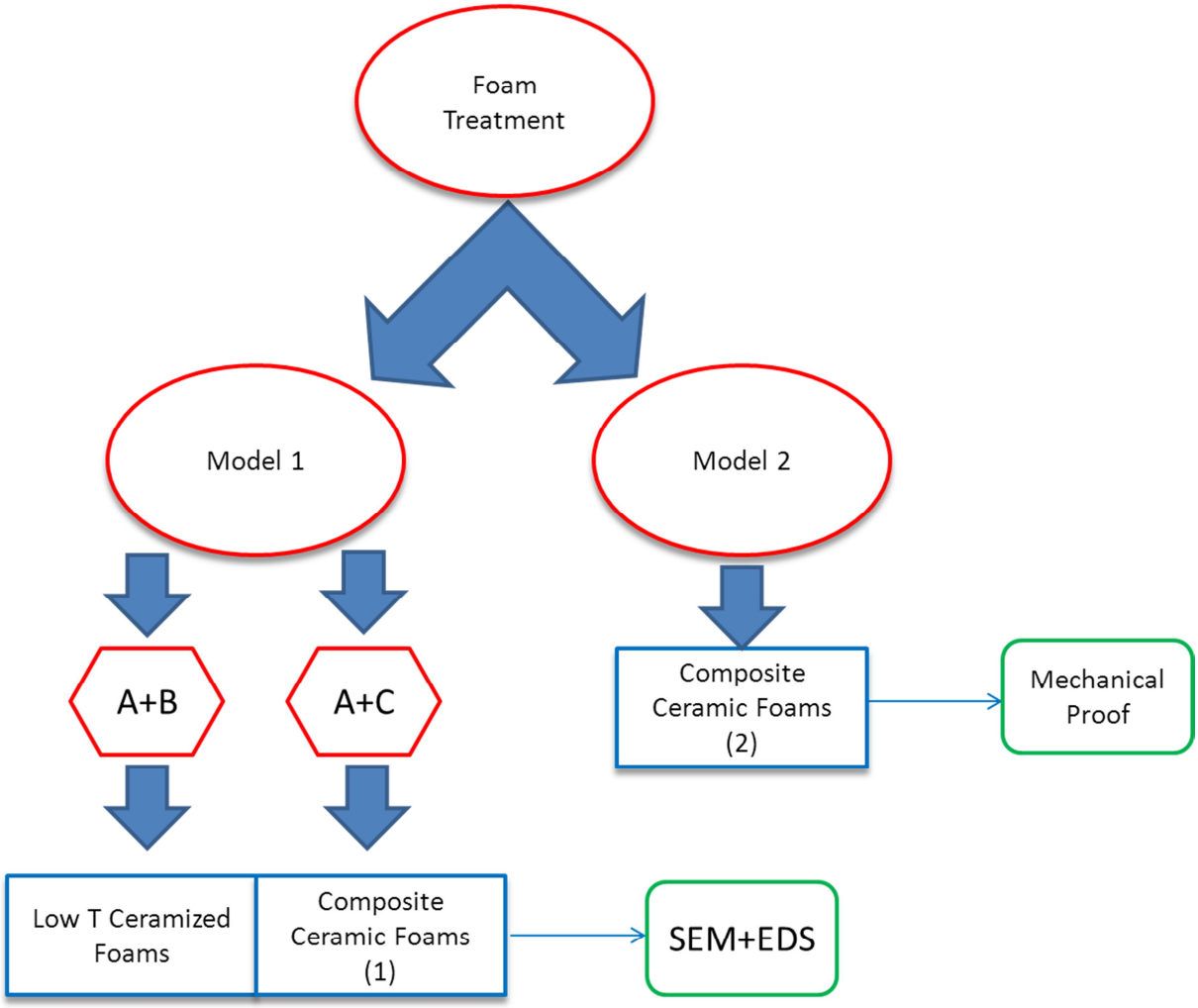

Figure 13 - Foam production and characterization.

3. CHARACTERIZATION AND INSTRUMENTS.

The techniques used to characterize the samples have been:

- X-Ray Diffraction (XRD);
- X-Ray fluorescence (XRF);
- X-ray Photoelectron Spectroscopy (XPS);
- Scanning Electron Microscope and, with the same instrument, Energy Dispersive Spectroscopy (SEM+EDS);
- Compressive strength.

The first four analysis have been use to characterize Composite Ceramic Powders and Foams (1), while the last one has been used for mechanical proof of Composite Ceramic Foams (2) (Figure 13).

3.1 *X-Ray Diffraction*.

The materials produced were subjected to XRD analysis to identify the phases contained therein. The technique used, called XRPD (X-ray powder diffraction), is based on elastic-scattering: the macroscopic phenomenon of diffraction arises from the sum of all electromagnetic waves spread from the atoms that are arranged along the same lattice planes family (Figure 14). This is constructive interference and thus the spectrum peak occurs when it satisfies Bragg's law:

$$n\lambda = 2d\,sen\theta \tag{7}$$

Where θ is the angle of incidence, d is the distance between adjacent crystallographic planes, λ is the wavelength of incident monochromatic radiation and n is a whole number.

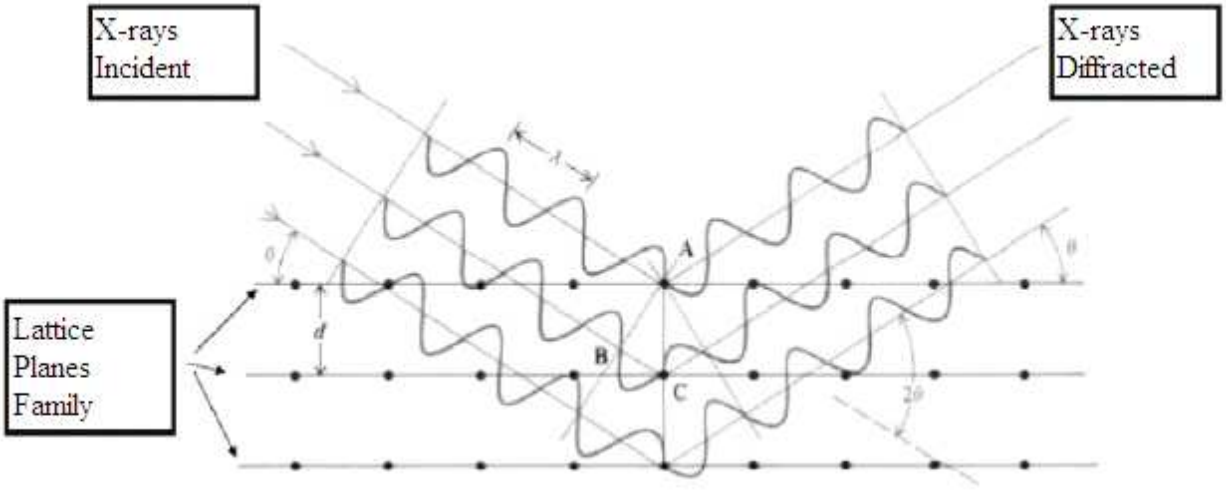

Figure 14 - X-ray diffraction on crystal planes.

The width and intensity of the diffracted radiation depend on the position of the atoms in the elementary cell: the sample is crystalline as much as the signals are intense and narrow on the spectrum.

The diffractogram (or pattern) of the sample is obtained by plotting the intensity of the beam diffracted with respect to the angle of diffraction 2θ.

The samples analyzed were hand grinded and then placed on a slide, in order to obtain a thin and uniform layer (Figure 15): dust behaves like a diffraction grating for the incident radiation.

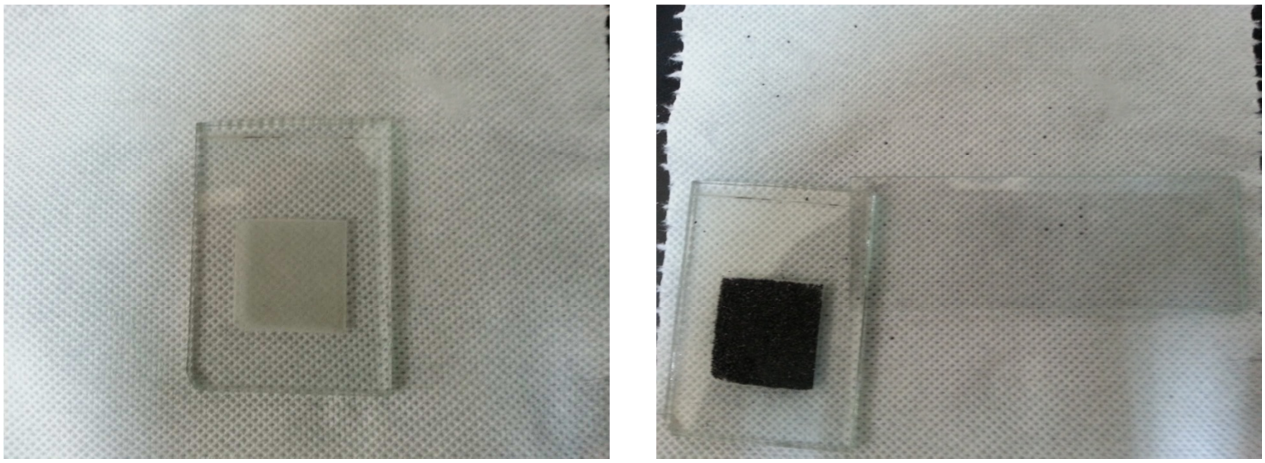

Figure 15 - Slide and XRD sample.

The qualitative analysis of XRD spectrum consists in identification of crystalline phases that constitute the pattern. This analysis is performed in two steps:

1. selection of the elements that should constitute the phases: software excludes the phases which don't contain the indicated elements;
2. manual selection of the best diagram chosen by the software.

Thanks to X'PERT HIGHSCORE software it was possible to compare the diffractograms of the samples with data in the database, to identify the different phases.

Figure 16 - X-ray diffractometer.

Number	Samples
1	1-1
2	2-1
3	3-1
4	4-1
5	1-4
6	1_1
7	1_2
8	1_3
9	1_4
10	ZrB_2
11	1-1fs

Table 15 - XRD Samples.

3.2 *X-Ray Fluorescence (XRF).*

X-ray fluorescence (XRF) is the emission of characteristic "secondary" (or fluorescent) X-rays from a material that has been excited by bombarding with high-energy radiation, like X-rays or gamma rays. The phenomenon is widely used for elemental analysis and chemical analysis, particularly in the investigation of metals, glass, ceramics and building materials.

When materials are exposed to short-wavelength X-rays or to gamma rays, ionization of their component atoms may take place. Ionization consists of the ejection of one or more electrons from the atom, and may occur if the atom is exposed to radiation with an energy greater than its ionization potential. X-rays and gamma rays can be energetic enough to expel tightly held electrons from the inner orbitals of the atom. The removal of an electron in this way renders the electronic structure of the atom unstable, and electrons in higher orbitals "fall" into the lower orbital to fill the hole left behind. In falling, energy is released in the form of a photon, the energy of which is equal to the energy difference of the two orbitals involved. Thus, the material emits radiation, which has energy characteristic of the atoms present. The term *fluorescence* is applied to phenomena in which the absorption of radiation of a specific energy results in the re-emission of radiation of a different energy, generally lower.

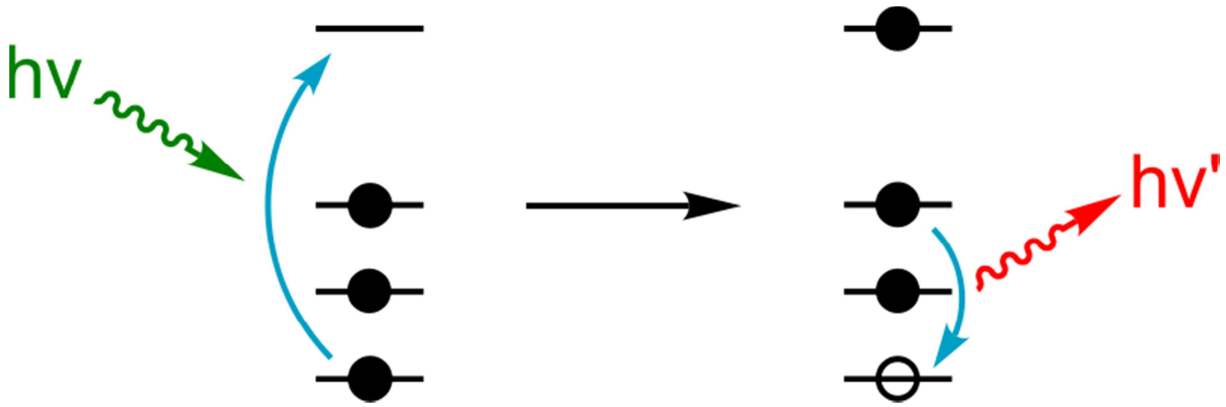

Figure 17 - Physics of X-ray fluorescence in a schematic representation.

Each element has electronic orbitals of characteristic energy. Following removal of an inner electron by an energetic photon provided by a primary radiation source, an electron from an outer shell drops into its place. Each of these transitions yields a fluorescent photon with a characteristic energy equal to the difference in energy of the initial and final orbital. The wavelength of this fluorescent radiation can be calculated from Planck's Law:

$$\lambda = h \cdot c / E \tag{8}$$

The fluorescent radiation can be analyzed either by sorting the energies of the photons (energy-dispersive analysis) or by separating the wavelengths of the radiation (wavelength-dispersive analysis). Once sorted, the intensity of each characteristic radiation is directly related to the amount of each element in the material.

In this experiment the energy dispersive analysis has been used (Figure 18): the fluorescent X-rays emitted by the material sample are directed into a solid-state detector which produces a "continuous" distribution of pulses, the voltages of which are proportional to the incoming photon energies. This signal is processed by a software which produces analytical data.

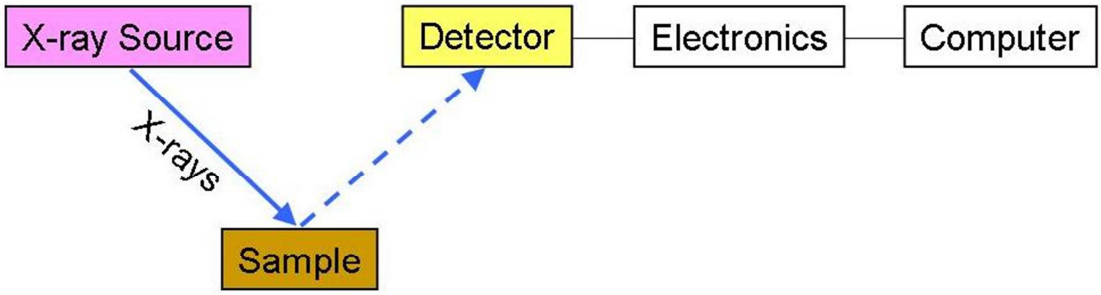

Figure 18 - Schematic arrangement of XRF spectrometer.

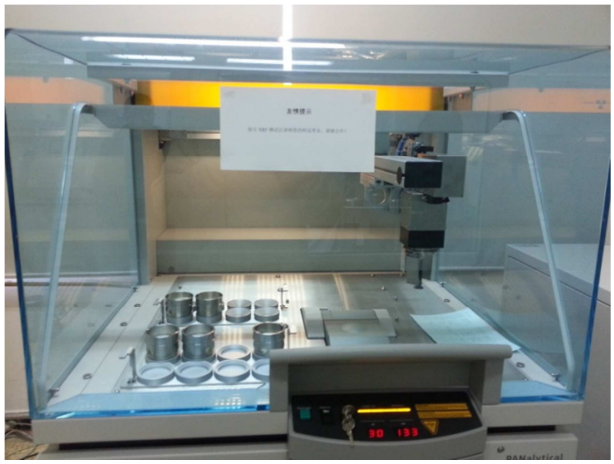

Figure 19 - XRF spectrometer.

SAMPLES:

- powders have been hand grinded and put into a cylinder, set in a press (Figure 21), in order to obtain a flat layer;
- in succession boric acid has been added (H_3BO_3, white powder); quantity must be high enough to become the substratum of the sample;
- cylinder has been removed;
- press has been closed;
- sample+H_3BO_3 have been pressed at ~30 MPa for 1 min;
- once ready, sample has been taken out (Figure 20) from press.

Once samples are ready, they have been arranged in XRF spectrometer (Figure 19)

Figure 20 - XRF sample.

Figure 21 - Press used to prepare XRF samples.

Number	Samples
1	1-1
2	2-1
3	3-1
4	4-1
5	1-4
6	1_1
7	1_2
8	1_3
9	1_4
10	1-1fs

Table 16 - XRF Samples.

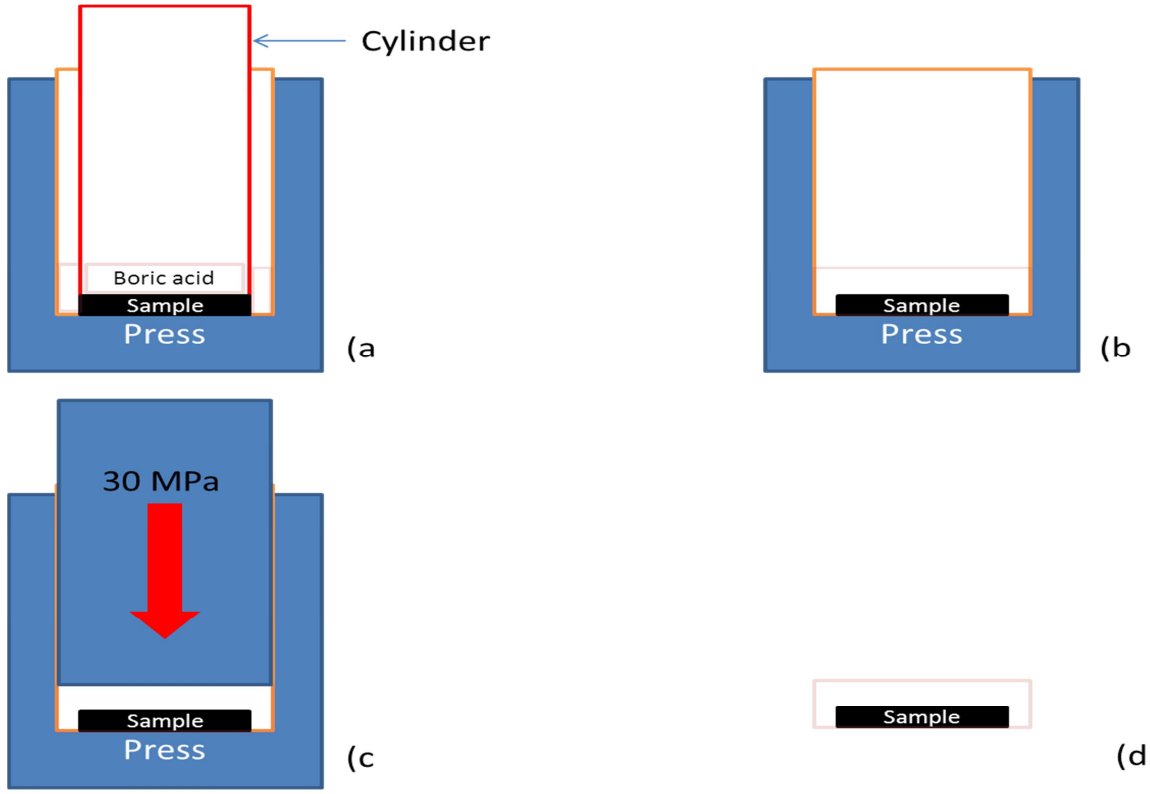

Figure 22- Sample schematic process: a) add powder and boric acid inside cylinder, set in the press (boric acid must be added also around the cylinder); b) remove cylinder; c) apply ~30MPa for 1 min; d) take out the sample.

3.3 *X-ray Photoelectron Spectroscopy (XPS).*

X-ray photoelectron spectroscopy (XPS) is a quantitative spectroscopic technique that measures the elemental composition, empirical formula, chemical state and electronic state of the elements that exist within a material. XPS spectra are obtained by irradiating a material with a beam of X-rays while simultaneously measuring the kinetic energy and number of electrons that escape from the top 1 to 10 nm of the material being analyzed. XPS requires ultra-high vacuum (UHV) conditions.

XPS is a surface chemical analysis technique that can be used to analyze the surface chemistry of a material in its "as received" state, or after some treatment. Because the energy of an X-ray with particular wavelength is known, the electron binding energy of each of the emitted electrons can be determined by using an equation that is based on the work of Ernest Rutherford (1914):

$$E_{\text{binding}} = E_{\text{photon}} - (E_{\text{kinetic}} + \phi) \tag{9}$$

where E_{binding} is the binding energy (BE) of the electron, E_{photon} is the energy of the X-ray photons being used, E_{kinetic} is the kinetic energy of the electron as measured by the instrument and ϕ is the work function of the spectrometer (not the material).

A typical XPS spectrum is a plot of the number of electrons detected, sometimes per unit time (ordinate), versus the binding energy of the electrons detected (abscissa). Each element produces a characteristic set of XPS peaks at characteristic binding energy values that directly identify each element that exists in or on the surface of the material being analyzed. These characteristic peaks correspond to the electron configuration of the electrons within the atoms (1s, 2s, 2p, 3s, etc). The number of detected electrons in each of the characteristic peaks is directly related to the amount of element within the area (volume) irradiated. To generate atomic percentage values, each raw XPS signal must be corrected by dividing its signal intensity (number of electrons detected) by a “relative sensitivity factor” (RSF) and normalized over all of the elements detected.

To count the number of electrons at each kinetic energy value, with the minimum of error, XPS must be performed under ultra-high vacuum (UHV) conditions because electron counting detectors in XPS instruments are typically one meter away from the material irradiated with X-rays.

It is important to note that XPS detects only those electrons that have actually escaped into the vacuum of the instrument. The photo-emitted electrons that have escaped into the vacuum of the instrument are those that originated from within the top 10 to 12 nm of the material. All of the

deeper photo-emitted electrons, which were generated as the X-rays penetrated 1– 5 micrometers of the material, are either recaptured or trapped in various excited states within the material. For most applications, it is, in effect, a non-destructive technique that measures the surface chemistry of any material.

The ability to produce Chemical State information from the topmost 1-12 nm of any surface makes XPS a unique and invaluable tool for understanding the chemistry of any surface either as received, or after physical or chemical treatments. Because modern systems use monochromatic X-ray sources, XPS measurements leave the surface free of any degradation with few exceptions.

Quantitative accuracy depends on several parameters such as: signal-to-noise ratio, peak intensity, accuracy of relative sensitivity factors, correction for electron transmission function, surface volume homogeneity, correction for energy dependency of electron mean free path, and degree of sample degradation due to analysis.

Under routine work conditions, where the surface is a mixture of contamination and expected material, the accuracy ranges from 80-90% of the value reported in atomic percent values.

Tables of binding energies (Bes) that identify the shell and spin-orbit of each peak produced by a given element are included with modern XPS instruments, and can be found in various handbooks and websites. Because these experimentally determined Bes are characteristic of specific elements, they can be directly used to identify experimentally measured peaks of a material with unknown elemental composition.

Figure 23 – XPS spectrometer.

SAMPLES:

- a square piece of carbon tape has been joined to a clean aluminum foil;
- ceramic powder has been hand grinded and applied on carbon tape;
- the sample has been covered with another aluminum foil and compacted at 20 Mpa for 1 min;
- after pressing, a square has been cut (about less than 1 cm each side) and the aluminum layers removed;
- this square has been joined to a specific specimen holder, that will be set in the spectrometer.

To avoid samples contamination, it's important to use gloves and tools to handle powders.

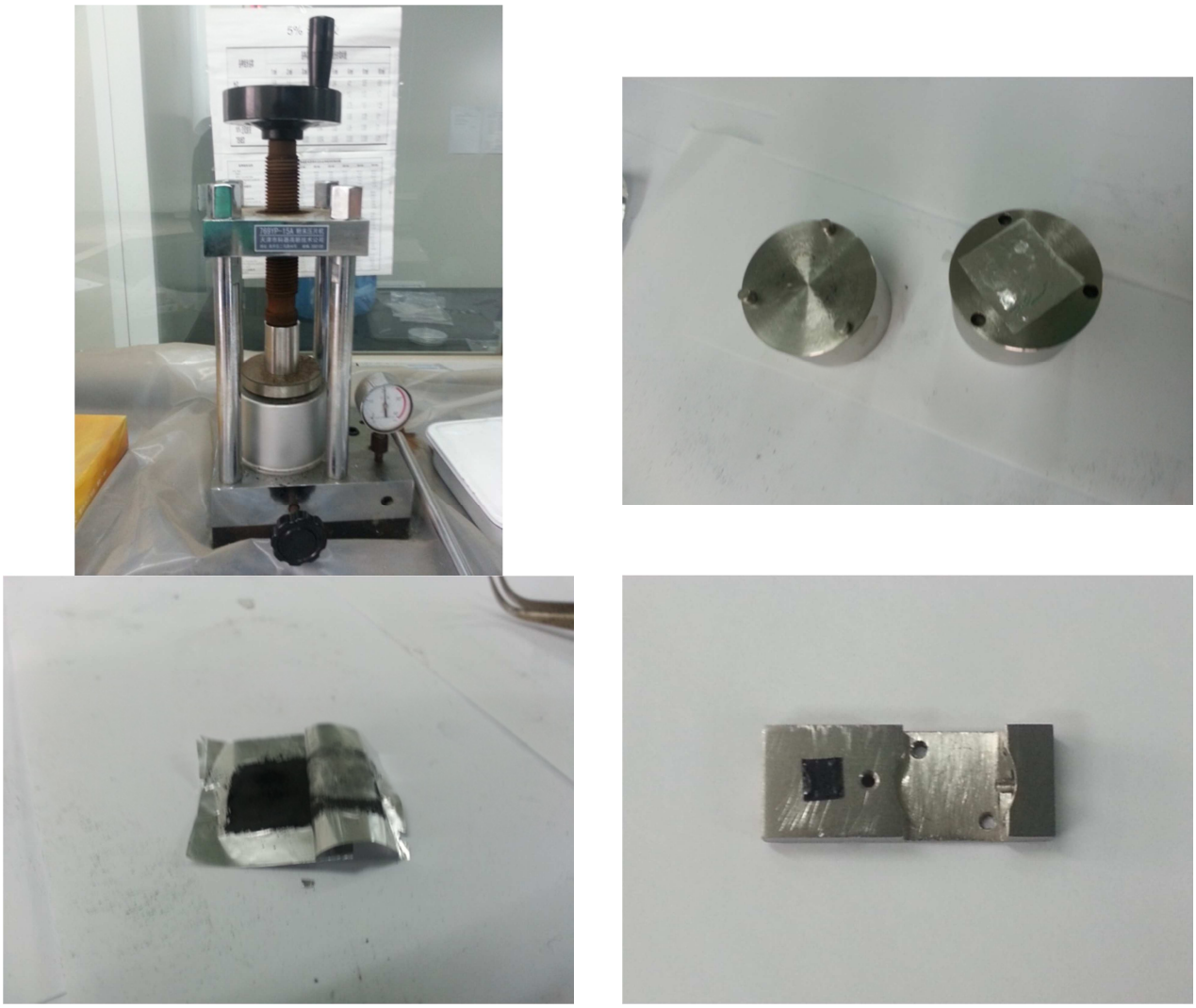

Figure 24 – Form top: press; covered sample before pressing; powder taken-out from press; sample ready to be set in spectrometer.

Number	Samples
1	1-1

Table 17 – XPS sample.

3.4 *Scanning Electron Microscope and Energy Dispersive Spectroscopy*.

Scanning Electron Microscope.

The scanning electron microscope (SEM) is a tool which allows analysis of the various signals produced by the interaction of the electrons beam with the sample. Information on the morphology of the samples are obtained by the processing of these signals.

The main elements of the SEM are shown in :

- electronic column, where the electron beam is created;
- vacuum chamber, where the electron beam interacts with the sample;
- various types of detectors that capture the signals of the interaction beam-sample and transfer them to the software;
- screen, which changes the signal in picture.

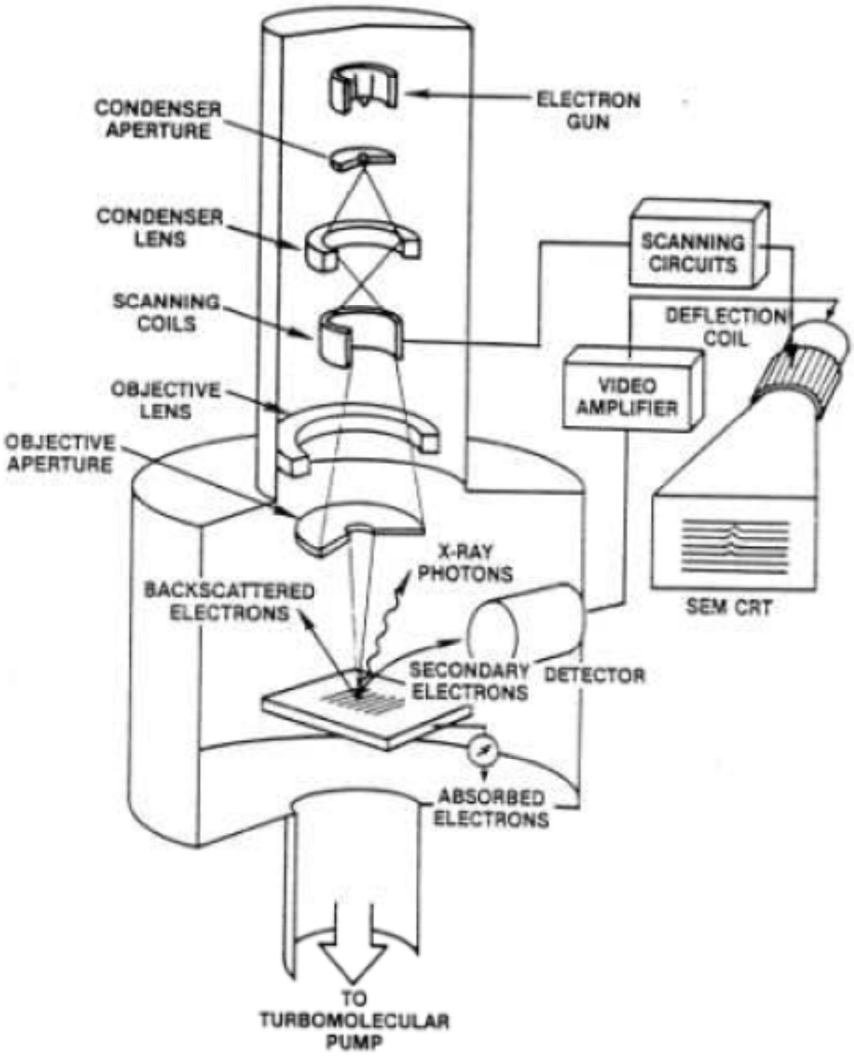

Figure 25 – SEM's operating diagram.

The electronic source, in the top of the column, generates an electron beam, using a filament (usually tungsten) that, led to high temperature, produces electrons due to thermionic effect.

The electrons are then accelerated, in the way to obtain an energy variable between a few hundred and some tens of thousands of eV (200eV to 30 keV), thanks to an anode placed under the filament.

The obtained beam is focused by a series of electromagnetic lenses and fissures within the column.

It exits the column and hits the sample within the under vacuum chamber.

Signals produced are various, the most important are:

1) *Secondary electrons*: their image represents the morphological structure of sample; contrast is determined by the topographical features of the surface.
2) *Backscattered electrons*: they give information that is related to the chemical composition and phase shape.
3) *X-ray*: another signal used for compositional analysis.

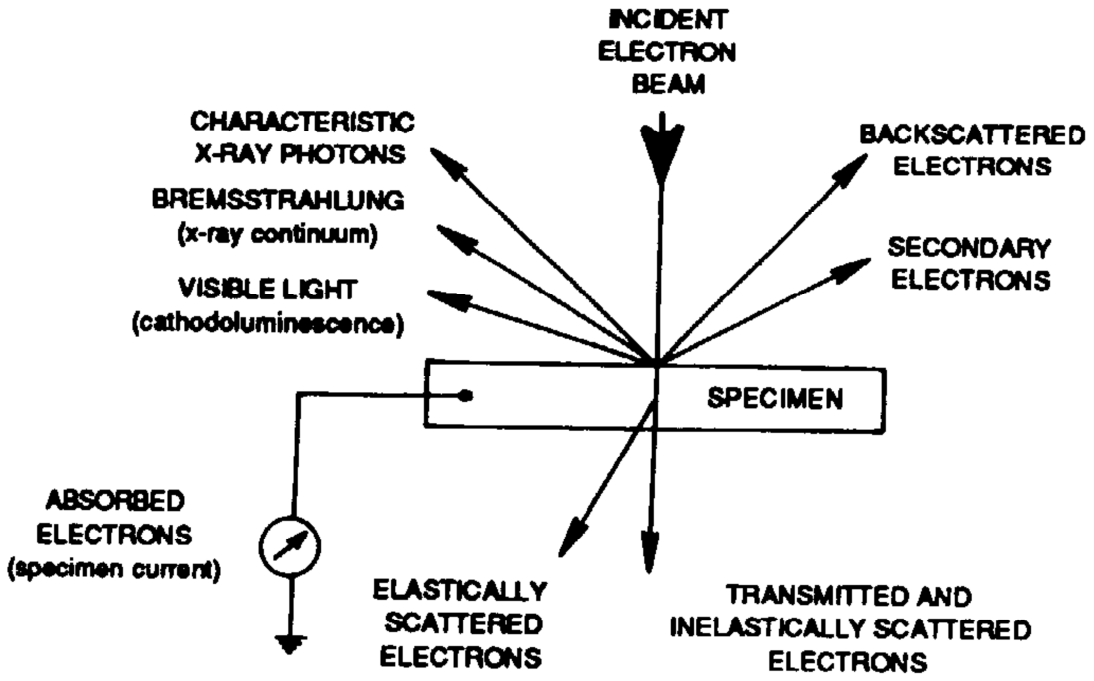

Figure 26 – Signals generated by sample and electron beam interaction.

For conventional imaging in the SEM, specimens must be electrically conductive, at least at the surface, and electrically grounded to prevent the accumulation of electrostatic charge at the surface. Nonconductive specimens tend to charge when scanned by the electron beam, and especially in secondary electron imaging mode, this causes scanning faults and other image artifacts. They are therefore usually coated with an ultrathin coating of electrically conducting material, deposited on the sample either by low-vacuum sputter coating or by high-vacuum evaporation.

Energy Dispersive Spectroscopy.

It is a technique used to collect and determine the energy and number of X-rays that are given-off by atoms in a material. These radiations can result from numerous physical processes, all of which involve excitation of a sample by some energy source (high-energy electrons beam), transitions of electrons in the sample between different energy states, and the emission of excess energy from the sample in the form of X-rays. This process is known as X-Ray Fluorescence.
In this case the analysis, that have been carried out, have given only qualitative result.

SAMPLES:

- Composite Ceramic Powders have been hand grinded;
- Composite Ceramic Foams(1) and Low T Ceramized Foam have been ripped to shreds;
- Pieces of carbon tape, with different shape, have been joined to specimen holder (Figure 28);
- Samples have been joined to carbon tape, position has been noted down (Figure 28);
- Samples have been coated by low-vacuum sputter technique (Figure 27) with two different conducting materials:
    - powders with gold ultrathin coating;
    - foams with carbon nanoparticles.
- Once ready, samples have been set in the microscope (Figure 29).

Number	Samples
1	1-1
2	2-1
3	3-1
4	4-1
5	1-4
6	Low T Ceramized Foam 1_1
7	Low T Ceramized Foam 1_2
8	Low T Ceramized Foam 1_3
9	Low T Ceramized Foam 1_4
10	Composite Ceramic Foam (1) 1_1
11	Composite Ceramic Foam (1) 1_2
12	Composite Ceramic Foam (1) 1_3
13	Composite Ceramic Foam (1) 1_4

Table 18 – SEM and EDS samples.

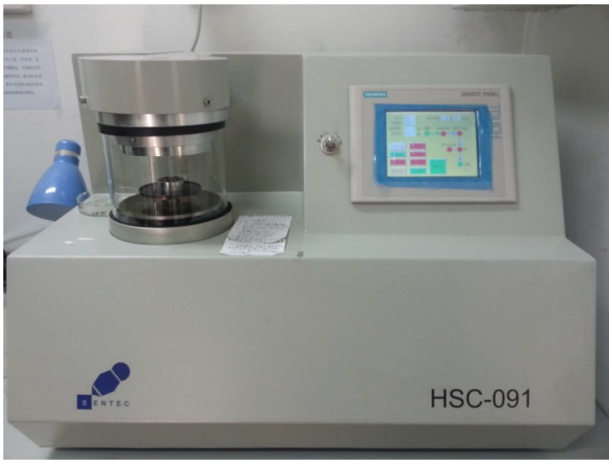

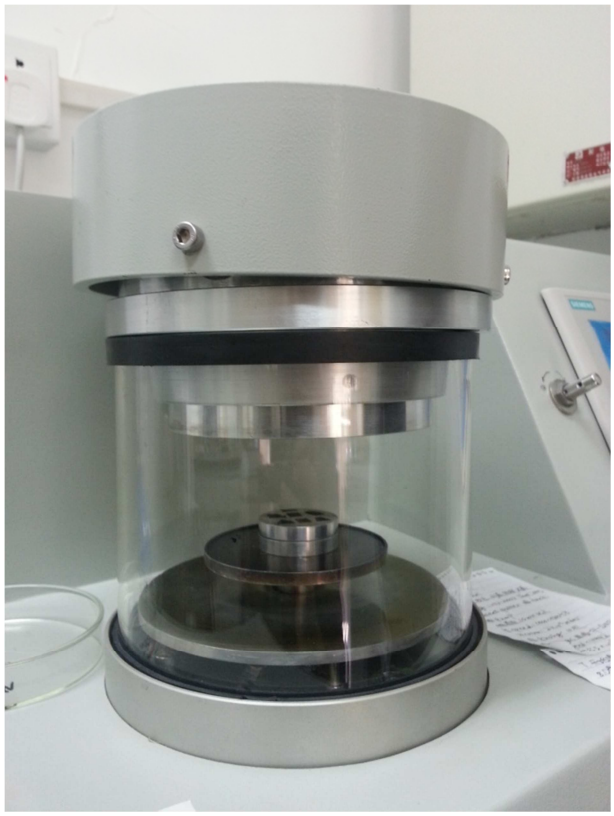

Figure 27 – Low-vacuum sputter instrument.

Figure 28 – Composite Ceramic Powders coated with gold and position noted down.

Figure 29 – Scanning Electron Microscope.

3.5 *Compressive strength*.

The mechanical proofs were made using a machine at controlled displacement (Figure 31); five samples per composition were subjected to the test.

The equipment consists of two circular platforms: a fixed one, on which the sample is placed, and a movable one with controlled movement to compress the regular shape pieces of Composite Ceramic Foam(2) (Figure 32).

When the speed of advancement of the head has been set (0,5 mm/min), the machine registers a stress proportional to the displacement (Δl). A load cell produces an electric signal directly proportional to the force (F) exerted on the sample, minute by minute.

The signal is appropriately processed and displayed on the computer monitor.

The relative deformation (ε) and the compression strain (σ) to which every single sample is subjected, can be calculated knowing the area A of the face of the sample on which the load F acts, by the two equations:

$$\varepsilon = \Delta l / l \tag{10}$$

$$\sigma = F / A \tag{11}$$

where *l* is the thickness of the sample.

The curve provided by the machine shows in the abscissa the displacement (Δl) and in the ordinate the force (F); when the two equations are applied, it is possible to obtain a second diagram (Figure 30) with ε% in x-axis and σ_{compr} in y-axis.

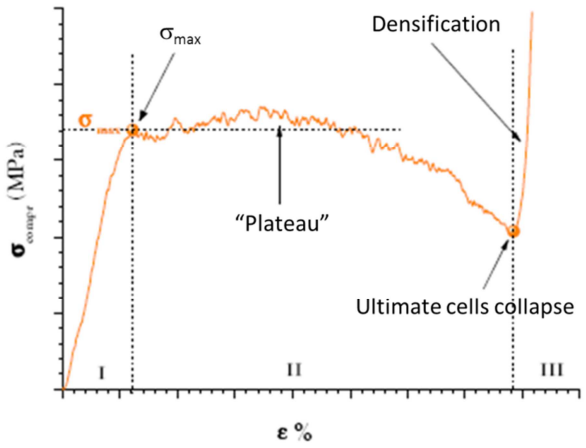

Figure 30 - σ / ε% graph of a generically specimen.

The diagrams obtained from compression tests, show a trend in which it is observed an initial peak (I) to maximum compression strain σ_{max}, a subsequent plateau (II) and a final zone (III), in which the load increases very rapidly.

In zone I, the porous compound deforms elastically up to reach the peak of maximum effort (σ_{max}). In this area the walls of the cells flex under the stress of compression, without breaking: the sample offers a structural resistance to compression.

In zone II, the strain remains almost constant: the load decreases due to the rupture of the cells by brittle fracture, but at the same time the friction, that is created between the fragments of the already broken walls, increases. In this area there is a balance between the collapse of the cells and the densification.

After this phase the ultimate cells collapse begins (zone III), caused by brittle fracture of the walls and the “densification” of the cellular structure: the opposing walls of each cell touch each other and the strain begins to grow rapidly due to the strong friction which is generated between the powders. In this stage there is no longer any recognizable cellular structure.

Figure 31 – Instrument for mechanical proof.

Number	Samples
1	Composite Ceramic Foam(2) 1_1
2	Composite Ceramic Foam(2) 1_2
3	Composite Ceramic Foam(2) 1_3
4	Composite Ceramic Foam(2) 1_4

Table 19- Mechanical proof samples.

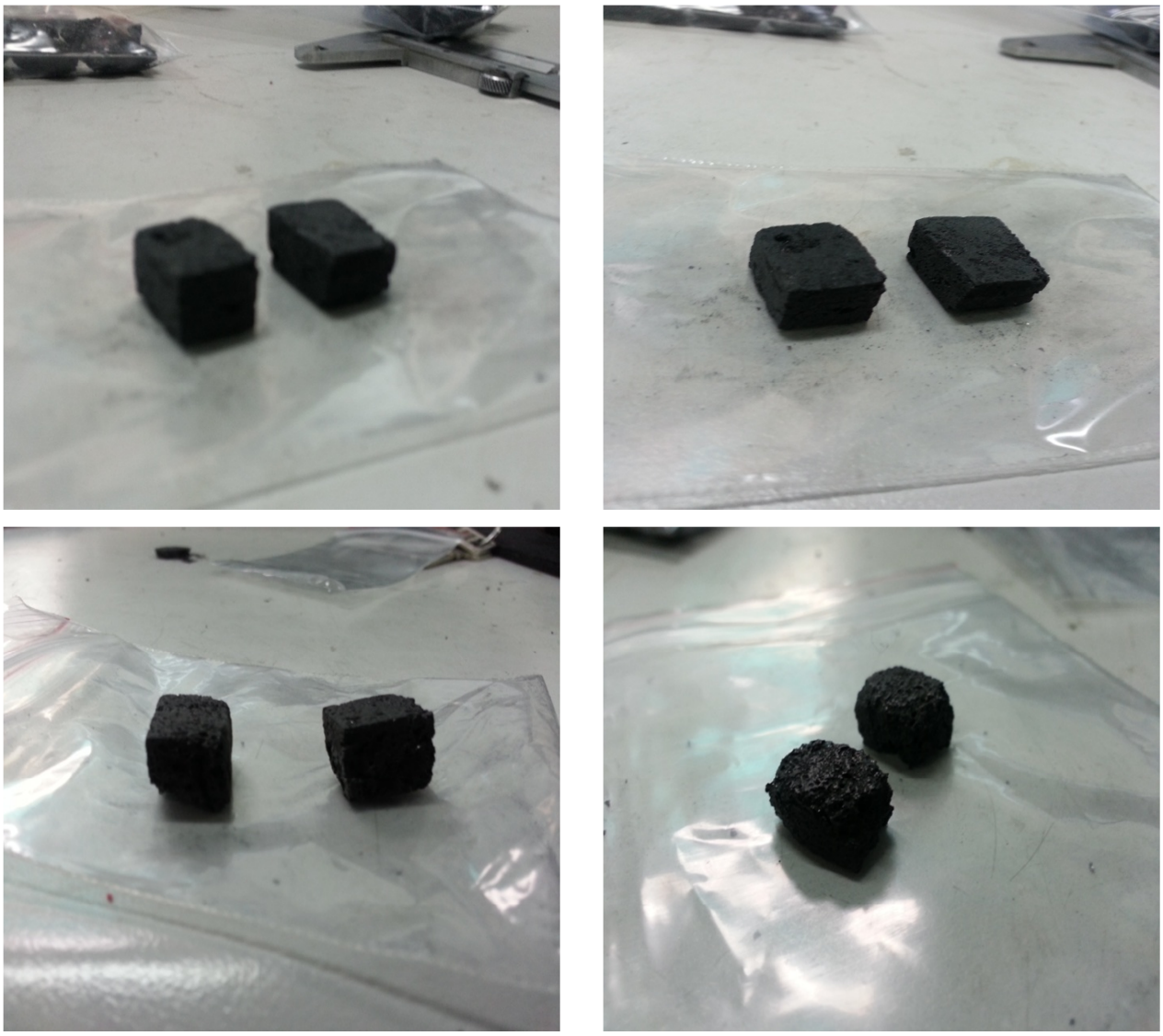

Figure 32 – Composite Ceramic Foams (2) for mechanical proof; top: left, 1_1; right, 1_2; down: left, 1_3; right, 1_4.

4. RESULTS AND DISCUSSION.

4.1 *Ceramic yield*.

In Table 20 all ceramic yields are shown.

Number	Samples name	Th ZrB_2 wt%	Ceramic yield	C.y%	Th c.y.
1	1-1	65,4	0,357	35,7%	0,382
2	2-1	79,1	0,308	30,8%	0,358
3	3-1	85,0	0,296	29,6%	0,347
4	4-1	88,3	0,284	28,4%	0,341
5	1-4	32,1	0,473	47,3%	0,442
6	1_1	28,0	0,466	46,6%	0,450
7	1_2	16,3	0,547	54,7%	0,471
8	1_3	11,5	0,597	59,7%	0,479
9	1_4	8,9	0,596	59,6%	0,484
10	ZrB_2	100,0	0,325	32,5%	0,320
11	1-1fs	65,4	0,078	7,8%	0,382

Table 20 – Ceramic yields for Powder composition samples.

From Table 20 it can be noticed that:

- ✓ ZrB_2 theoretical ceramic yield value is approximately similar to the experimental one;
- ✓ 1-1fs shows a very low ceramic yield; the reason could be that solvent boiling caused a very high material loss.

For Powder composition the ceramic yield decreases by increasing ZrB_2 amount. It may be assumed that a mixtures rule has been followed, that is:

$$Th\ c.y. = \eta_{ZrB2} * (Th\ ZrB_2\ wt\%) + \eta_{SiC} * (1 - Th\ ZrB_2\ wt\%) \quad (12)$$

where *Th c.y.* is Theoretical ceramic yield of the ceramic composite, η_{ZrB2} is the ceramic yield of the zirconium diboride precursor, η_{SiC} is the ceramic yield of the silicon carbide precursor and *Th* ZrB_2 *wt%* is the theoretical weight fraction of zirconium diboride.

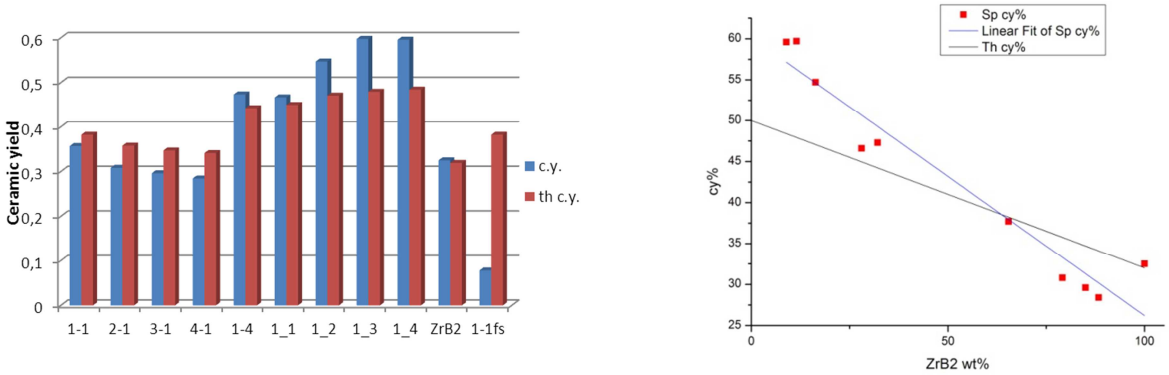

Figure 33 – Graphs: ceramic yield histogram shows differences between experimental values (blue columns) and theoretical ones (red columns); right graph shows ceramic yield trend versus theoretical zirconium diboride weight fraction.

In Figure 33 the right graph shows:

- a straight black line (Th cy%), that represents the Theoretical ceramic yield % of the system (12);
- red scatters (Sp cy%), they are the experimental Samples ceramic yields;
- a blue line, that is the Linear Fit of experimental results.

It's possible to see that Sp cy% values don't follow the mixtures law (black straight line); their trend is better described by a different line with different slope (blue one).

Histogram in Figure 33 shows the difference between theoretical ceramic yield (red columns) and experimental one (blue columns).

Sample	Yield	Y%
1_1	0,746	74,6%
1_2	0,832	83,2%
1_3	0,835	83,5%
1_4	0,832	83,2%

Table 21 - Yield for A Treatment in small furnace.

Sample	Average yield	A.y%
1_1	0,907	90,7%
1_2	0,900	90,0%
1_3	0,945	94,5%
1_4	0,893	89,3%

Table 22 - Yield for A Treatment in big furnace.

In Table 21 and Table 22 the different yields for the different furnace are illustrated: the small one (nitrogen atmosphere) has minor values than big one (argon atmosphere). The A Treatment has a max weight loss around ~25% (sample 1_1) for small furnace and ~11% (sample 1_4) for big one.
In Table 22 the values are an average result because more than one sample of each composition has been heat treated.

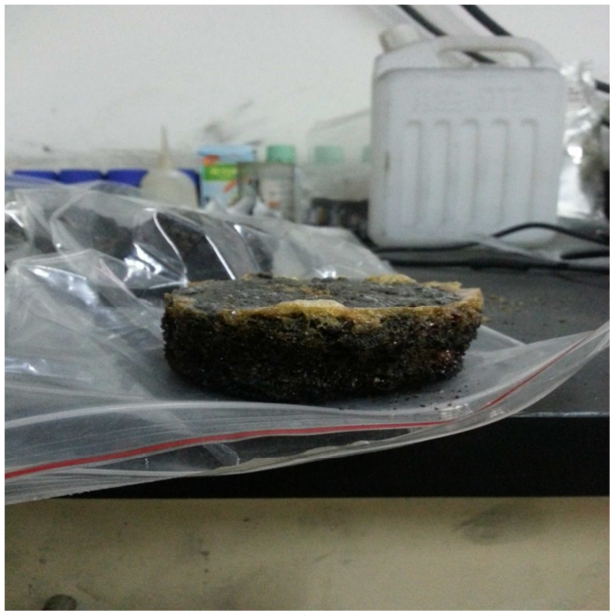

(a

(b

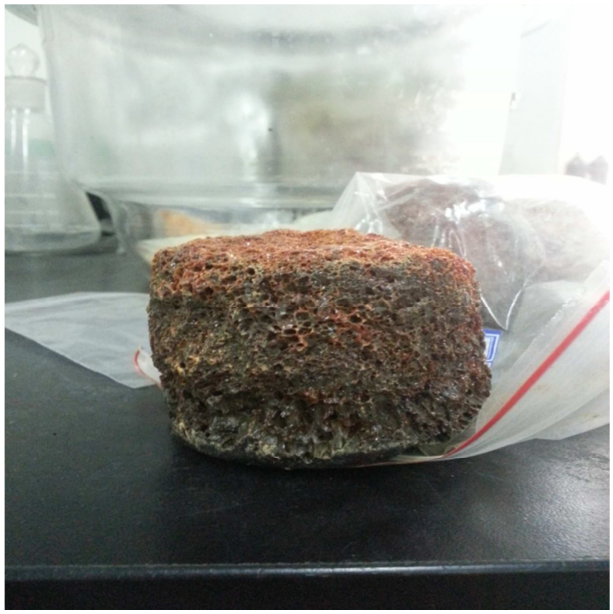

(c

(d

Figure 34 - Precursor foam from big furnace: a) 1_1 (100g); b) 1_2 (100g); c) 1_3 (200g); d) 1_4 (200g).

Sample	Ceramic Yield	C.y%
Low T Ceramized Foam 1_1	0,813	81,3%
Low T Ceramized Foam 1_2	0,853	85,3%
Low T Ceramized Foam 1_3	0,857	85,7%
Low T Ceramized Foam 1_4	0,855	85,5%

Table 23 - Yield for Treatment B (Model 1).

Sample	Ceramic yield	C.y%
Composite Ceramic Foam (1) 1_1	0,616	61,6%
Composite Ceramic Foam (1) 1_2	0,794	79,4%
Composite Ceramic Foam (1) 1_3	0,776	77,6%
Composite Ceramic Foam (1) 1_4	0,788	78,8%

Table 24 - Ceramic yield for Treatment C (Model 1).

Foam ceramic yield is slightly higher than Powder one with the same composition (es: Composite ceramic Foam (1) 1_1 = 61,6%, while powder 1_1 = 46,6%). This difference could be conferred to cross linking process: it causes high degrees of branching and high molecular weight, so there will be fewer oligomers and short chains that may volatilize at high temperatures and consequently the weight loss will be lower.

Yields of Low T Ceramized Foams are respectively higher than Composite Ceramic Foam (1). Generally for polymer derived ceramic the conversion process from organic to inorganic material can be considered terminated between 800 ° C and 1000 ° C and it is normally associated to a weight loss varying between 10% and 30%, then typical ceramic yields are between 70% and 90%. The step of thermal decomposition takes place around 300 ° C and 400 ° C and most of the weight loss of the polymer is due to the cleavage of chemical bonds and the release of gaseous byproducts. At higher temperatures (>1000°C), dehydrogenation and carbothermal reduction give a further contribution to the overall weight loss, although these phenomena are much less significant than thermal decomposition [34]. This is why Composite Ceramic Foam (1) yields are lower than Low T Ceramized Foam one.

Figure 35 - Composite Ceramic Foam (1).

4.2 *XRD*.

In the follow figures Composite Ceramic Powder patterns are shown.

Principal recorded phases are:

- silicon carbide (SiC);
- zirconium diboride (ZrB_2);
- zirconium carbide (ZrC), it's a product of reaction between Zr-precursor and carbon excess.

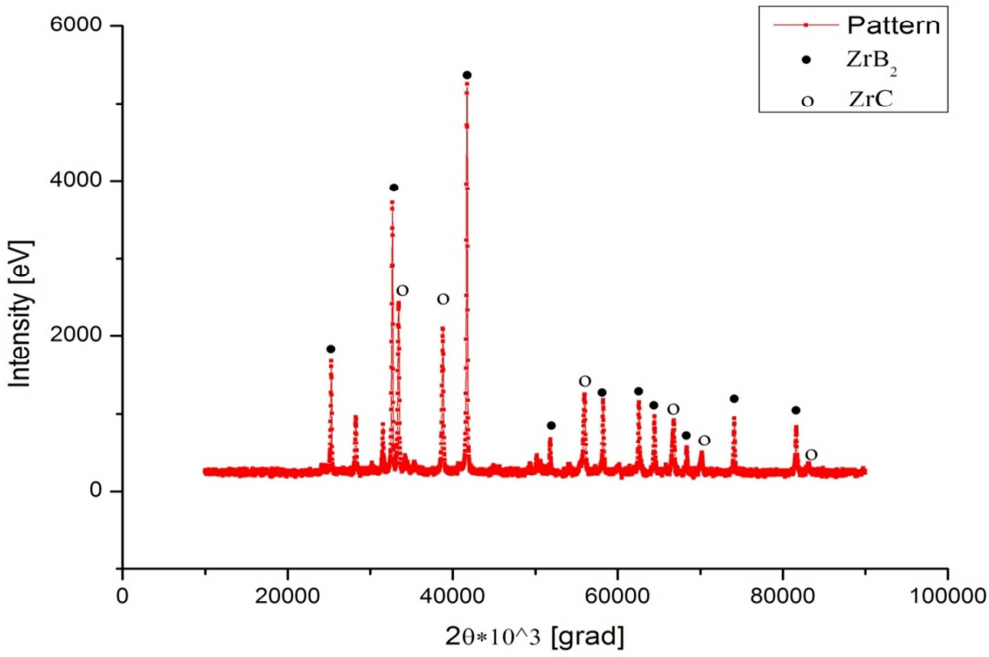

Figure 36 - ZrB_2 pattern.

In Figure 36 ZrB_2 pattern shows that from pyrolysis of pure zirconium diboride precursor solution a ZrB_2/ZrC composite ceramic powder has been obtained.

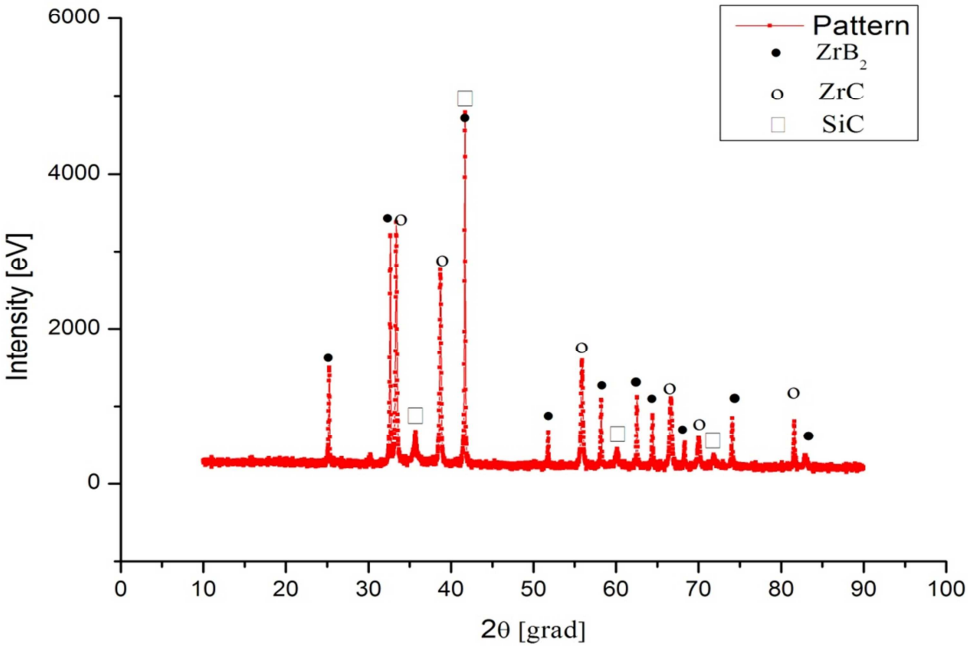

Figure 37 - 1-1 Composite Ceramic Powder's Pattern.

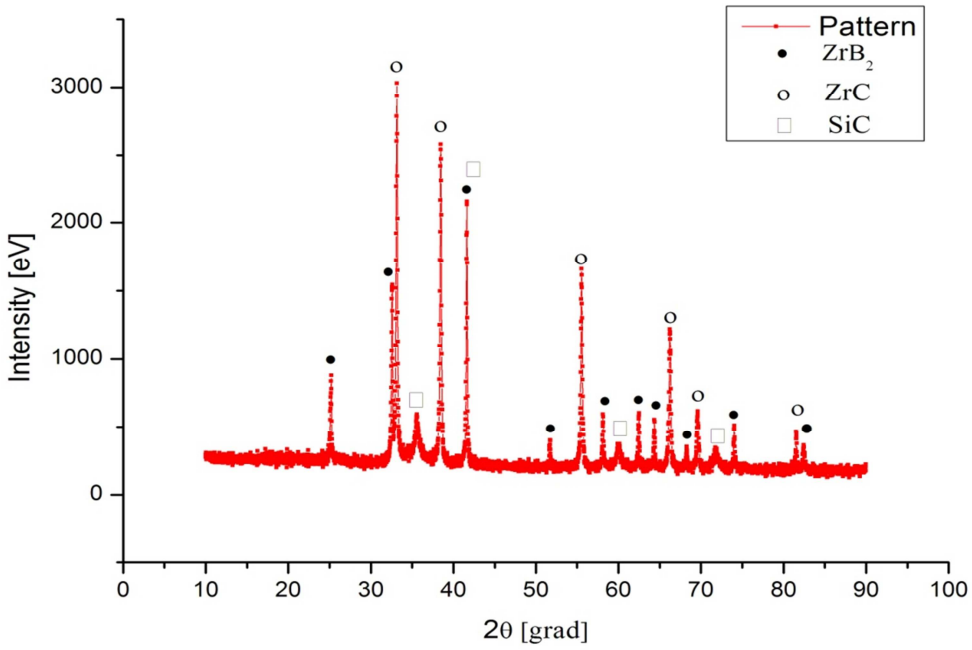

Figure 38 - 1-1fs Composite Ceramic Powder's pattern.

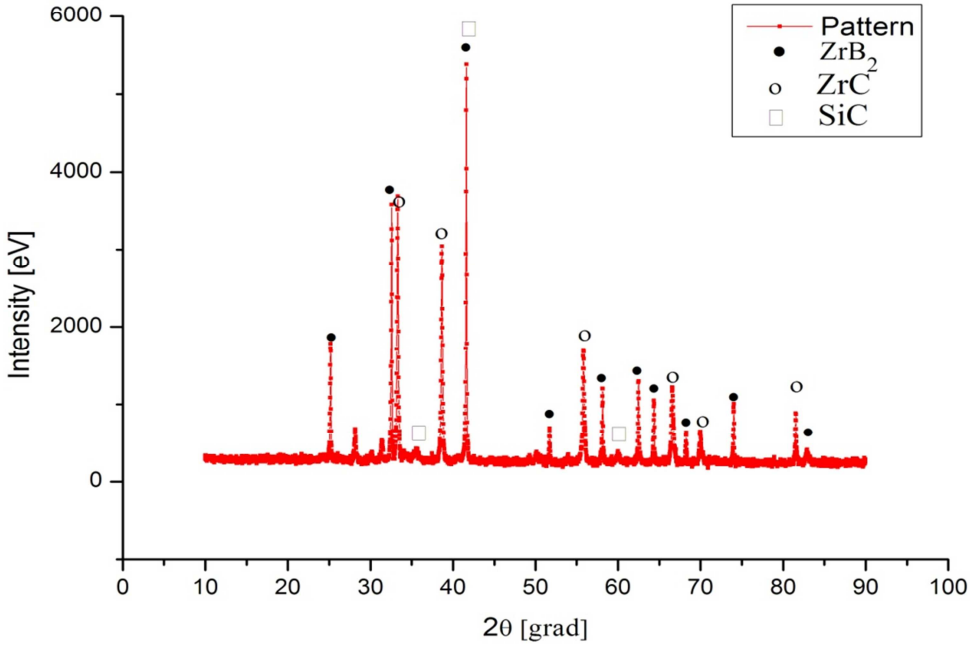

Figure 39 - 2-1 Composite Ceramic Powder's Pattern.

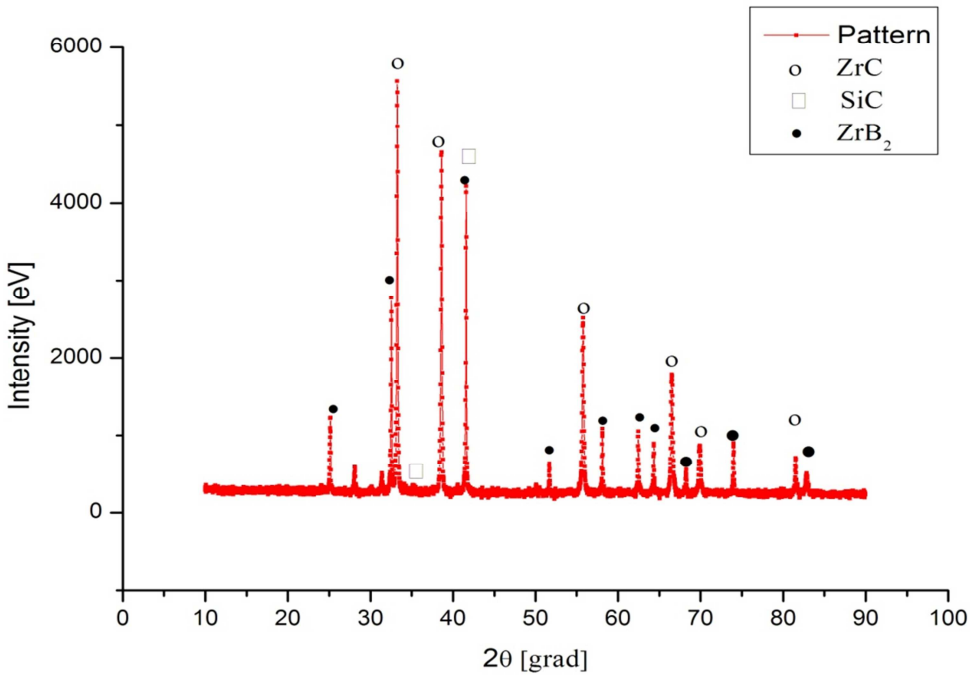

Figure 40 - 3-1 Composite Ceramic Powder's pattern.

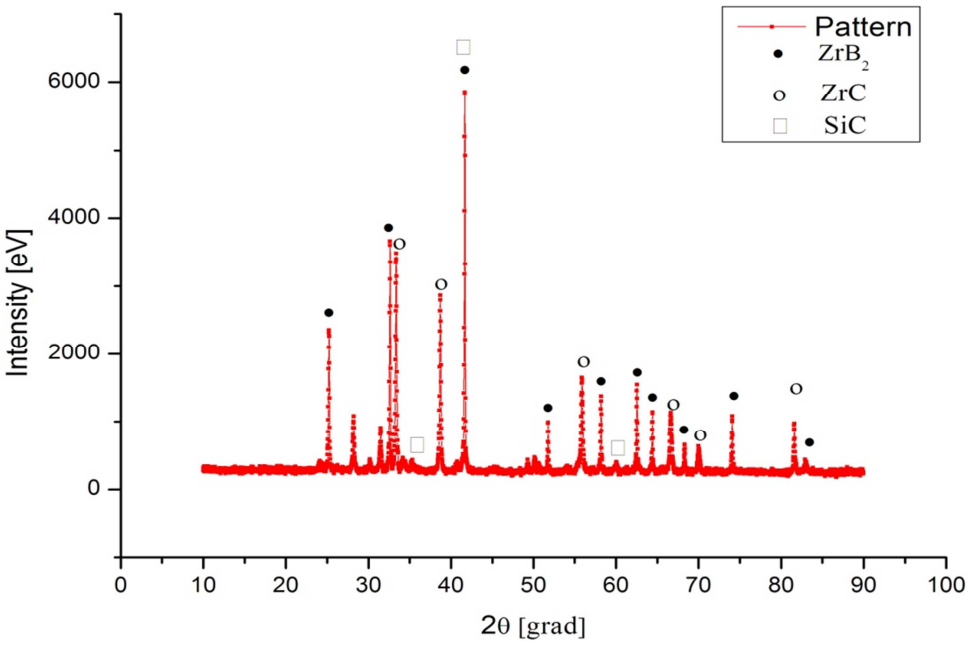

Figure 41 - 4-1 Composite Ceramic Powder's pattern.

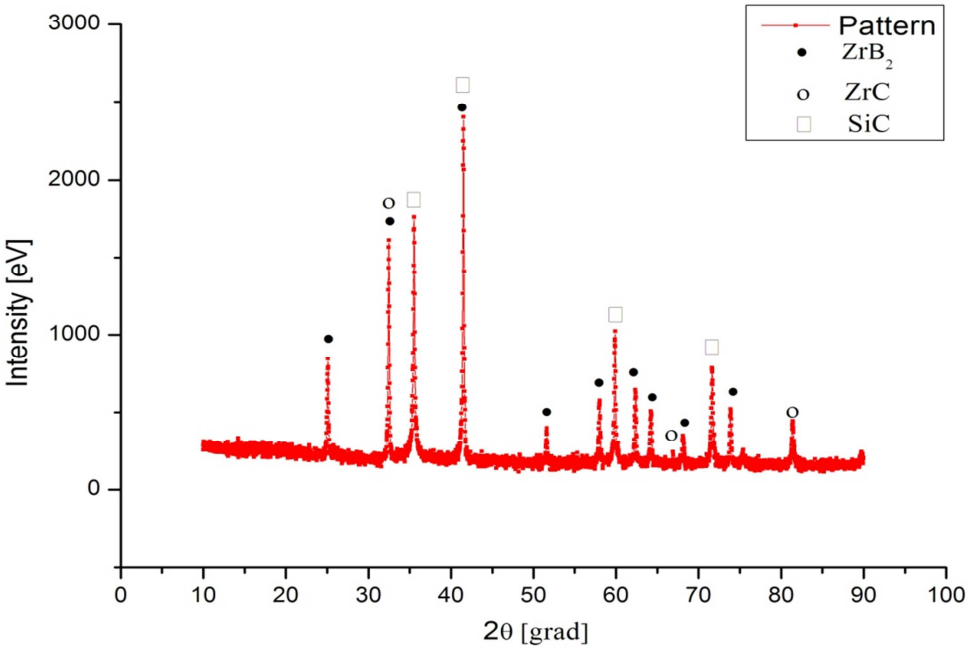

Figure 42 - 1-4 Composite Ceramic Powder's pattern.

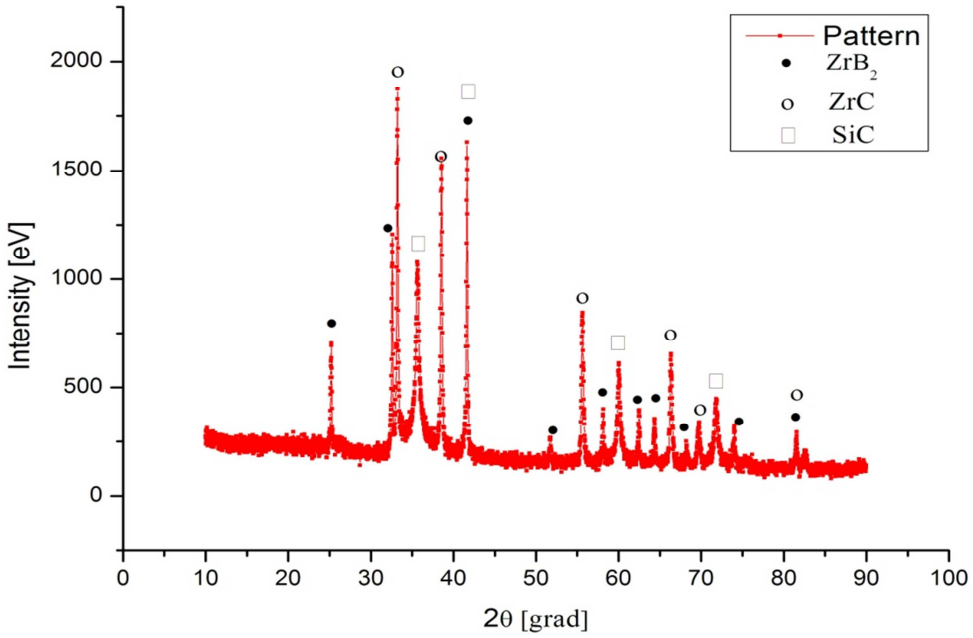

Figure 43 - 1_1 Composite Ceramic Powder's pattern.

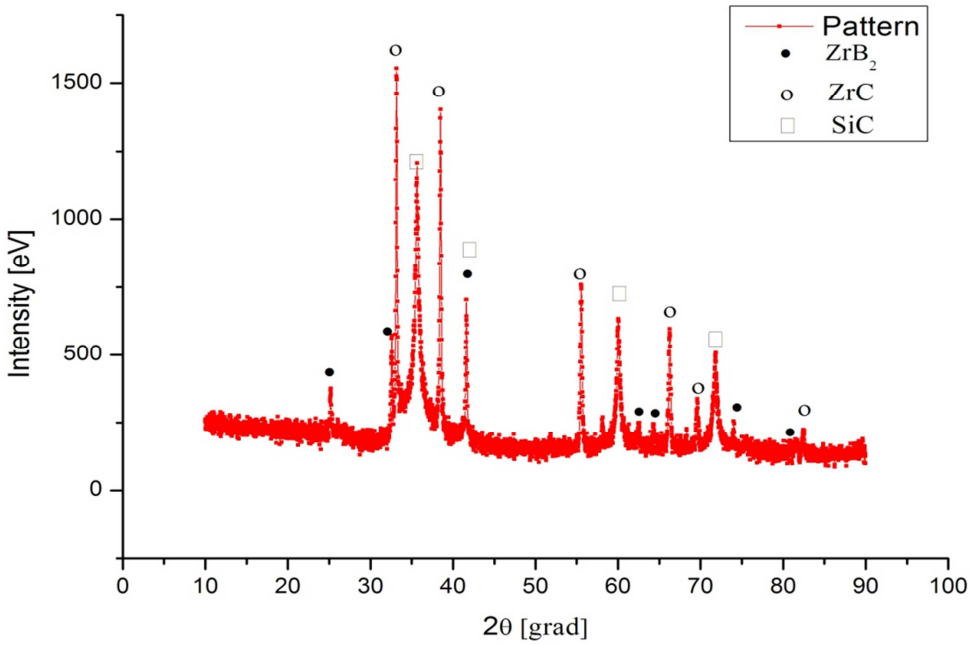

Figure 44 - 1_2 Composite Ceramic Powder's pattern.

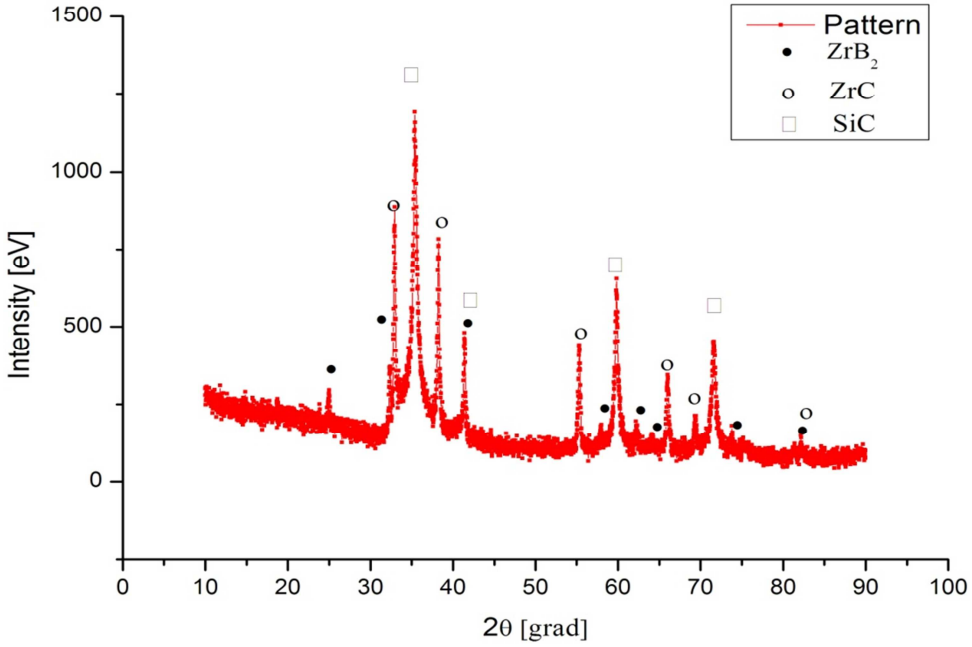

Figure 45 - 1_3 Composite Ceramic Powder's pattern.

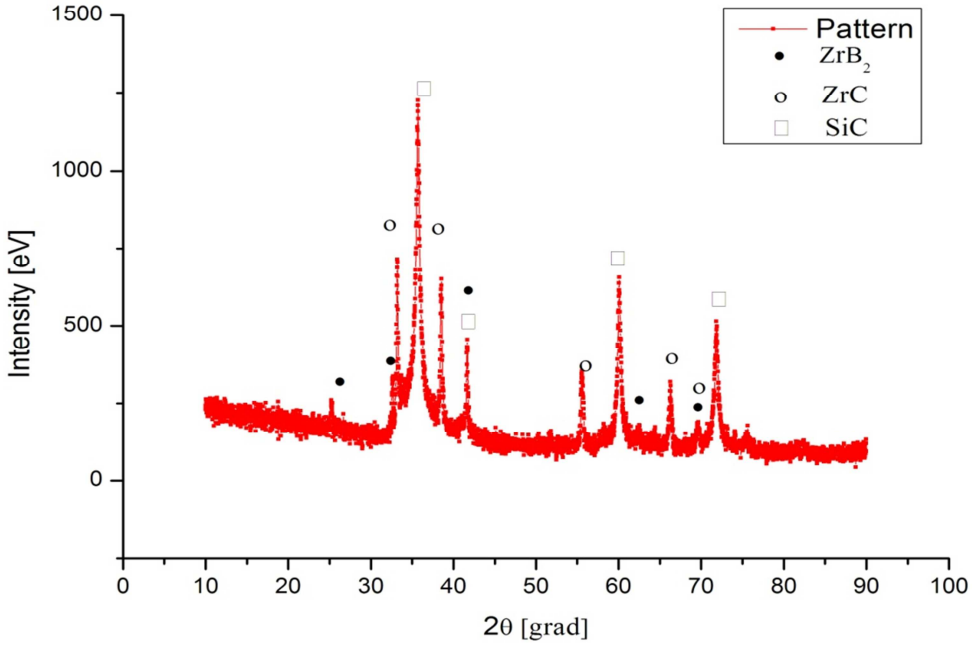

Figure 46 - 1_4 Composite Ceramic Powder's pattern.

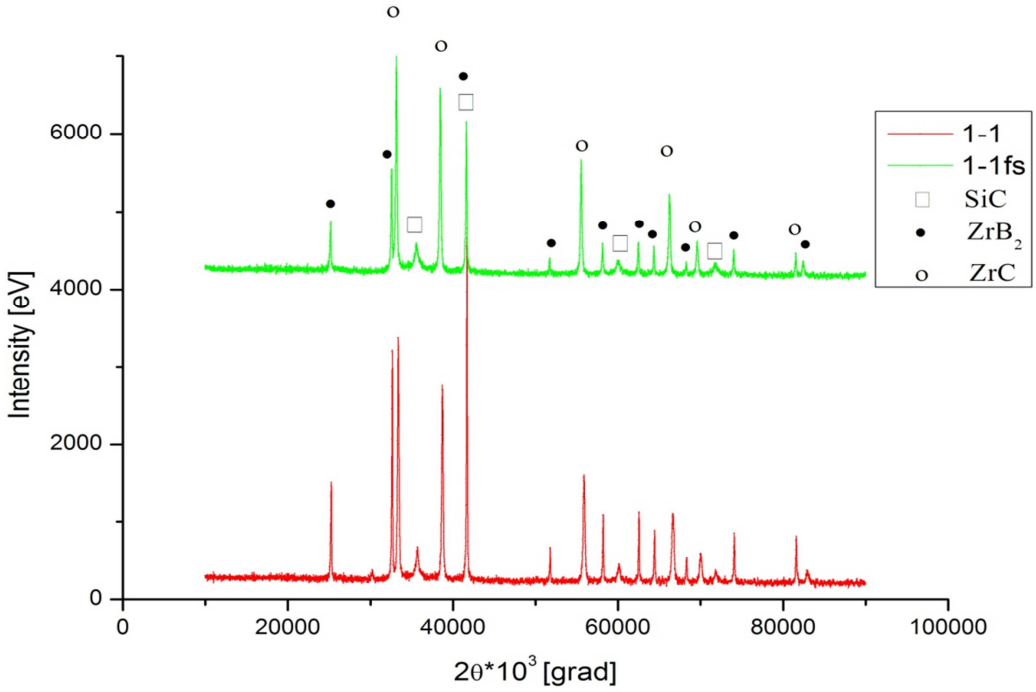

Figure 47 - 1-1 and 1-1fs patterns comparison.

Figure 47 shows the difference between powders with same composition (1-1), but one is obtained by pyrolysis of polymeric powder (1-1) and the other by polymeric solution(1-1fs).

About 1-1fs, zirconium carbide peaks are more intense than zirconium diboride ones; the opposite situation is described for 1-1. The solution, if compared to the powder, develops more ZrC phase than ZrB_2.

Scientific articles [35,36] describe that polymer derived silicon carbide crystallized in β-SiC (cubic); it has four fundamental peaks at 35°, 59° and 71°. It may be supposed that concentration remains constant because the peaks intensity doesn't change.

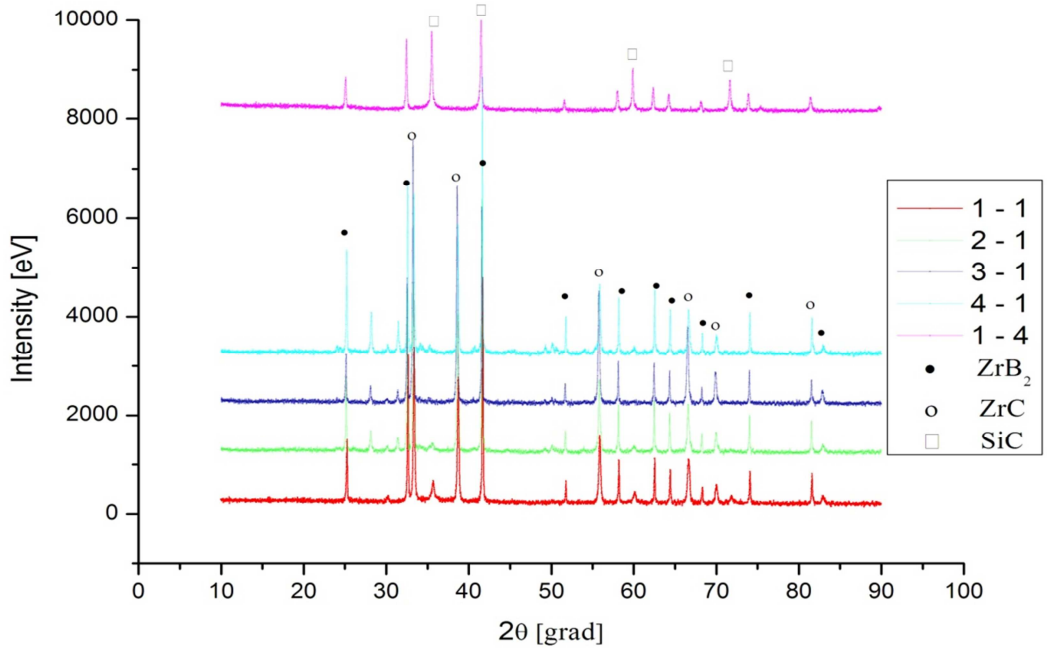

Figure 48 - Composite Ceramic Powder patterns comparison (Powder composition).

For Powder composition (Figure 48) it is possible to see that increasing zirconium diboride amount ZrB_2 and ZrC peaks intensity increases too. About 1-4 pattern shows that ZrB_2 and ZrC intensity signals are mostly reduced or they totally disappear.

To confirm this affirmation, in patterns illustrated in Figure 49 SiC peaks intensity increases from 1_1 to 1_4, while zirconium diboride and zirconium carbide signals go down.

From 1-1 to 4-1 powder patterns (Figure 48) there are some peaks between 27° and 32°; these are caused by zirconia [32]. The ZrO_2 presence is due to an oxygen excess, deriving from Zr-containing precursor and low carbon concentration level. The O_2 can be reduced by C by these reactions, during heat treatment:

$$ZrO_2(s) + B_2O_3(s) + C(s) \longrightarrow ZrB_2(s) + CO(g) \quad [15]\ \{5\}$$

$$ZrO_2(s) + 2C(s) \longrightarrow ZrC(s) + 2CO(g) \quad \{6\}$$

For Powder composition samples 2-1, 3-1 and 4-1 carbon concentration is not high enough to reduce zirconia.

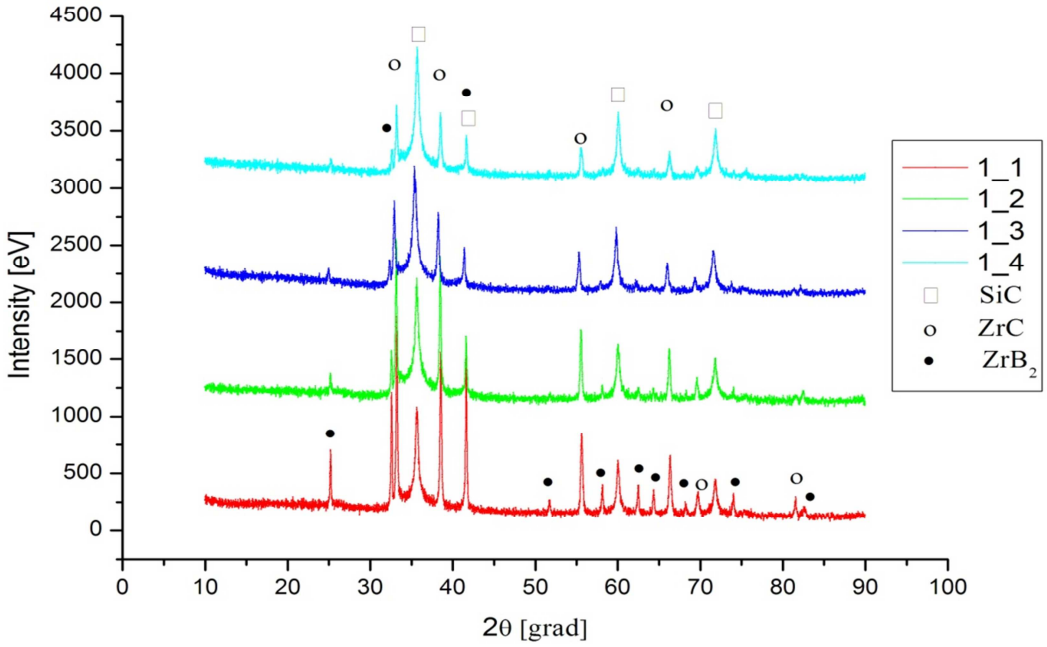

Figure 49 - Composite Ceramic Powder patterns comparison (Foam composition).

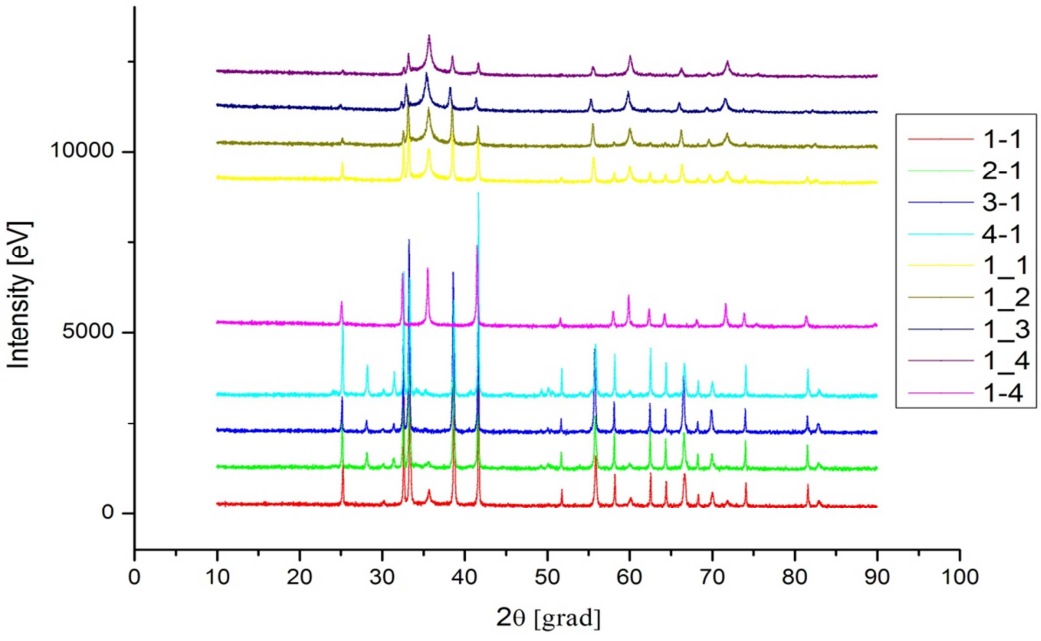

Figure 50 - All patterns.

The zirconium carbide concentration has been calculated by means of peaks area and the results are illustrated in Table 25; ZrB_2/ZrC means the weight fraction of zirconium diboride with respect to zirconium carbide.

Powder Sample	**ZrB_2/ZrC**	**Th ZrB_2 wt%**
1-1	0,421	65,4
2-1	0,447	79,1
3-1	0,313	85,0
4-1	0,477	88,3
1-4	0,540	32,1
1_1	0,385	28,0
1_2	0,165	16,3
1_3	0,286	11,5
1_4	0,309	8,9
ZrB_2	0,600	100,0

Table 25 - ZrB_2/ZrC weight fraction.

Graph in Figure 51 describes ZrB_2/ZrC trend versus Theoretical zirconium diboride weight fraction; it approximately follows a nonlinear curve (red line). There is a MAX peak around Th ZrB_2 wt% = ~ 50%; it means that for that composition there is a ZrB_2/ZrC/SiC composite ceramic with zirconium diboride concentration higher than zirconium carbide.

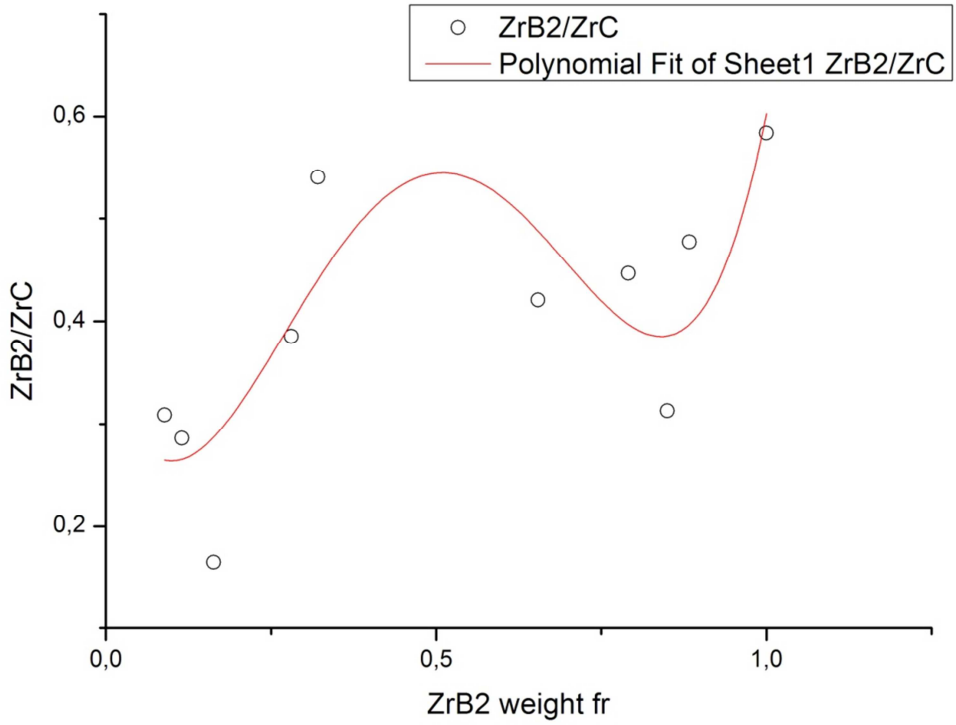

Figure 51 - ZrB_2/ZrC graph.

4.3 *XRF*.

From XRF analysis quantitative results (weight fraction, wt%) have been obtained. Because of instrument low sensibility, it hasn't been possible to measure weight concentration of elements with atomic weight lower than sodium (Na).

The only measured elements are zirconium (Zr) and silicium (Si); from results (Table 26) it's impossible to understand which phase composition of samples (ZrB_2, SiC, SiO_2, B_2O_3, ZrO_2, ZrC, etc.) is present.

Powder Sample	Zr wt%	Si wt%	Th Zr wt%	Th Si wt%	Δ Zr wt%	Δ Si wt%
1-1	59,4	40,6	65,4	34,6	6,0	-6,0
1-1fs	55,6	44,4	65,4	34,6	9,8	-9,8
2-1	83,3	16,7	79,1	20,9	-4,2	4,2
3-1	99,0	1,0	85,0	15,0	-14,0	14,0
4-1	96,7	3,3	88,3	11,7	-8,4	8,4
1-4	19,9	80,1	32,1	67,9	12,2	-12,2
1_1	13,1	86,9	28,0	72,0	14,9	-14,9
1_2	8,3	91,7	16,3	83,7	8,0	-8,0
1_3	7,3	92,7	11,5	88,5	4,2	-4,2
1_4	5,4	94,6	8,9	91,1	3,5	-3,5

Table 26 - XRF results.

In Table 26 results are showed: *Zr wt%* and *Si wt%* are weight fraction data that come from machine, *Th Zr wt%* and *Th Si wt%* are respective theoretical values, *Δ Zr wt%* and *Δ Si wt%* represent the difference between theoretical value and experimental one .

It can be noticed that modulus differences are included in a range between 3,5% and 14%. These errors could be attributed to instrumental imprecision and patchy phase separation.

Oxygen concentration hasn't been determinated because the experiment hasn't been performed in vacuum so the O_2 in the air and the adsorbed one may compromise the results.

4.4 *XPS*.

From XPS qualitative results have been obtained; they describe the phases that are present in Composite Ceramic Powder 1-1 by analysis of binding energy (B.E. [eV]).
XPS data have been analyzed and fitted by *XPS PEAK 41* and then plotted by *OriginPro 8.5*. In y-axis Raw [count/s] is the signal elaborated by the machinery, while in x-axis B.E. [eV] is the electrons binding energy.
In each graph three fundamental lines can be distinguished:

- *Raw*: black line with black squares, it represents the signal elaborated by the machinery;
- *Intensity*: red line with red circles, it represent the fitting line of the program;
- *Background*: blue line with blue triangles.

The others curves are the single signal of compound binding, which added together frame the red curve (Intensity).
In the ensuing figures and tables all the results about detected electrons binding energies are described.

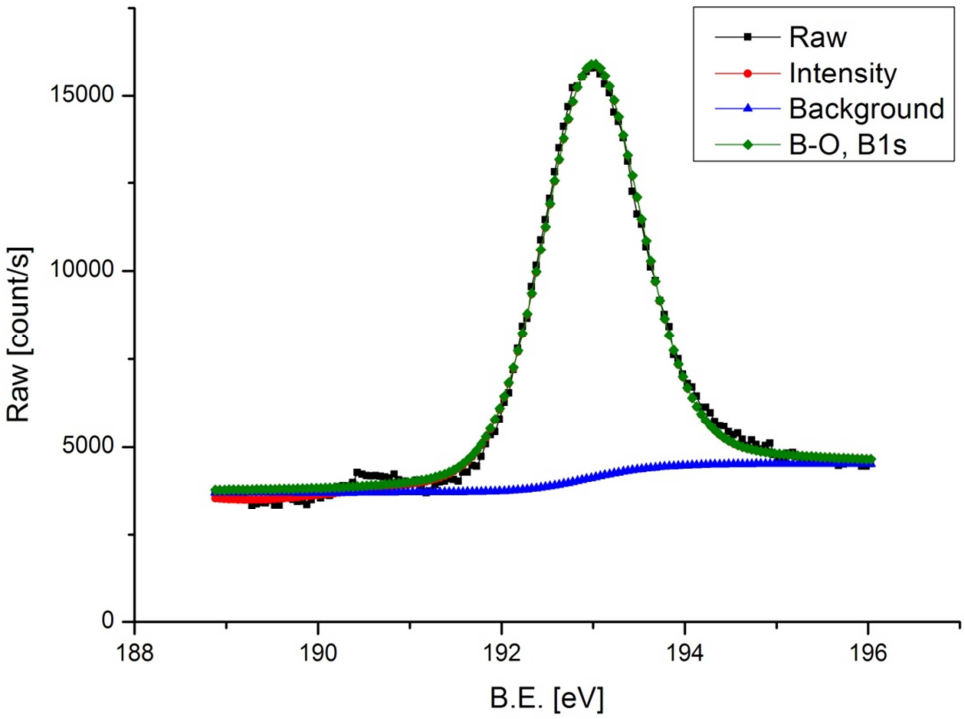

Figure 52 - B - 1s orbital.

In binding energy range represented in Figure 52, the graph peak represents B-O binding energy relative to B-1s orbital; this indicates the presence of boria (B_2O_3) in the powder.

Binding	Sp value [eV]
B - O	192,98

Table 27 – B - 1s, compounds binding energy.

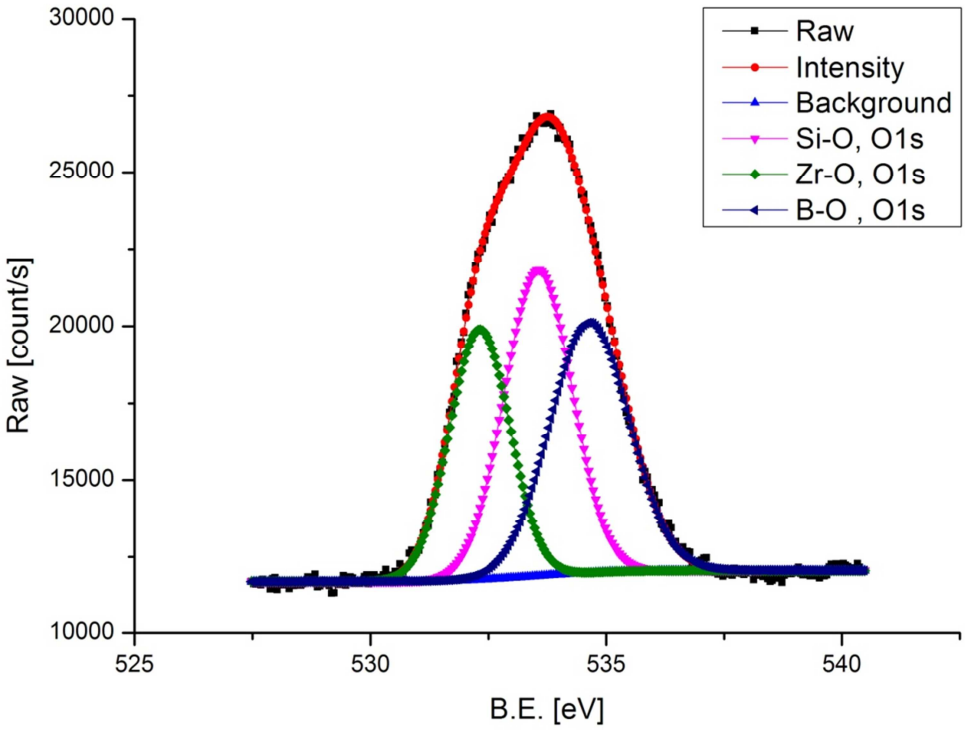

Figure 53 - O - 1s orbital.

In binding energy range represented in Figure 53, the graph peaks represent:

- Blue line, B-O binding energy, this confirms the presence of boria (B_2O_3);
- Green line, Zr-O binding energy, it indicates zirconia presence (ZrO);
- Pink line, Si-O binding energy, it means silica presence (SiO_2).

All these peaks are related to O - 1s orbital.

Binding	Sp value [eV]
Zr - O	532,33
Si - O	533,58
B - O	534,63

Table 28 - O - 1s orbital, compounds binding energy.

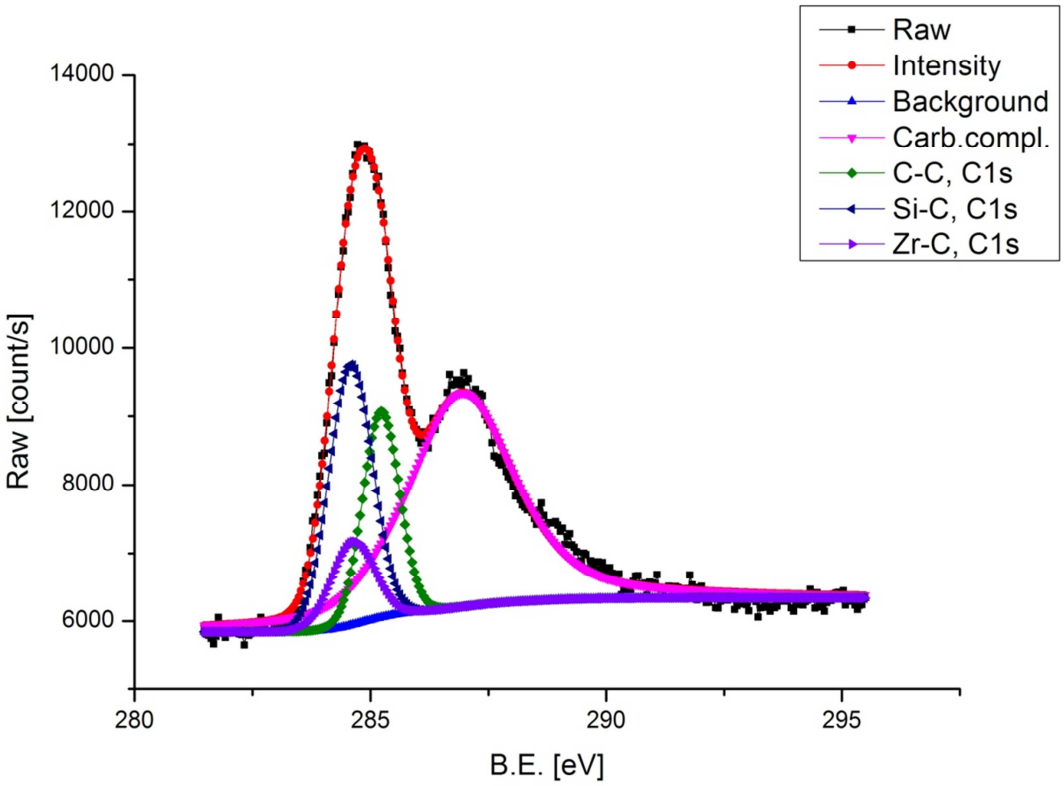

Figure 54 - C - 1s orbital.

In binding energy range represented in Figure 54, the graph peaks represent:

- Blue line, Si-C binding energy, this indicates the presence of (B_2O_3);
- Green line, C-C binding energy, it indicates presence of solid carbon;
- Purple line, Zr-C binding energy, it means zirconium carbide presence (ZrC);
- Pink line (carb.compl.), it indicates the presence of Si – C – O bond[32].

All these peaks are related to C - 1s orbital.

Binding	Sp value [eV]
Si – C	284,58
Zr – C	284,63
C – C	285,23
Carb.compl. (Si – C – O)	286,93

Table 29 - C - 1s orbital, compounds binding energy.

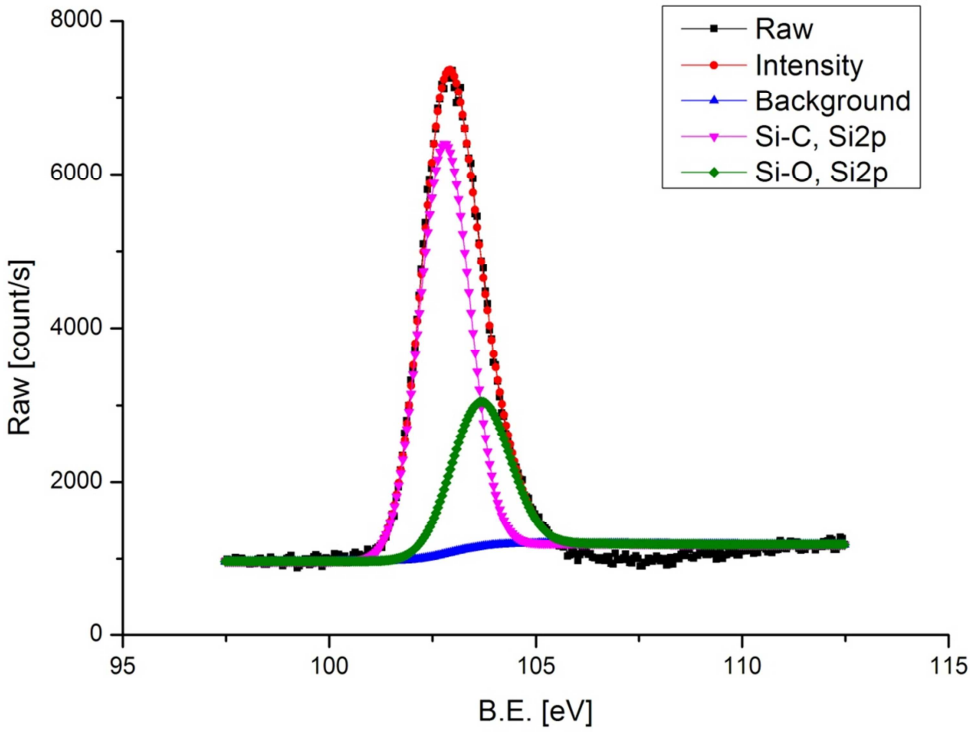

Figure 55 - Si - 2p orbital.

In binding energy range represented in Figure 55, the graph peaks represent:

- Green line, Si-O binding energy, it confirms silica presence (SiO_2);
- Pink line, Si-C binding energy, it indicates the presence of silicon carbide or a complex Si – C – O.

The two peaks are related to Si – 2p orbital.

Binding	Sp value [eV]
Si – C	102,78
Si – O	103,68

Table 30 - Si - 2p orbital, compounds binding energy.

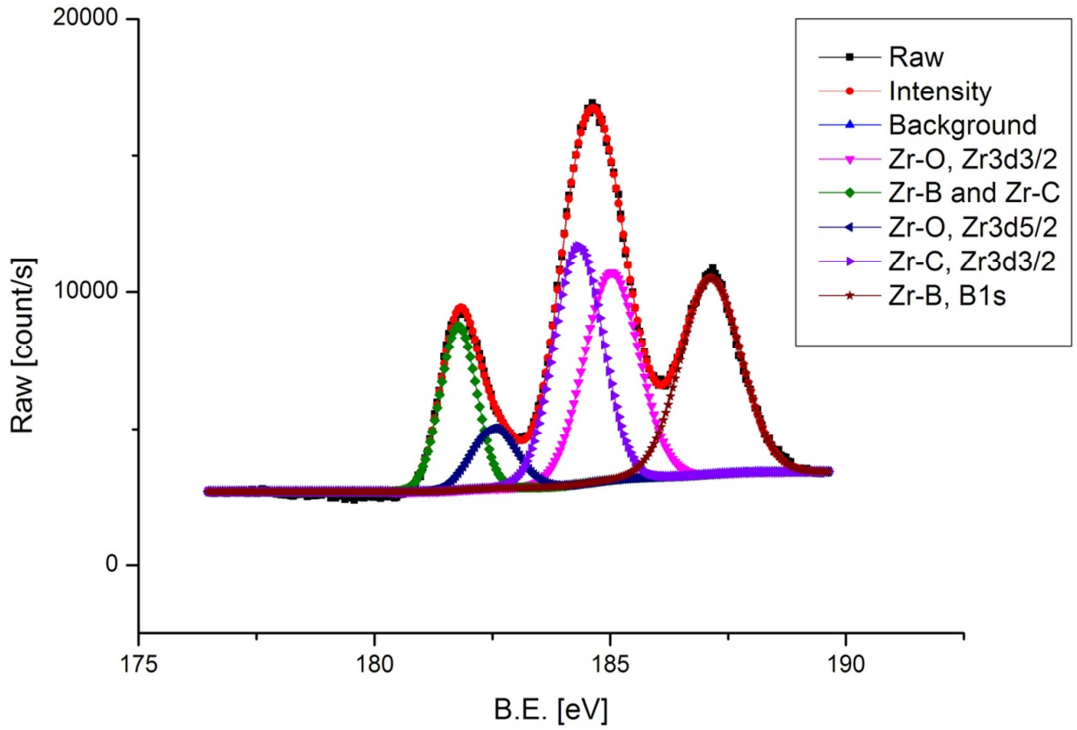

Figure 56 - Zr - 3d and B - 1s orbitals.

In binding energy range represented in Figure 55, the graph peaks represent:

- Blue line, Zr-O binding energy of $Zr3d_{5/2}$ orbital, this confirm the presence of zirconia (ZrO);
- Green line, it is an overlap of other 2 single signals: Zr-B binding energy (181,80 eV), about ZrB_2 presence; Zr-C binding energy (181,60 eV), that confirms ZrC existence;
- Purple line, Zr-C binding energy, it means zirconium carbide presence (ZrC);
- Pink line, Zr-O binding energy of $Zr3d_{3/2}$ orbital;
- Vermillion line, Zr-B binding energy of B1s orbital, that confirms the zirconium diboride presence.

Most of the peaks are related to Zr3d orbitals (3/2 and 5/2), one of them is about B1s orbital.

Binding	**Sp value [eV]**
Zr – B and Zr – C	181,80 ($Zr3d_{3/2}$)
Zr – B and **Zr – C**	181,60 ($Zr3d_{5/2}$)
Zr – O, $Zr3d_{5/2}$	182,58
Zr – C, $Zr3d_{3/2}$	184,33
Zr – O, $Zr3d_{3/2}$	185,03
Zr – B, B1s	187,13

Table 31 - Zr - 3d and B – 1s orbitals, compounds binding energy.

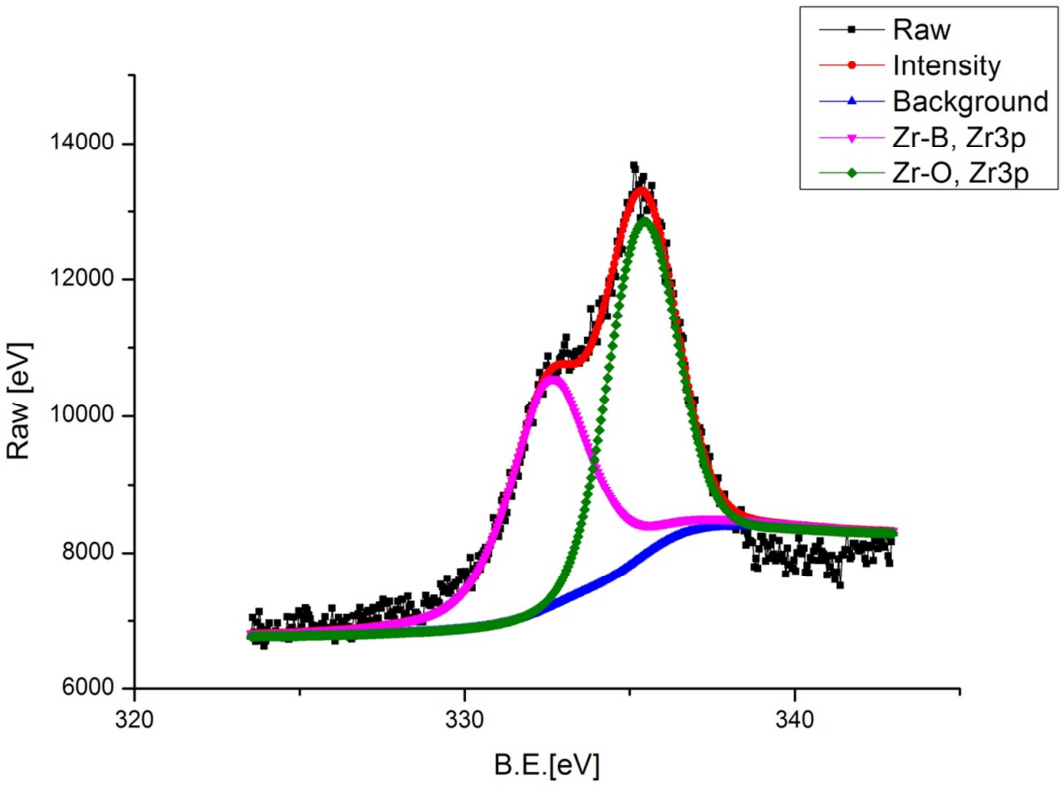

Figure 57 - Zr - 3p orbital.

In binding energy range represented in Figure 57, the graph peaks represent:

- Green line, Zr-O binding energy, it confirms zirconia presence (ZrO);
- Pink line, Zr-B binding energy, it highlights the presence of zirconium diboride (ZrB_2).

The two peaks are related to Zr3p orbital.

Binding	Sp value [eV]
Zr – B	332,63
Zr – O	335,33

Table 32 - Zr - 3p orbital, compounds binding energy.

Energy values reported in the tables have been assigned to the respective binding compound by comparison to values that have been found in internet database and scientific articles[32,33].

4.5 *SEM and EDS*.

Energy Dispersive Spectroscopy.

Just two samples with different composition have been chosen: 1-1 and 1-4 Composite Ceramic Powders .

EDS helps to understand which phases are represented in the pictures:

- light one is Zr-based phase;
- dark one is Si-based phase.

Because of low sensibility of instrument it has been possible to determine only the presence of elements with molecular weight higher than sodium (Na). Because of this reason, in the graphs (Figure 58,Figure 59) only silicon and zirconium peaks must be considered and it's not possible to understand the phase detected.

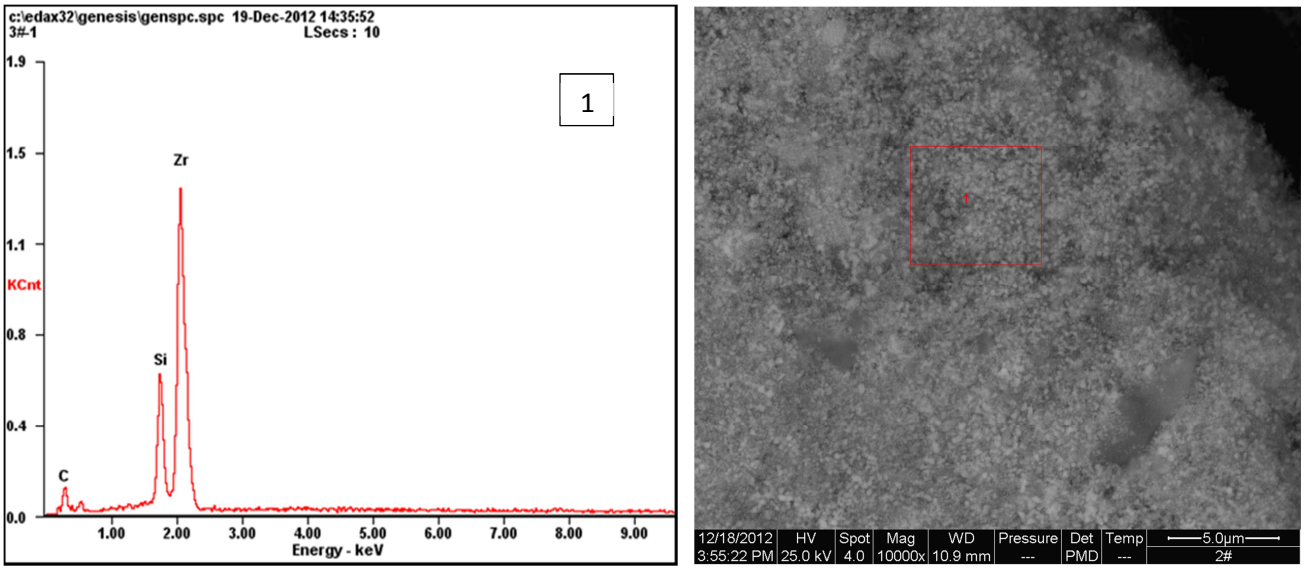

Figure 58 - EDS graph (left); SEM picture of 1-1 Composite Ceramic Powder, with Powder composition.

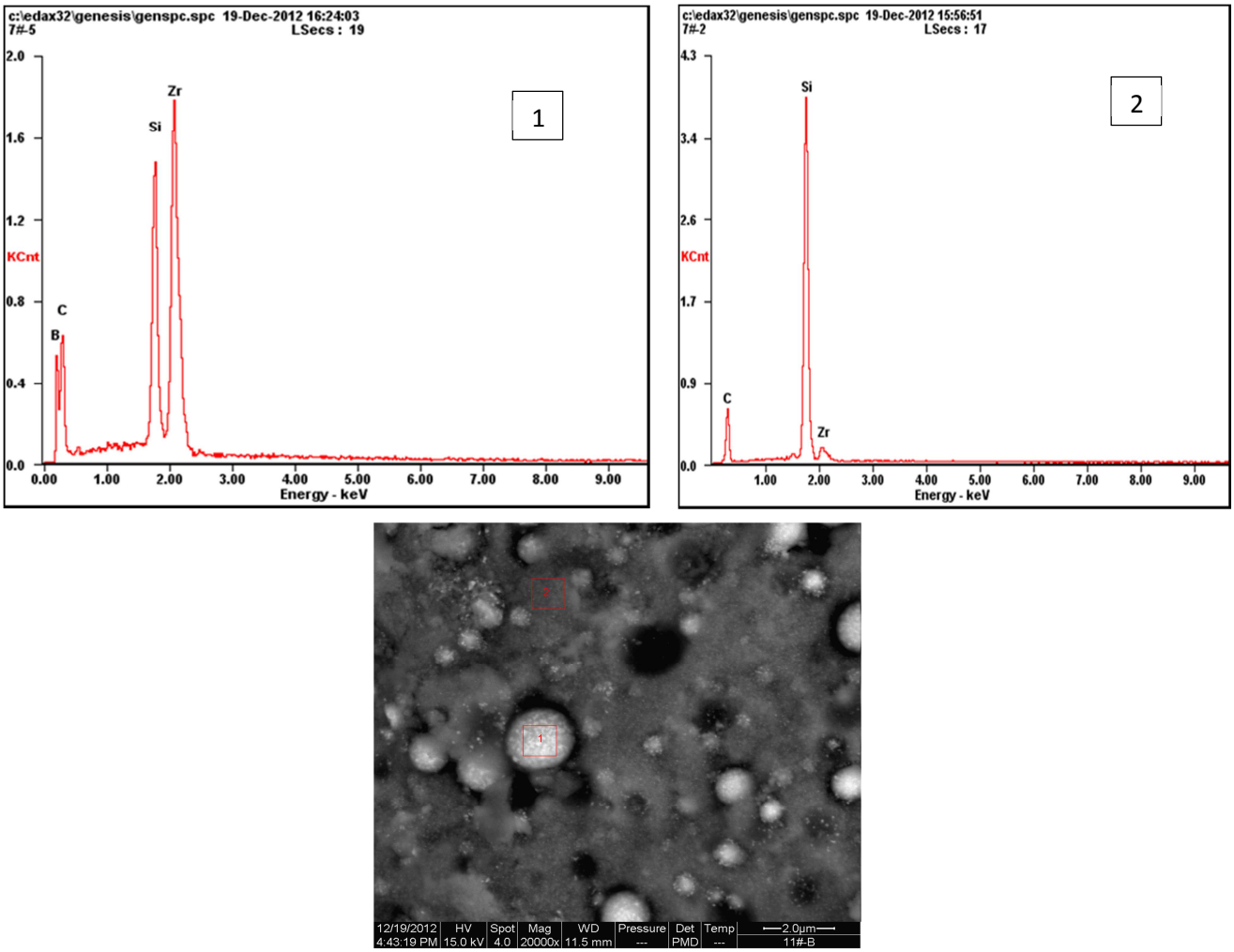

Figure 59 - EDS graphs (top); SEM picture of 1-4 Composite Ceramic Powder, with Powder composition.

Scanning Electron Microscope.

The follows SEM pictures are divided in:

- left column: *Secondary electrons* images;
- right column: *Backscattered electrons* images.

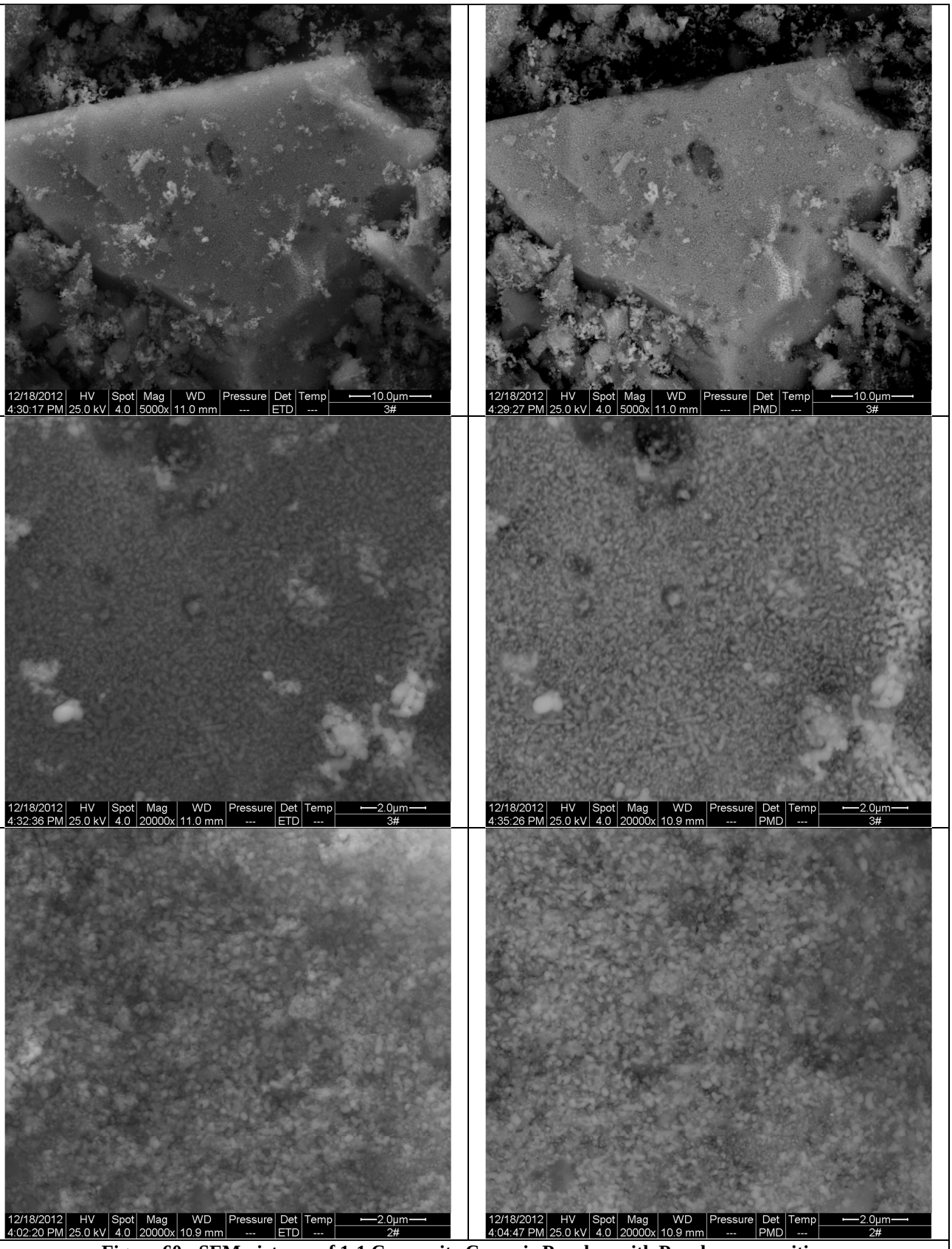

Figure 60 - SEM pictures of 1-1 Composite Ceramic Powder, with Powder composition.

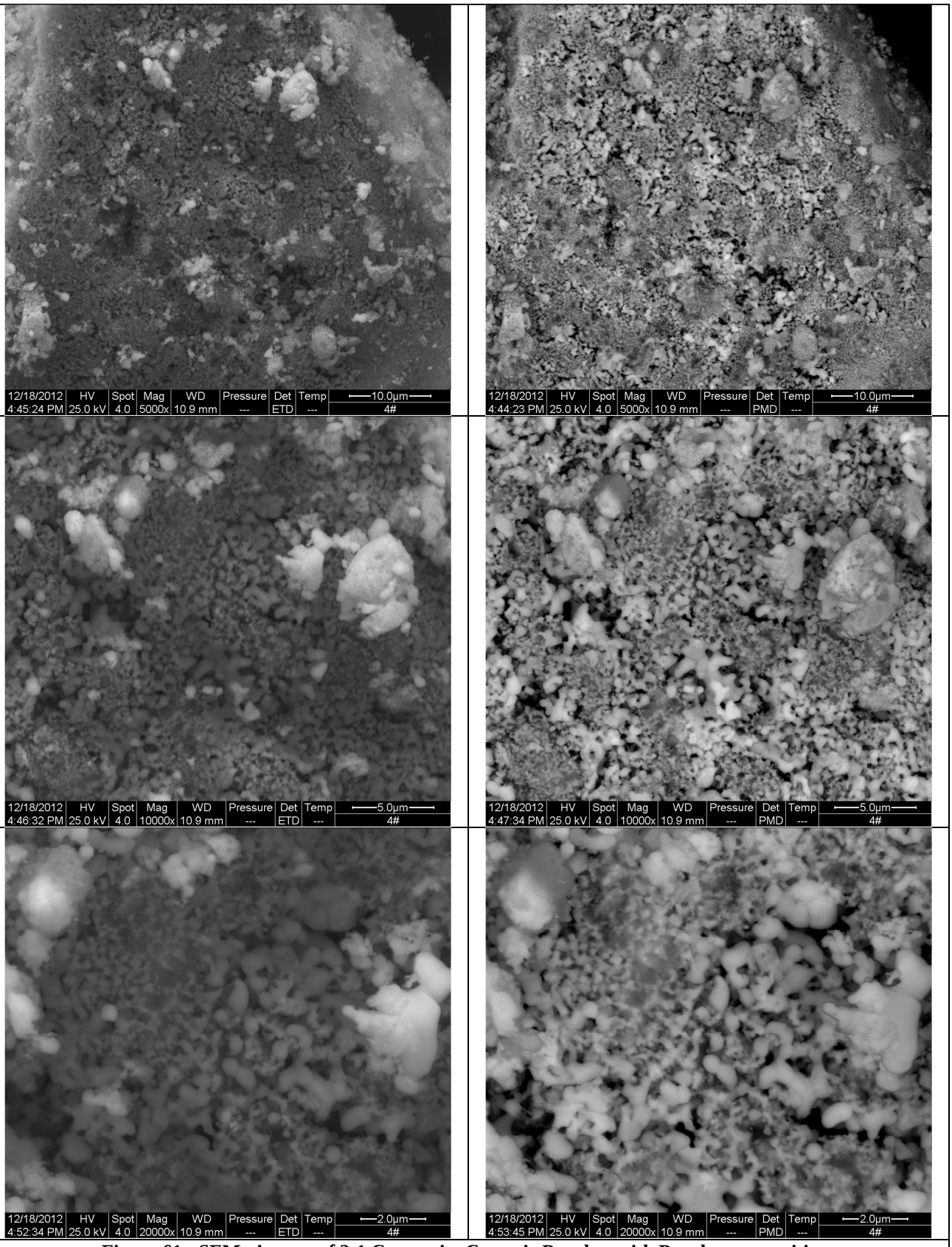

Figure 61 - SEM pictures of 2-1 Composite Ceramic Powder, with Powder composition.

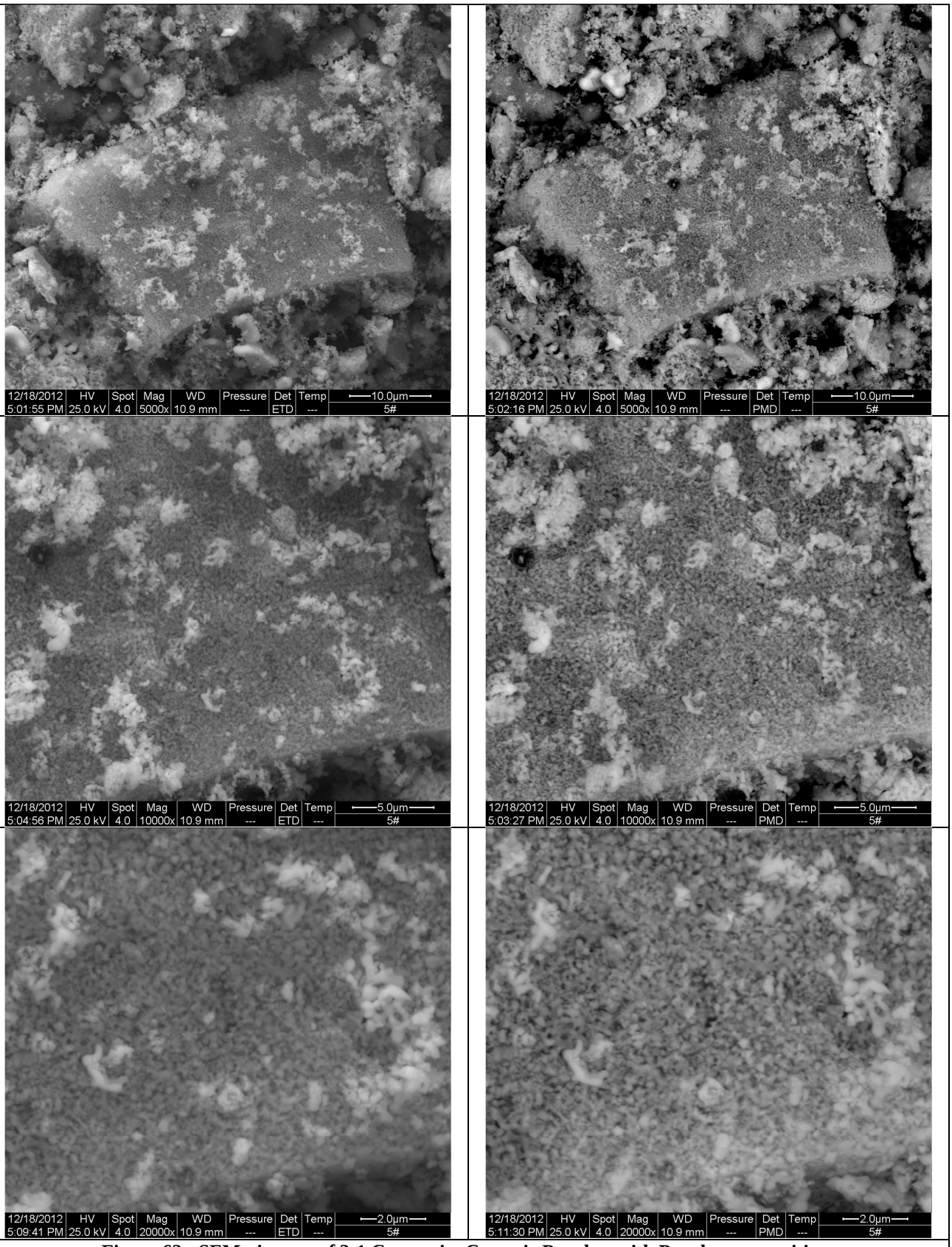

Figure 62 - SEM pictures of 3-1 Composite Ceramic Powder, with Powder composition.

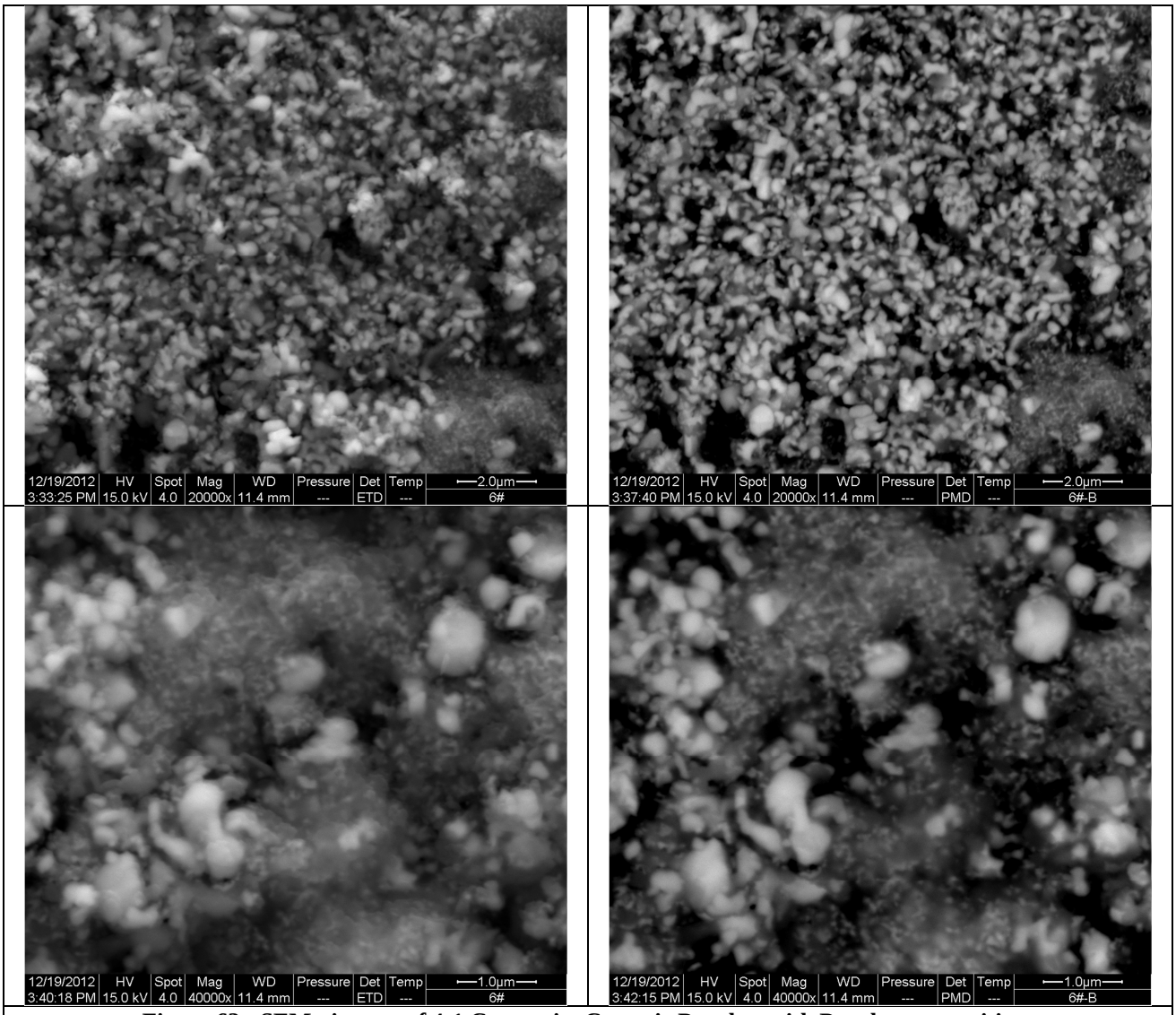

Figure 63 - SEM pictures of 4-1 Composite Ceramic Powder, with Powder composition.

Figure 60, Figure 61, Figure 62 and Figure 63 illustrate the first four compositions of Composite Ceramic Powder, with Powder composition. It's possible to see that the white phase (Zr-containing) is homogeneously and finely dispersed with nano dimensions (< 1 μm). Phase dimension increases from 1-1 to 4-1 together with ZrB_2 increasing amount.

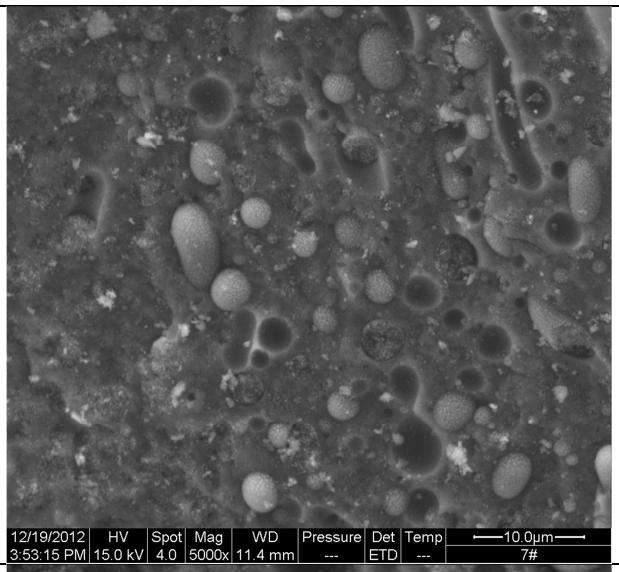
12/19/2012 | HV | Spot | Mag | WD | Pressure | Det | Temp | 10.0µm
3:53:15 PM | 15.0 kV | 4.0 | 5000x | 11.4 mm | --- | ETD | --- | 7#

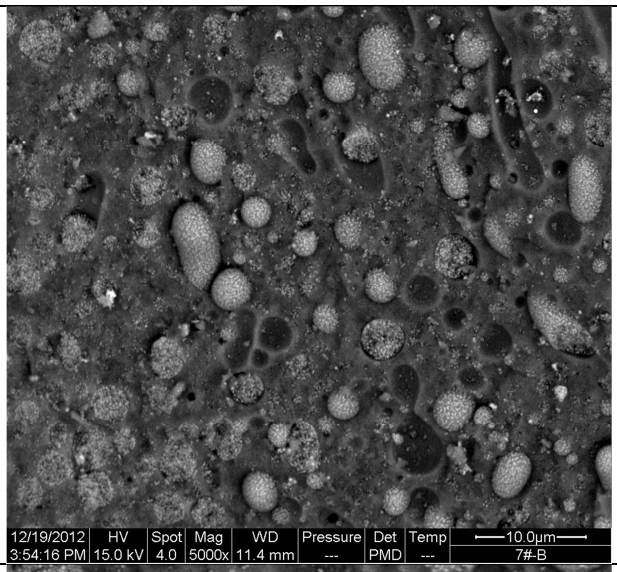
12/19/2012 | HV | Spot | Mag | WD | Pressure | Det | Temp | 10.0µm
3:54:16 PM | 15.0 kV | 4.0 | 5000x | 11.4 mm | --- | PMD | --- | 7#-B

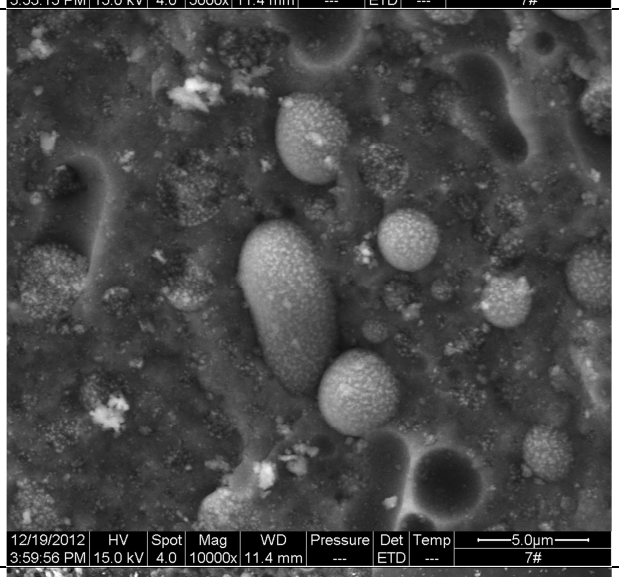
12/19/2012 | HV | Spot | Mag | WD | Pressure | Det | Temp | 5.0µm
3:59:56 PM | 15.0 kV | 4.0 | 10000x | 11.4 mm | --- | ETD | --- | 7#

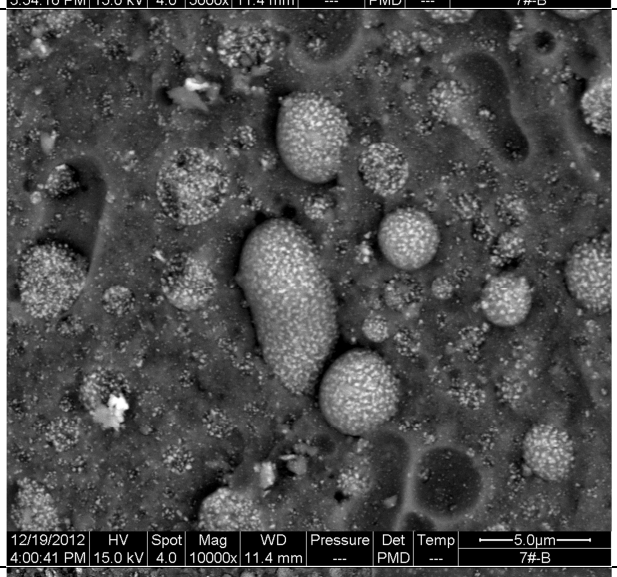
12/19/2012 | HV | Spot | Mag | WD | Pressure | Det | Temp | 5.0µm
4:00:41 PM | 15.0 kV | 4.0 | 10000x | 11.4 mm | --- | PMD | --- | 7#-B

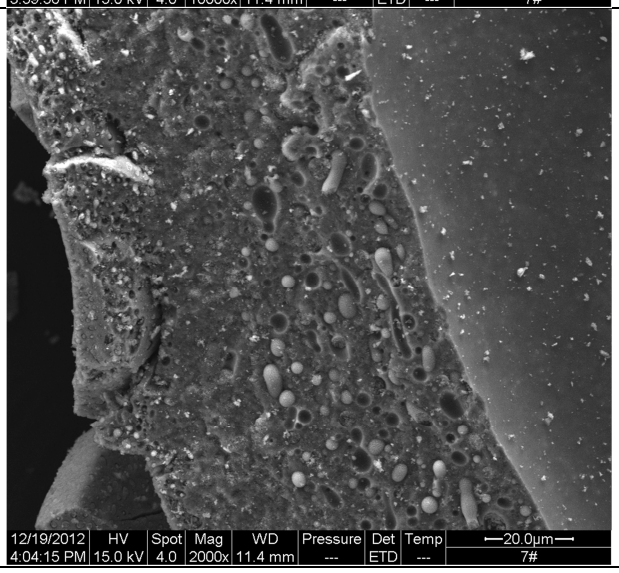
12/19/2012 | HV | Spot | Mag | WD | Pressure | Det | Temp | 20.0µm
4:04:15 PM | 15.0 kV | 4.0 | 2000x | 11.4 mm | --- | ETD | --- | 7#

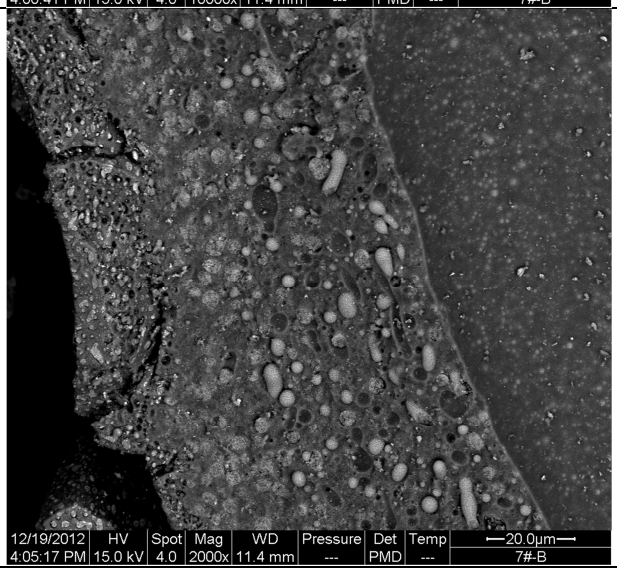
12/19/2012 | HV | Spot | Mag | WD | Pressure | Det | Temp | 20.0µm
4:05:17 PM | 15.0 kV | 4.0 | 2000x | 11.4 mm | --- | PMD | --- | 7#-B

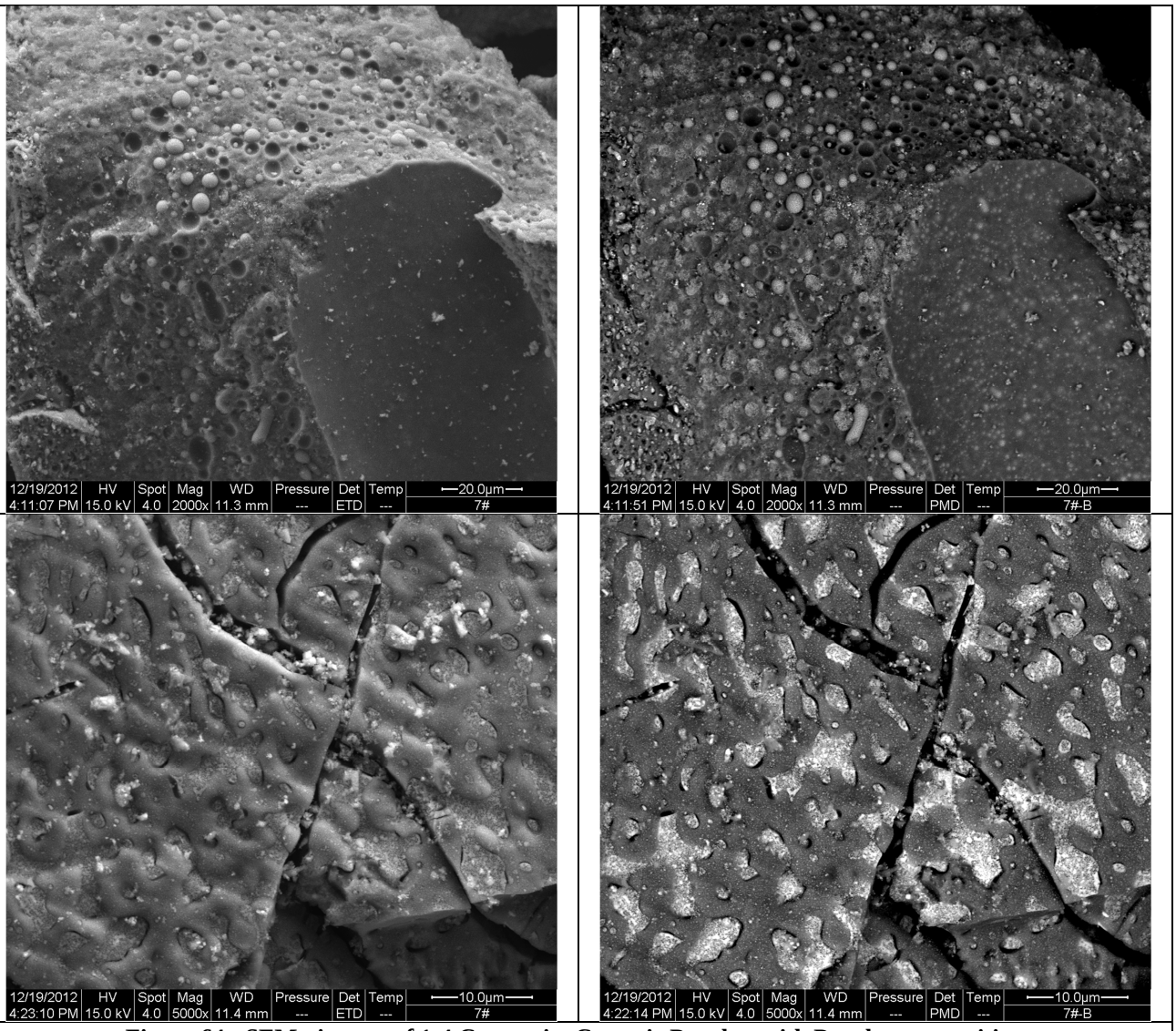

Figure 64 - SEM pictures of 1-4 Composite Ceramic Powder, with Powder composition.

In Figure 64 there are 1-4 Ceramic Composite Powder SEM pictures. Phase separation is totally different from previous samples. A matrix (dark phase, Si-rich) and a second dispersed compound (light phase, Zr-rich) with micrometer size can be recognized.

The white phase is also dispersed in Si-matrix with many nanometers size. Principally phases are spheroidal; there are also irregular shapes but always with rounded edges. A curved shape is due to separations phase happened while polymers were melted.

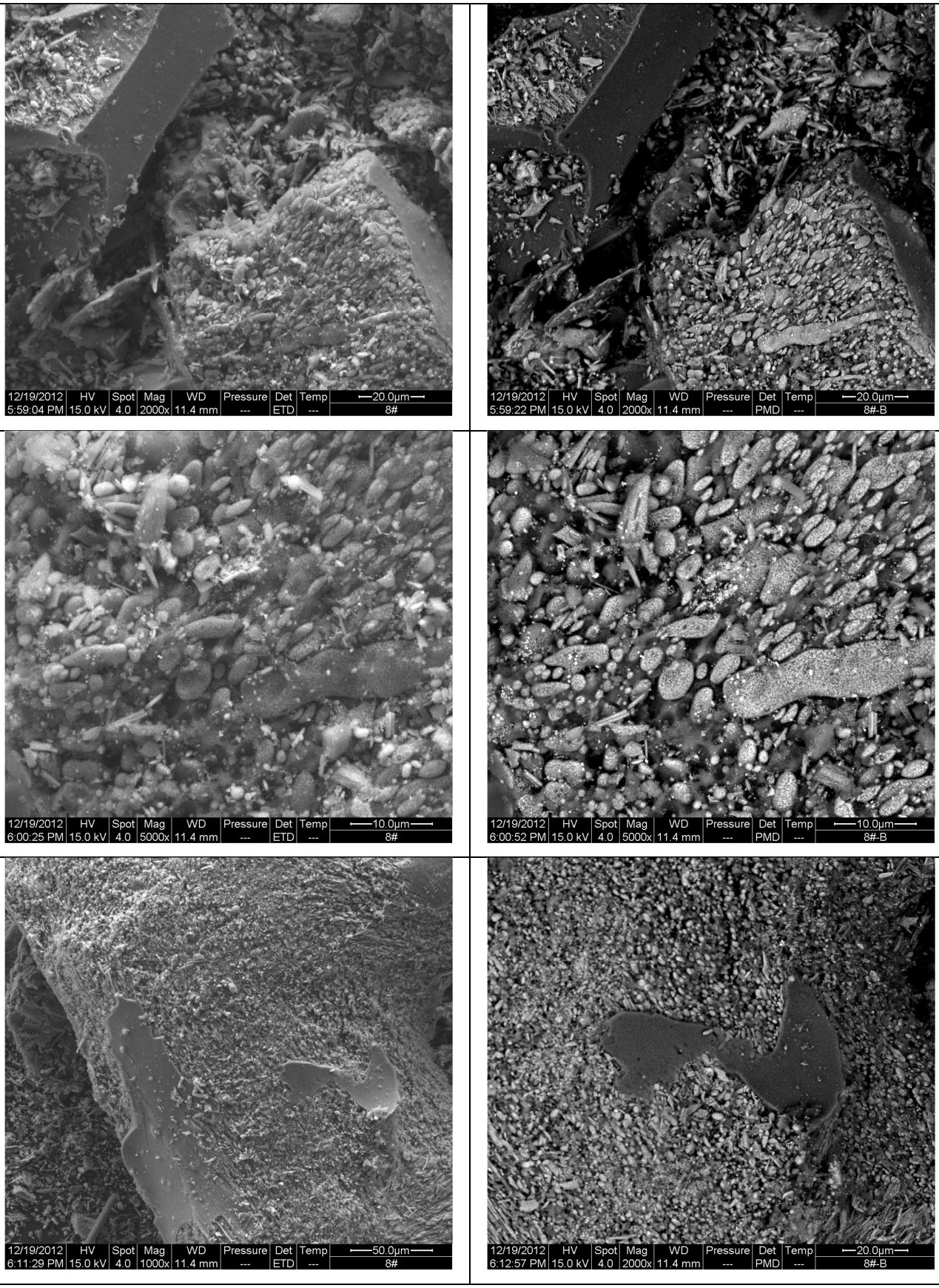

Figure 65 - SEM pictures of 1_1 Composite Ceramic Powder, with Foam composition.

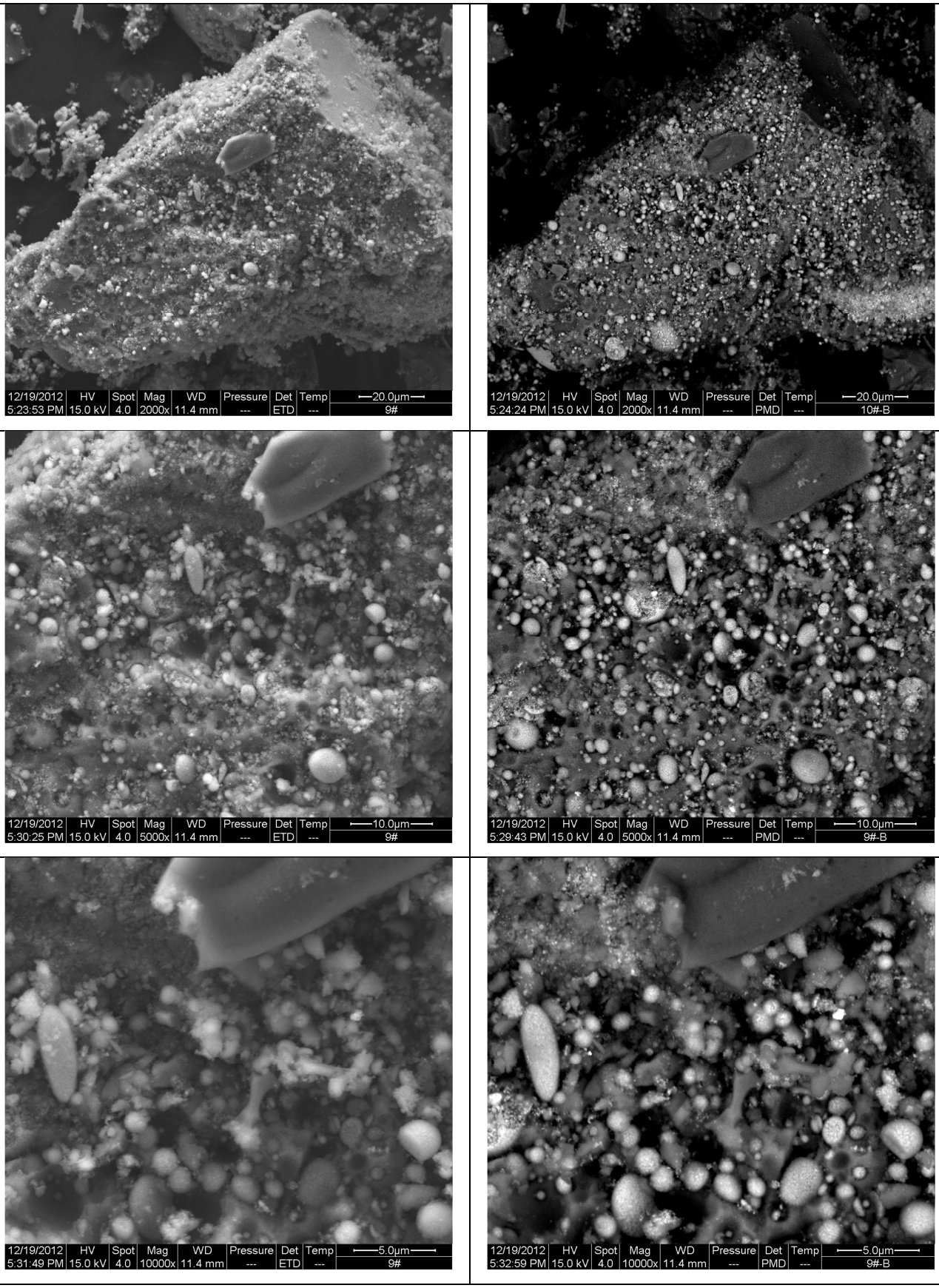

Figure 66 - SEM pictures of 1_2 Composite Ceramic Powder, with Foam composition.

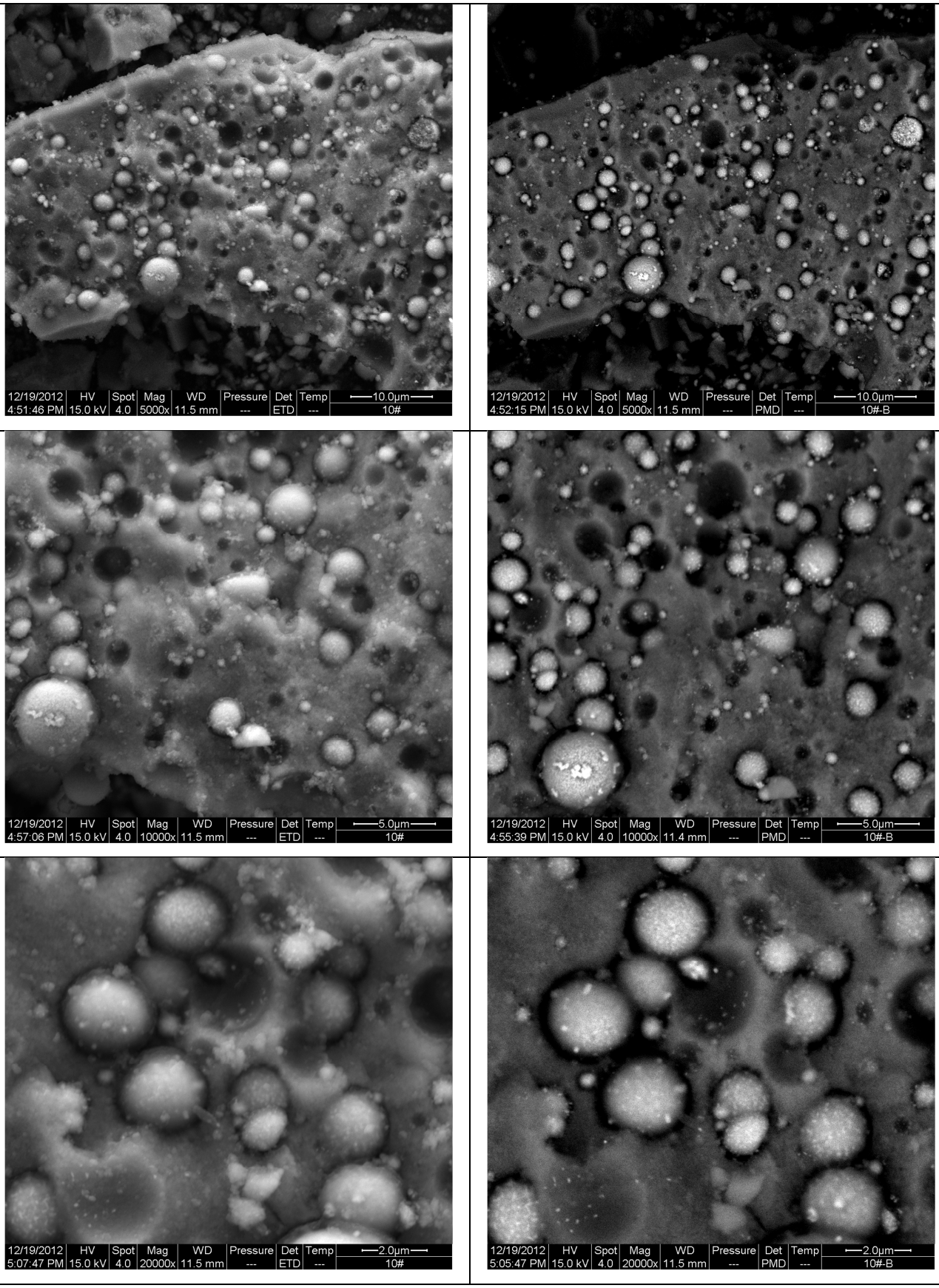

Figure 67 - SEM pictures of 1_3 Composite Ceramic Powder, with Foam composition.

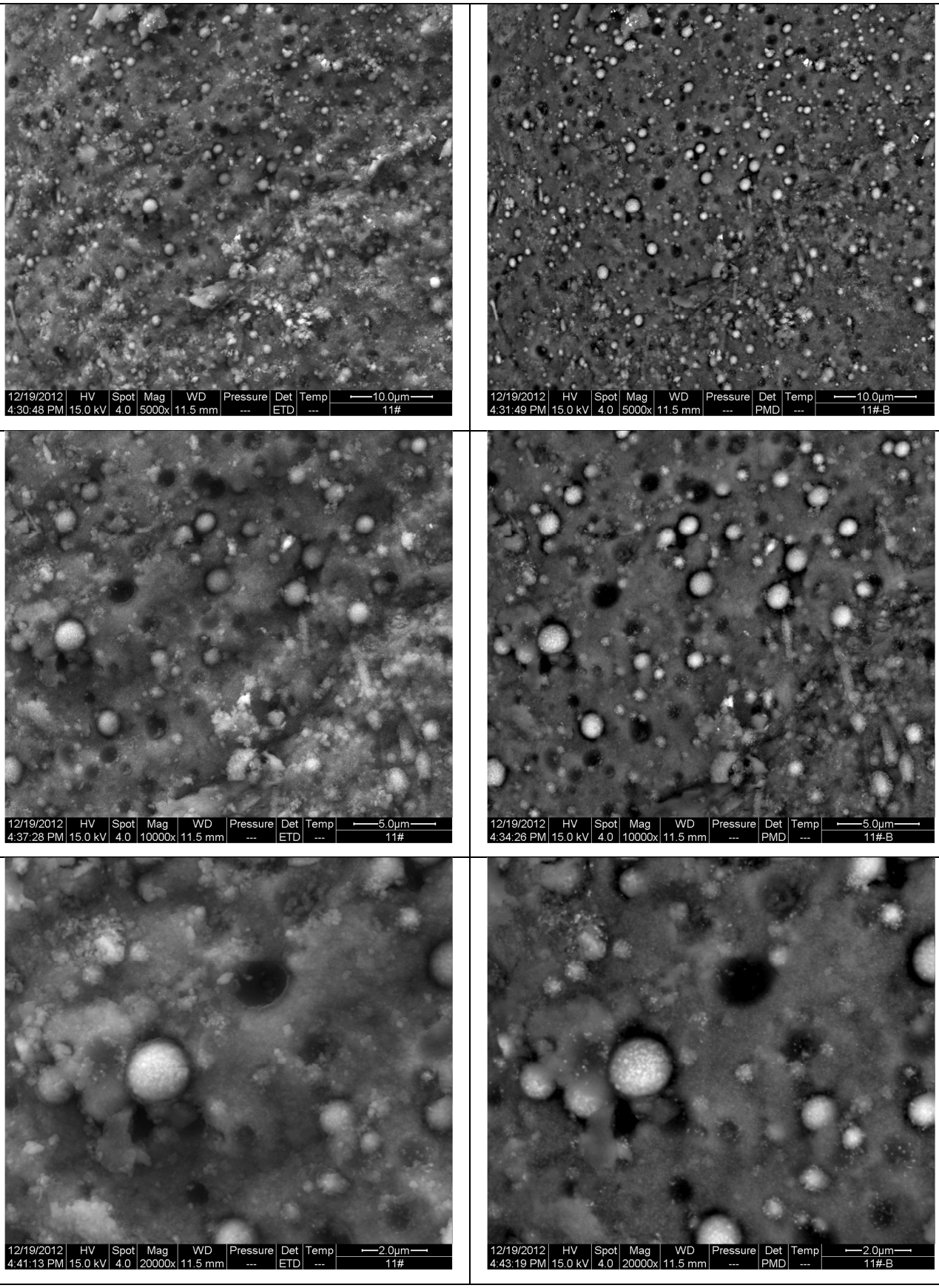

Figure 68 - SEM pictures of 1_4 Composite Ceramic Powder, with Foam composition.

From Figure 65 to Figure 68 1_1, 1_2, 1_3 and 1_4 Composite Ceramic Powders, with Foam composition, are illustrated. Separation phase is always present; increasing Si-amount, Zr-containing phases assume a regular spheroidal shape.

Obviously, decreasing Zr amount, the white phase becomes smaller from 1_1 to 1_4.

In Figure 69 phase separation changing versus composition (Th Zr wt%) is illustrated. Increasing zirconium diboride amount, it becomes more homogeneous and finely dispersed.

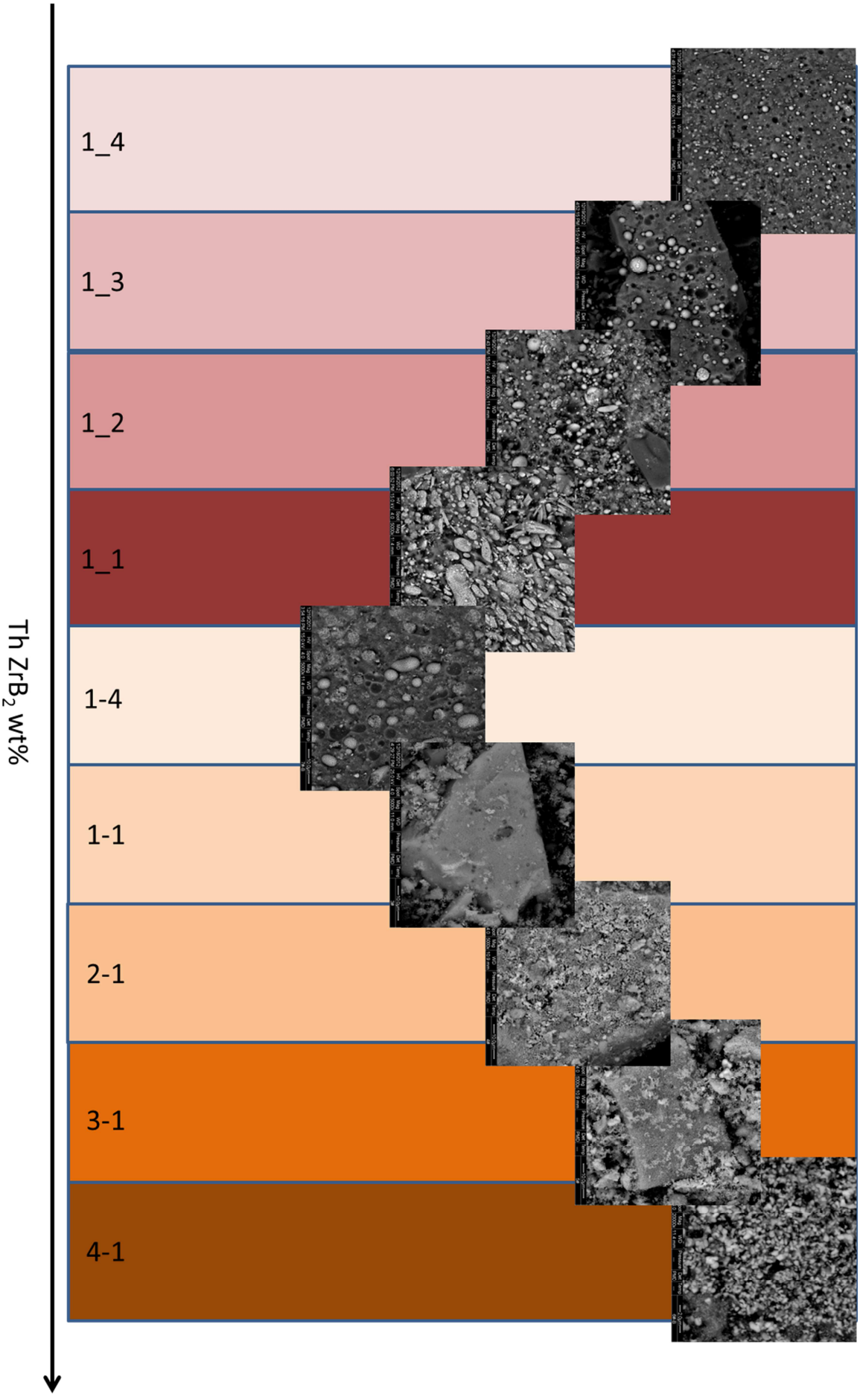

Figure 69 - Graph that shows different phase separation shape versus different powder composition.

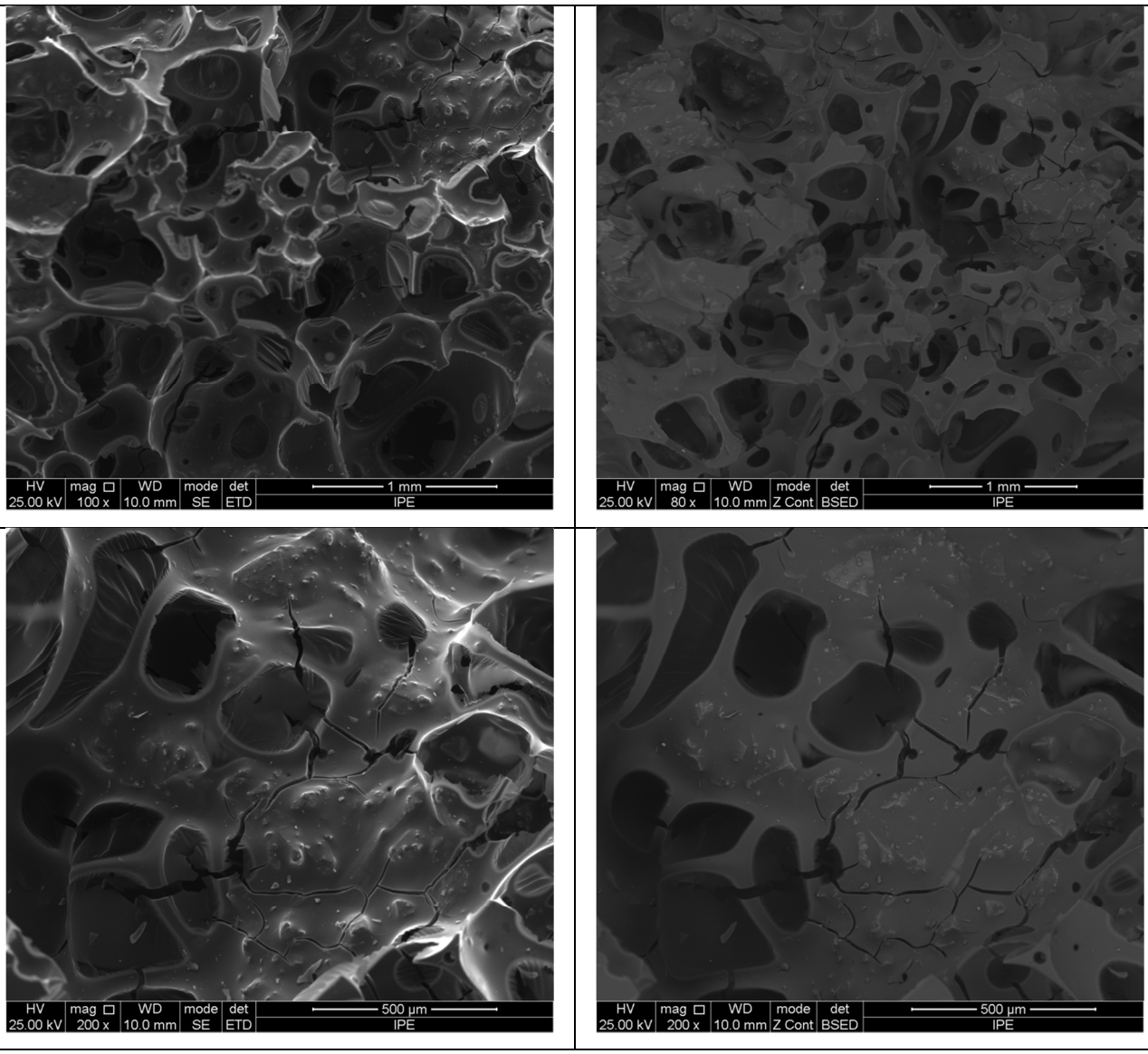

Figure 70 - SEM pictures of 1_1 Low T Ceramized Foam, with Foam composition.

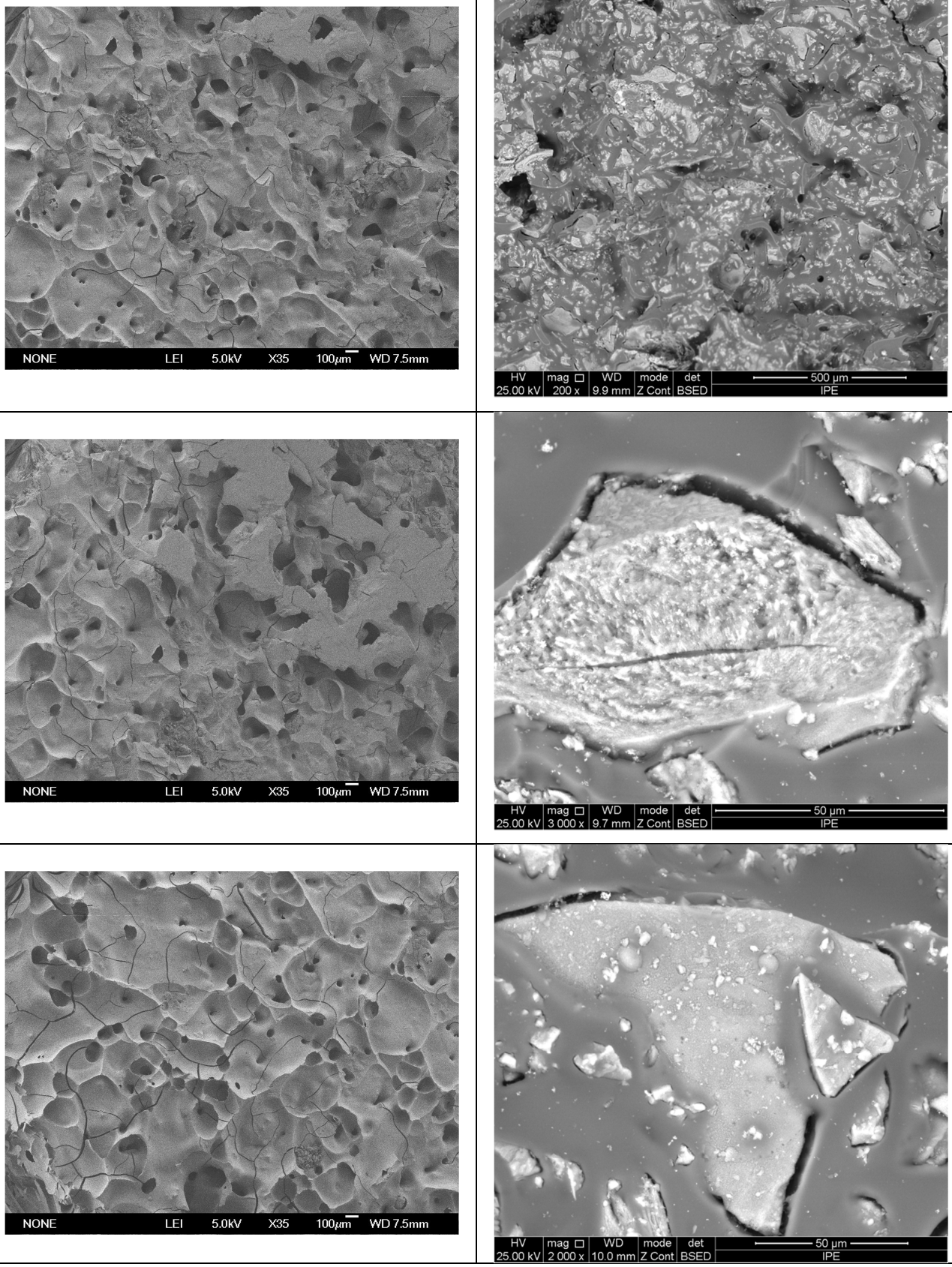

Figure 71 - SEM pictures of 1_1 Composite Ceramic Foam (1), with Foam composition.

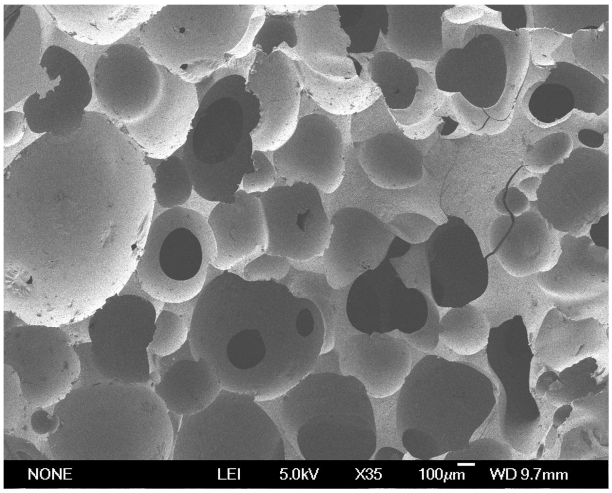

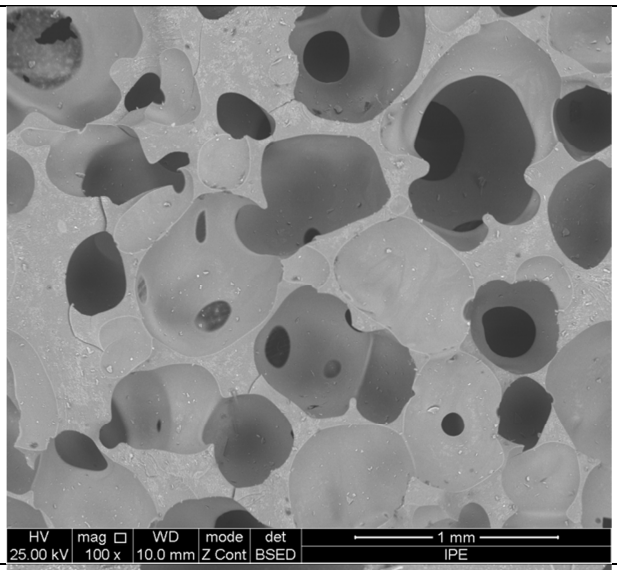

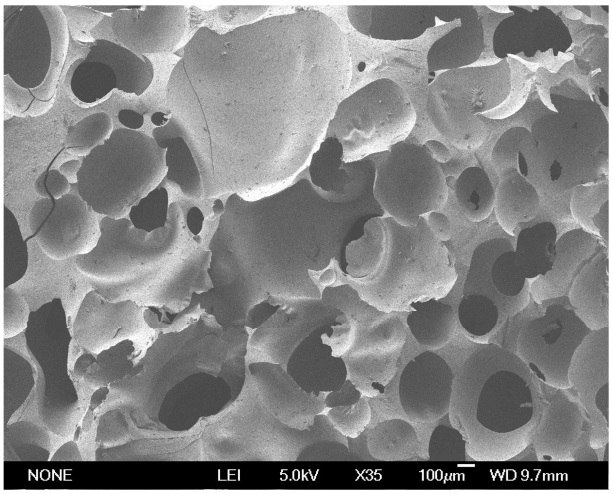

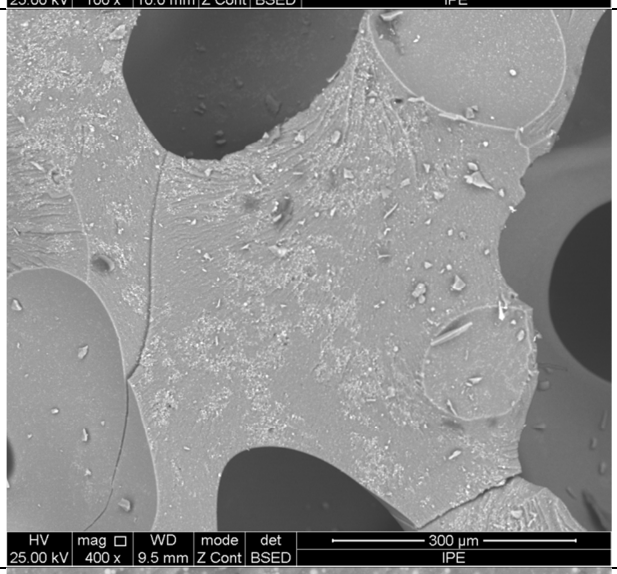

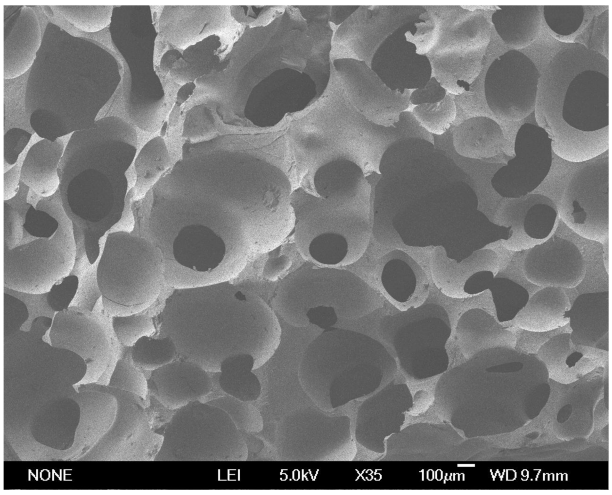

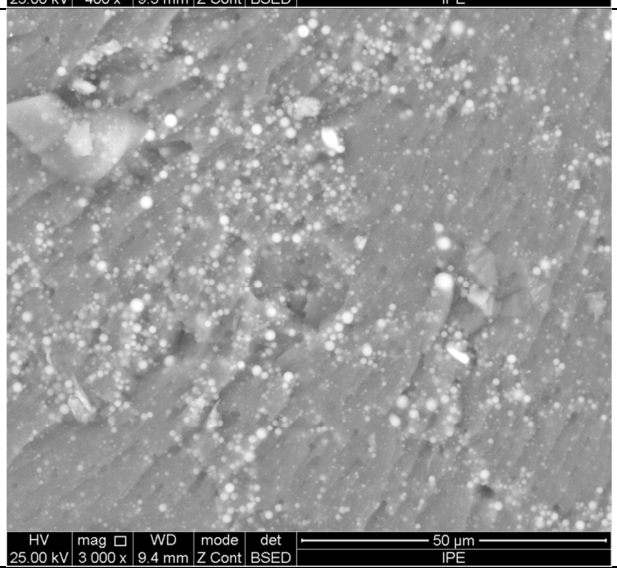

Figure 72 - SEM pictures of 1_2 Low T Ceramized Foam, with Foam composition.

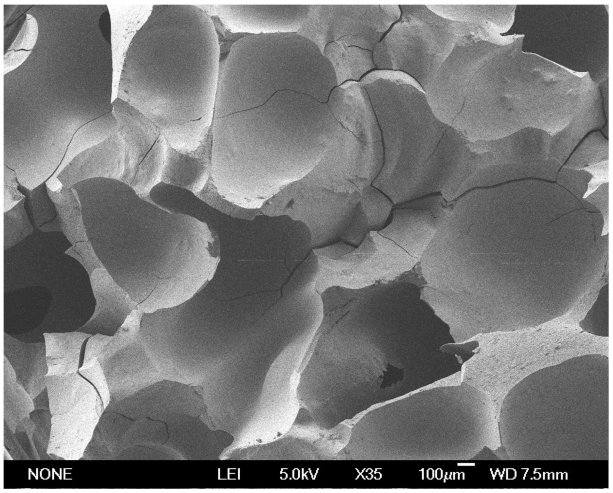

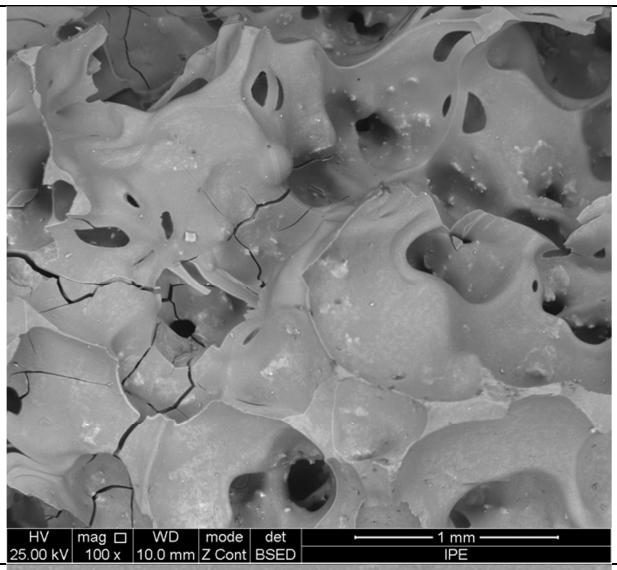

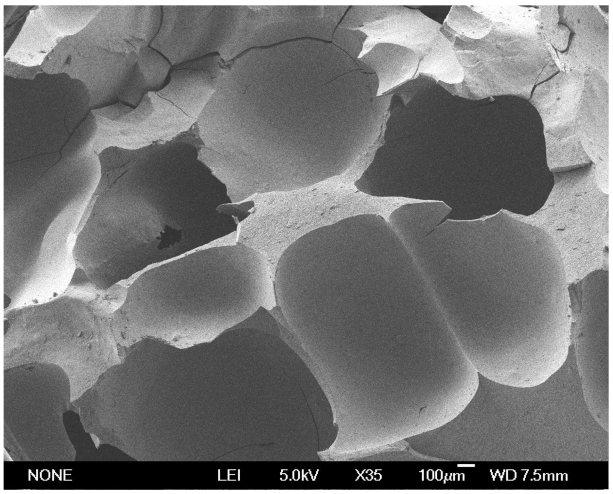

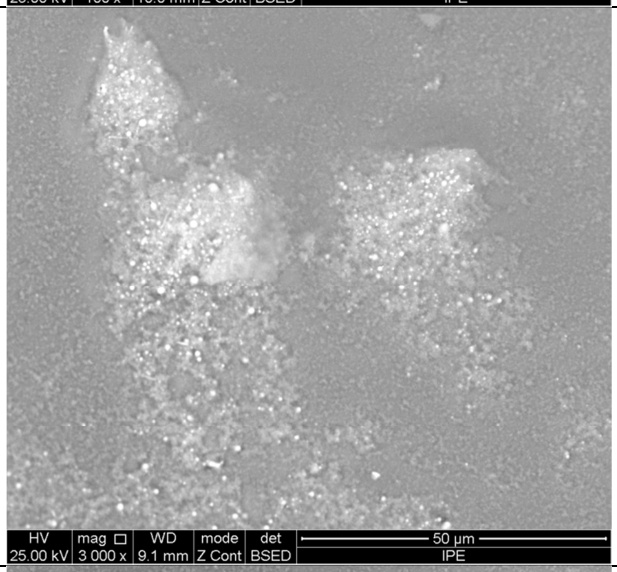

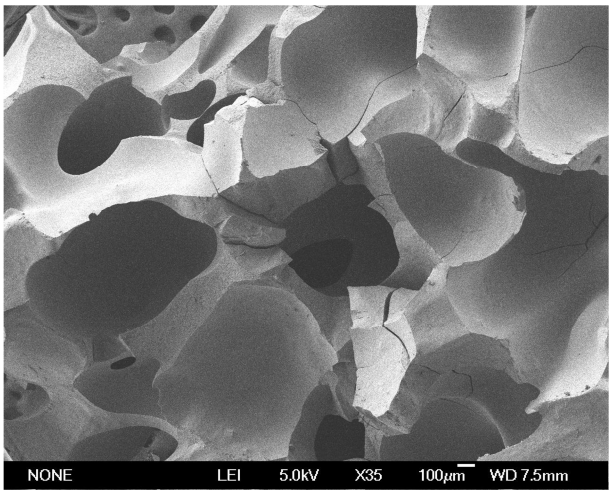

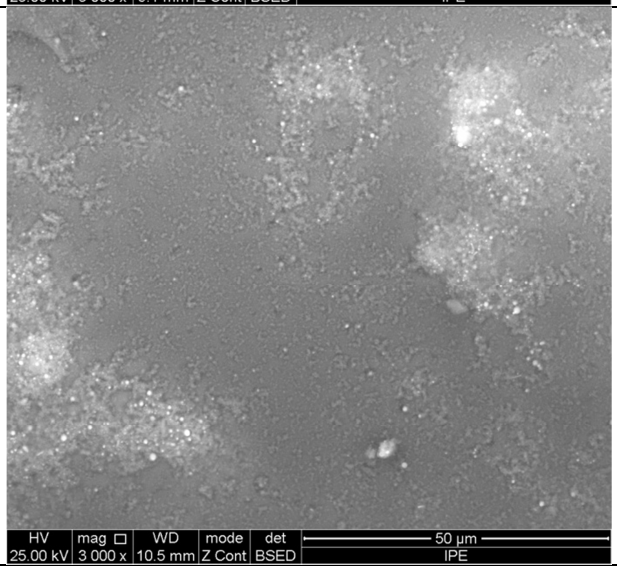

Figure 73 - SEM pictures of 1_2 Composite Ceramic Foam (1), with Foam composition.

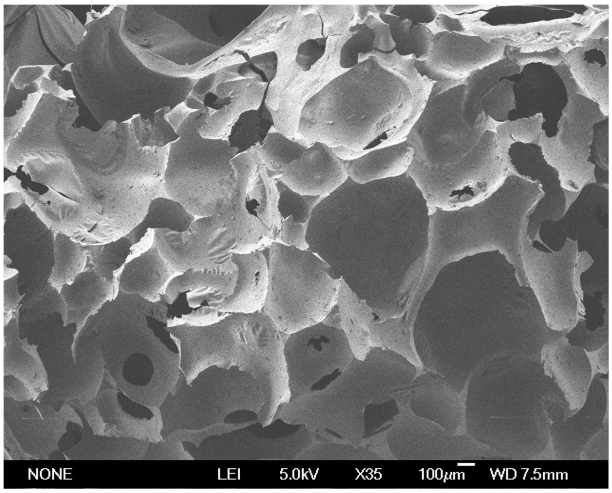

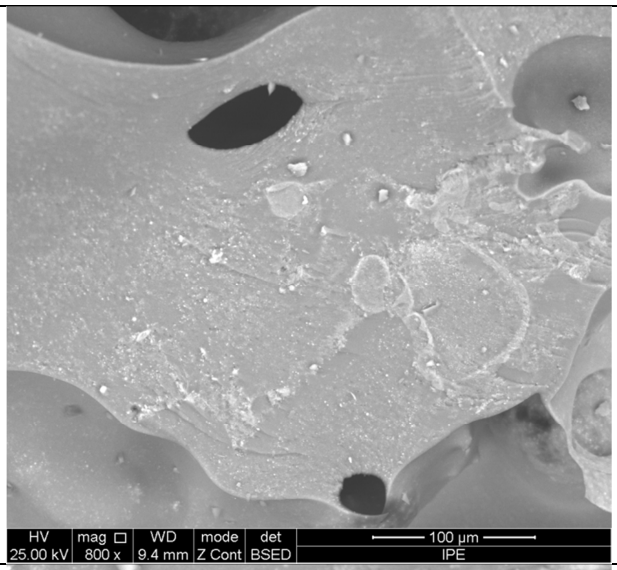

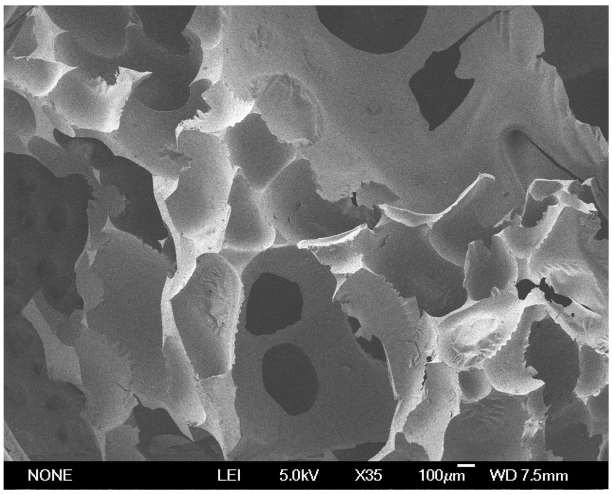

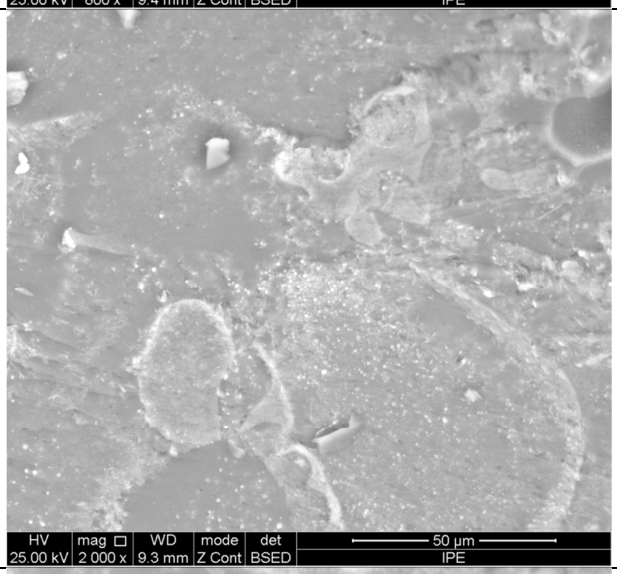

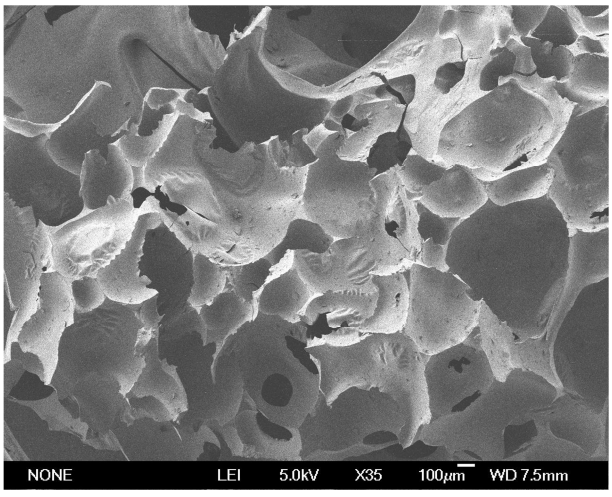

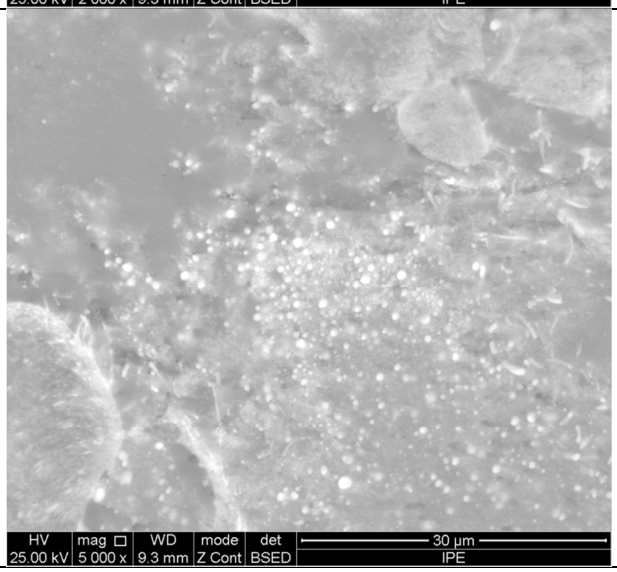

Figure 74 - SEM pictures of 1_3 Low T Ceramized Foam, with Foam composition.

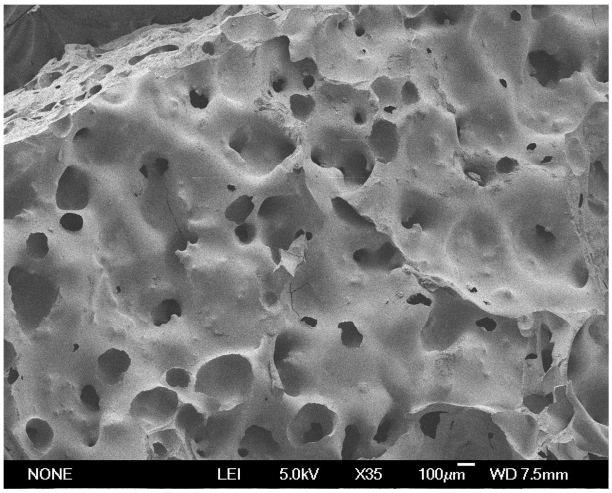

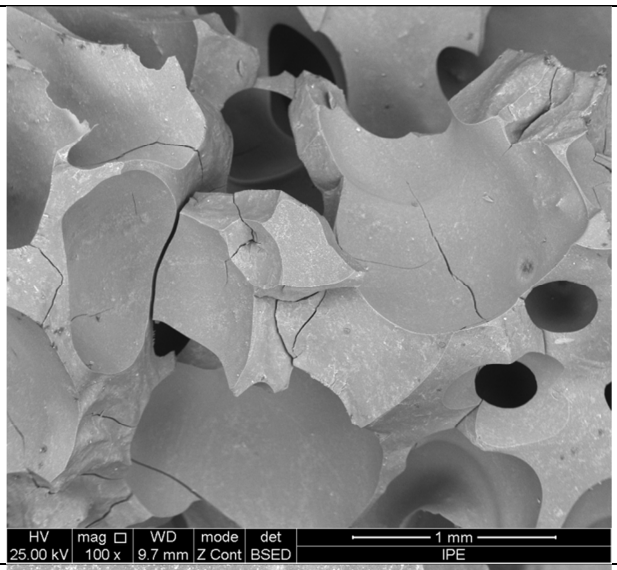

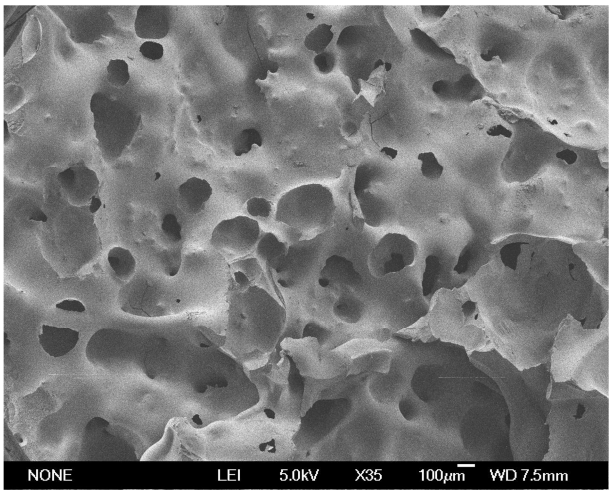

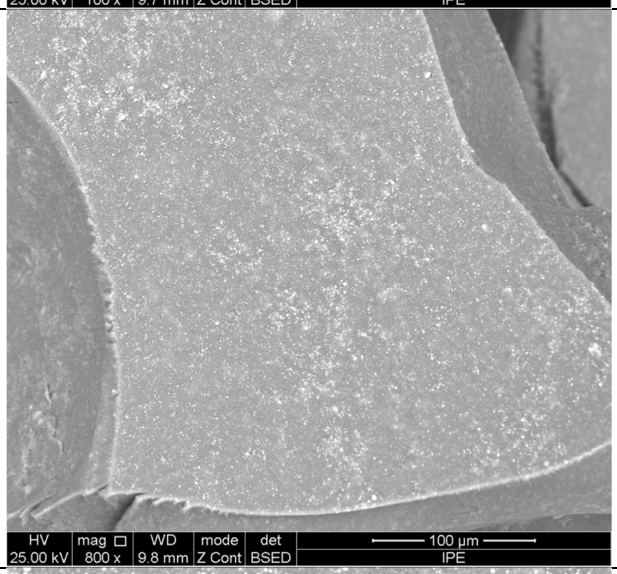

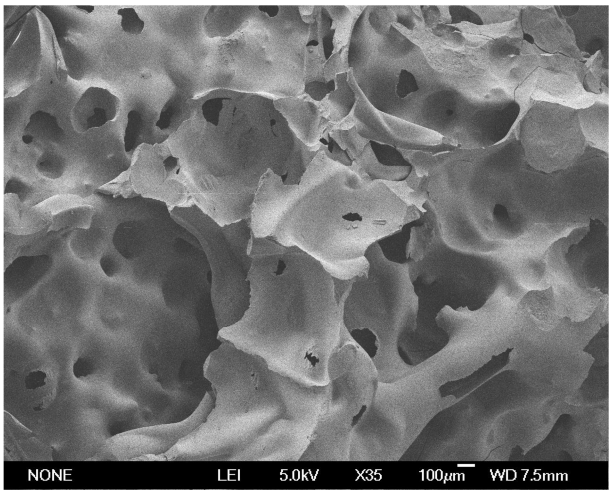

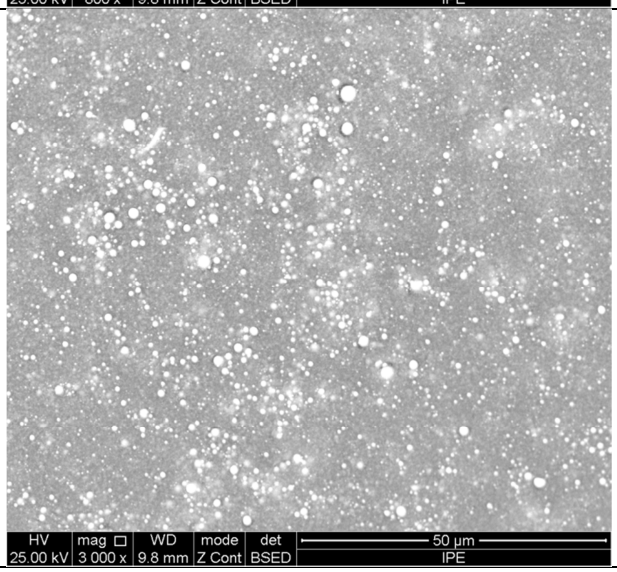

Figure 75 - SEM pictures of 1_3 Composite Ceramic Foam (1), with Foam composition.

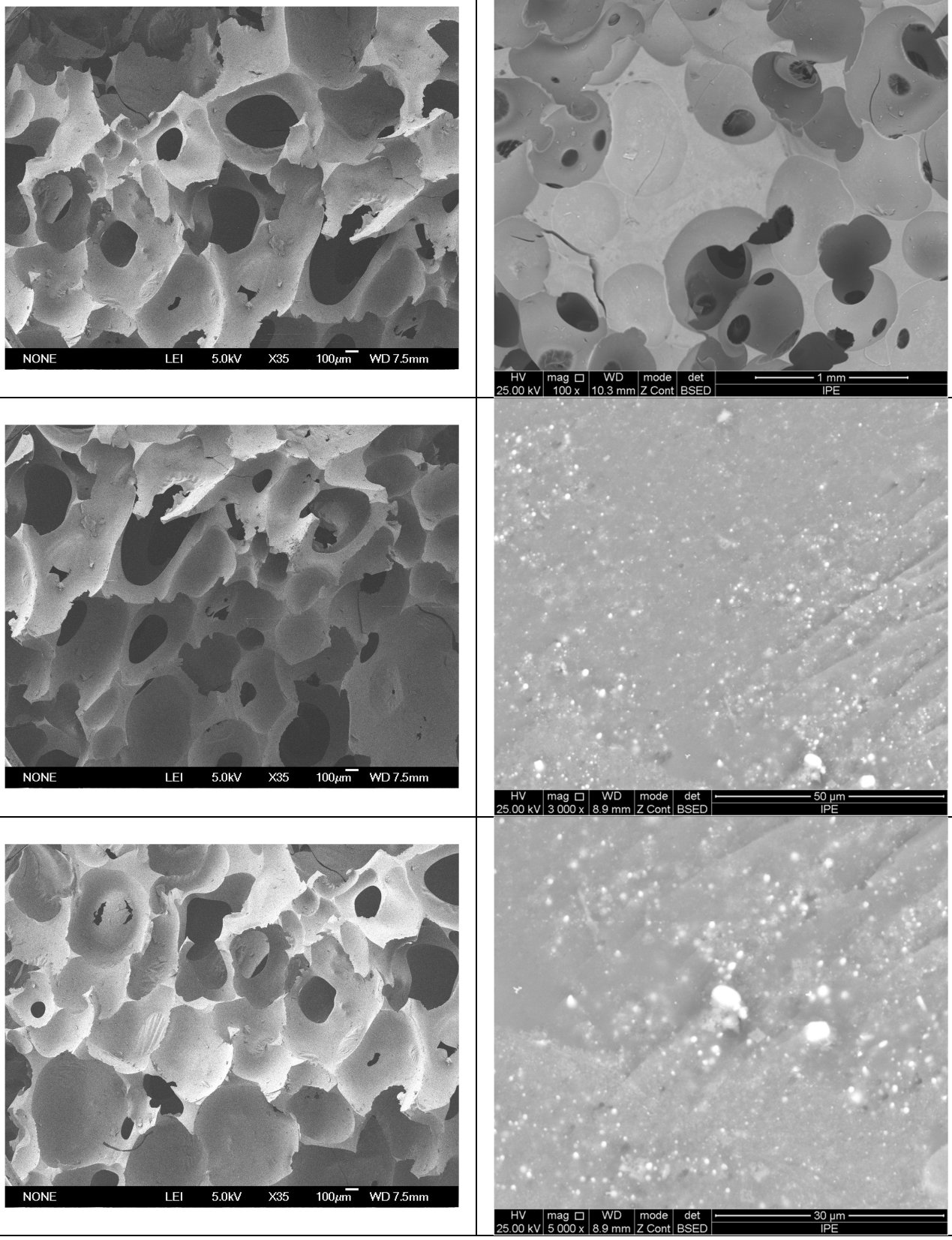

Figure 76 - SEM pictures of 1_4 Low T Ceramized Foam, with Foam composition.

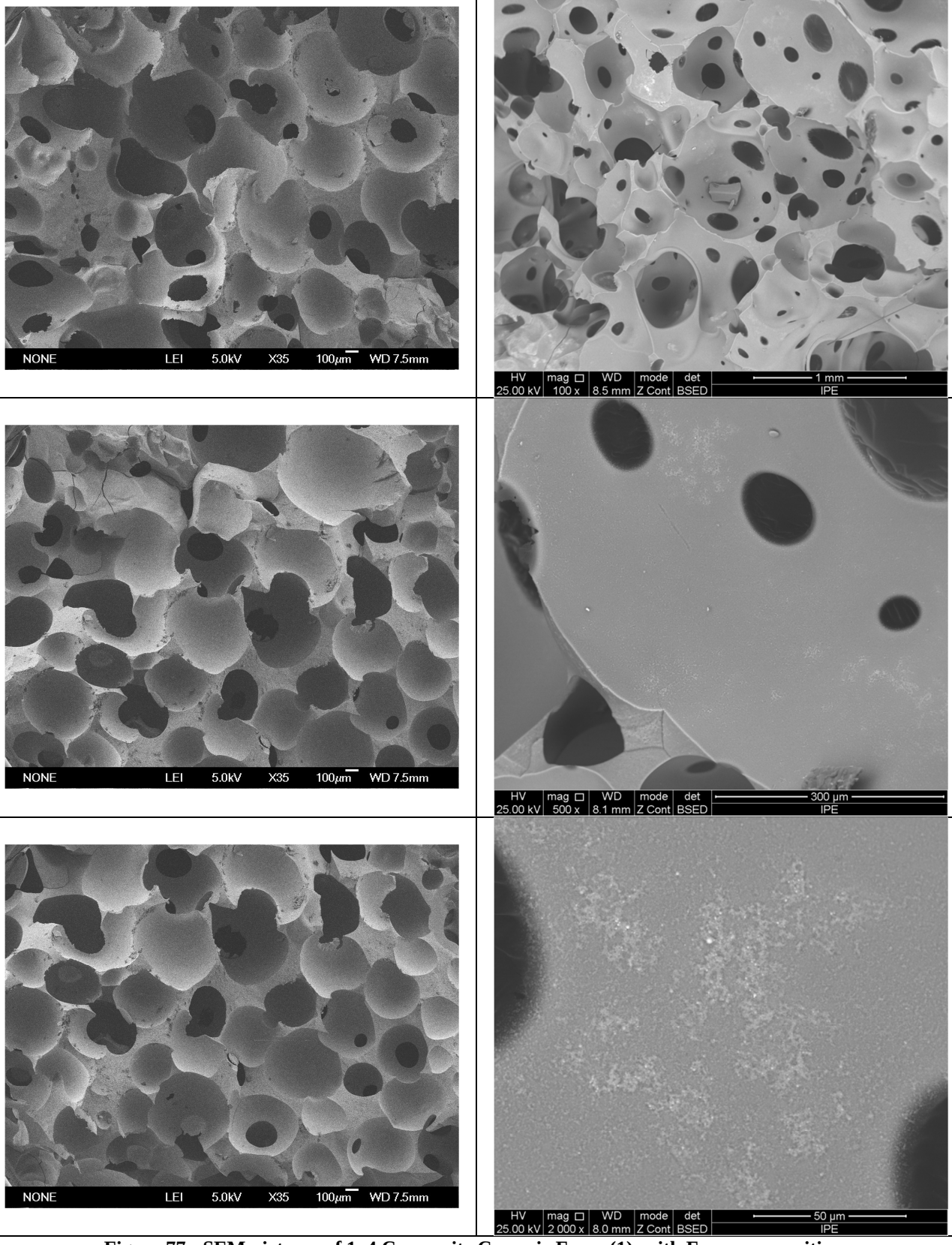

Figure 77 - SEM pictures of 1_4 Composite Ceramic Foam (1), with Foam composition.

The previous photos (from Figure 70 to Figure 77) show Low T Ceramized Foam (Precursor Foam heat treated at 1000°C) and Composite Ceramic Foam (1) (Precursor Foam heat treated at 1500°C). Secondary electrons pictures (left column) show a random porous structure in each sample at both treatment temperatures: pores have different shape and dimension.

About *Back scattered electrons* photos, the presence of the separation phase can be noted; the second compound becomes smaller and finely dispersed from 1_1 to 1_4 Foam composition. Contrary to the powder with same Foam composition (it means from Composite Ceramic Powder 1_1 to 1_4), in Composite Ceramic Foam the separated phase is smaller and more finely dispersed than respective Powder.

4.6 *Compressive Strength*.

Principal features that have been measured are:

- max strain σ_{max} [MPa] , the value has been read in the graph;
- E [MPa], Young's modulus (or elastic modulus) that has been obtained by Hooke's law :

$$\sigma = E * \varepsilon \qquad (13)$$

where σ and ε are read in the graph at the beginning and the end of *zone I* of each σ/ε specimens graphs.

In Table 33 the σ_{max} and E values are average results of the five specimen that have been tested.

Composite Ceramic Foam(2) sample	**Th ZrB_2 wt%**	**E [MPa]**	**σ_{max} [MPa]**	**E St. Dev. [MPa]**	**σ_{max} St. Dev [MPa]**
1_1	28,0	608,51	16,06	191,63	1,67
1_2	16,3	227,58	4,73	63,72	2,17
1_3	11,5	87,12	6,32	10,65	2,51
1_4	8,9	150,83	2,80	27,91	1,67

Table 33 - Elastic modulus E, σ_{max} and relative Standard Deviation values of each Composite Ceramic Foam(2).

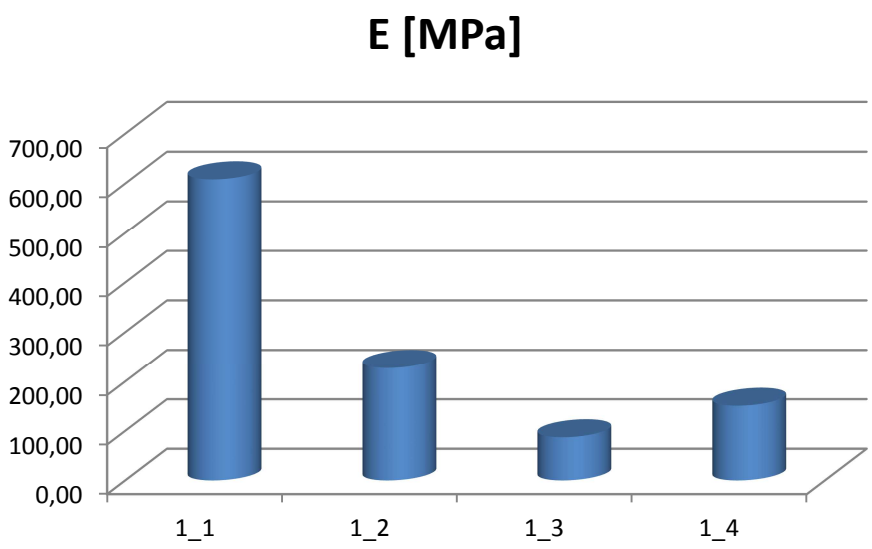

Figure 78 - Composite Ceramic Foam(2) Elastic Modulus histogram.

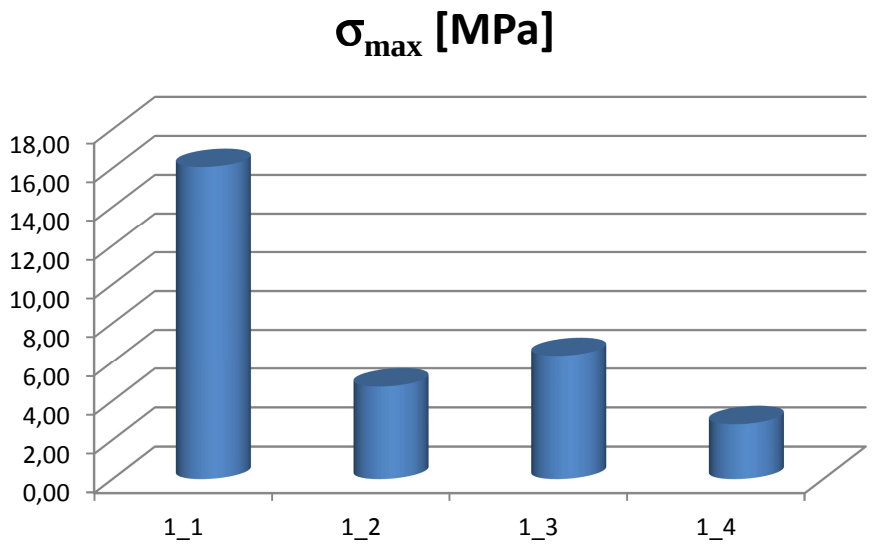

Figure 79 - Composite Ceramic Foam (2) σ_{max} histogram.

Modulus and max stress decrease with silicon carbide increasing amount, from Composite Ceramic Foam (2) 1_1 to Composite Ceramic Foam (2) 1_4. As it can be noticed in graphs (Figure 80,Figure 81), E and σ_{max} decreasing trend is described by polynomial fit (blue line) better than linear fit (red line).

It must be specified that elastic modulus values can be subjected to error; deformation (ε) values recorded include also the circular platforms deformation. For more precise values strain gage must be used: this measures just the sample deformation and it helps to obtain more correct information.

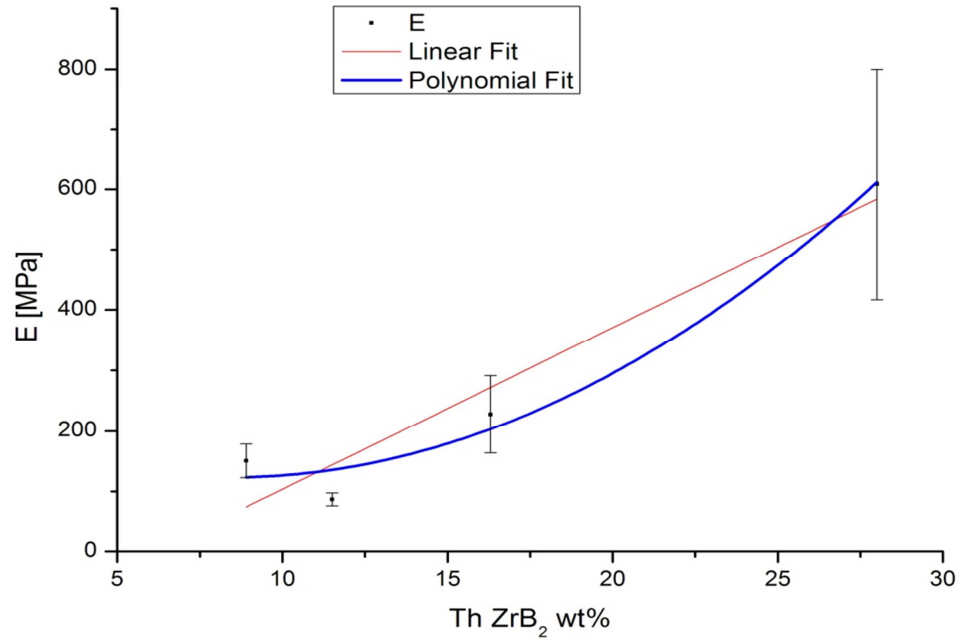

Figure 80 – Elastic modulus trend graph, with standard deviation for each composition.

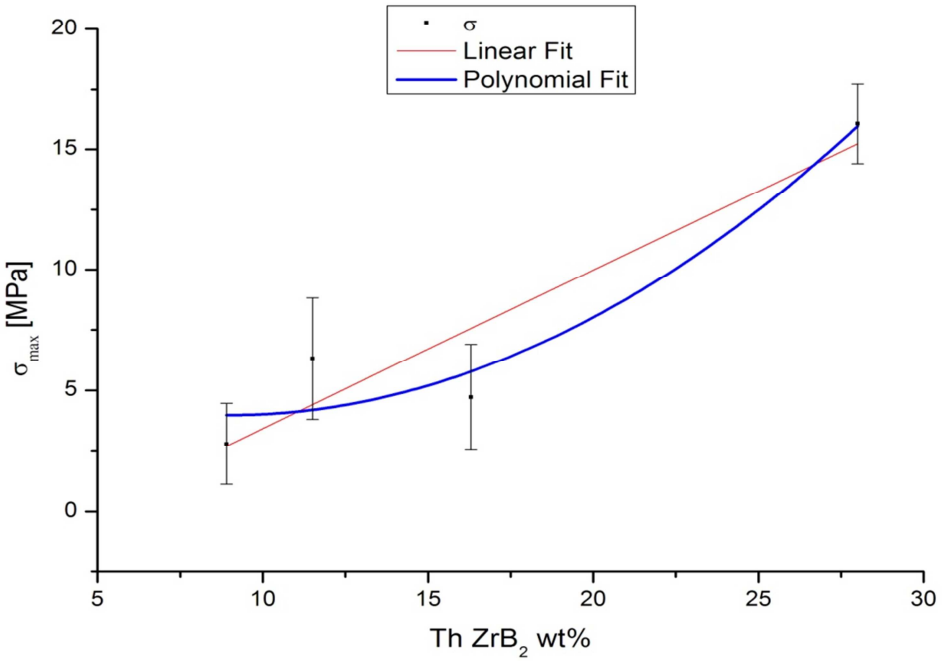

Figure 81 - σ_{max} trend graph, with standard deviation for each composition.

In Figure 82 some σ/ε curves of Composite Ceramic Foam (2) samples are shown. In most of them first (linear elastic) and second (plateau) zones are visible; every proof has been interrupted before the third zone beginning, because it was irrelevant to obtain data in those conditions.

Some linear elastic zones look segmented: this means that during the proof, some local damaging happens.

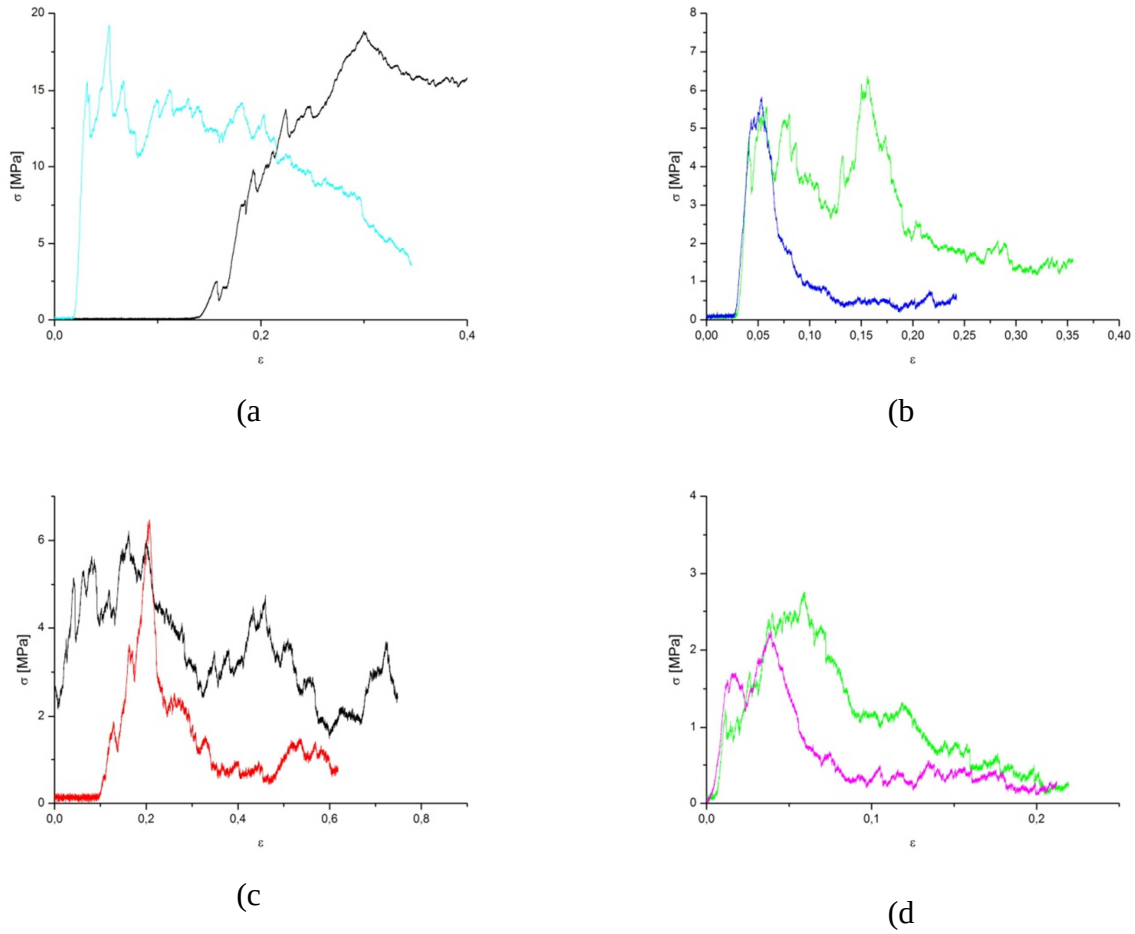

Figure 82 - Composite Ceramic Foam (2) compressive graphs: a) 1_1; b)1_2; c)1_3; d)1_4.

5. CONCLUSIONS.

This work has enabled to produce and characterize different polymer derived ceramics ZrB_2 based and modified adding different concentration of SiC.

The target was to obtain ZrB_2/SiC composite ceramic, but the results (X-ray Photoelectron Spectroscopy and Diffraction) show a presence of other phases:

- ZrC: crystalline zirconium carbide should be a result of secondary reactions between carbon excess (resulting from polymers) and Zr-containing precursor.;
- ZrO_2: crystalline zirconia caused by low carbon concentration level that can't reduce oxygen content in Zr-containing precursor [15];
- SiO_2 and B_2O_3: amorphous silica and boria originated by the same zirconia reason or by reaction with the air.

SEM powders pictures illustrate a different phase separation between Foam composition and Powder composition samples. Powders of first composition show a separated phase Zr-rich with spheroidal shape, or rounded vertices with micrometers dimensions.

As regards to Powder composition, samples show Zr-containing phase finely and homogeneously dispersed in Si-rich matrix.

In Figure 69 it can be noticed that there's a composition, between 1_4 and 1-1, in which Zr-containing phase starts to be dispersed with nano size dimensions.

As mentioned at the beginning, the addition of silicon carbide to zirconium diboride bulk ceramics increases sinterability, toughness and oxidation resistance. The last is one of the most important features for aerospace application. A more deepened study could help to find the optimal composition with best required features.

About oxidation resistance, the nano dispersed phase could improve it by forming an homogeneous and resistant protective layer composed by the three principal oxides (ZrO_2, SiO_2 and B_2O_3).

About Composite Ceramic Foam it has been noticed that phase separation is different from powder with same composition; this could be due to heat treatment at 500°C, at 1MPa of nitrogen atmosphere which could help to reduce separated phase dimensions.

It has been detected that this foam molding method has produced composite ceramic foams with good mechanical characteristics. More deepened researches could help to find the way to obtain better characteristics with alternative foaming molding.

Studies about this ZrB_2-polymer precursor and UHTCs are just at the beginning, so more research can be carried out to obtain new materials with excellent features, depending on usage.

BIBLIOGRAPHY.

1. Wuchina, E., et al. (2007). "UHTCs: ultra-high temperature ceramic materials for extreme environment applications". *The Electrochemical Society Interface*.
2. Jiecai Han, Ping Hu, Xinghong Zhang, Songhe Meng, Wenbo Han (2008). “Oxidation-resistant ZrB2-SiC composites at 2200°C”. *Composites Science and Technology*.
3. Jiecai Han, Ping Hu, Xinghong Zhang, Songhe Meng (2007). “Oxidation behavior of zirconium diboride-silicon carbide at 1800°C”. *Scripta Materialia*.
4. A.Chamberlain, W.Fahrenholtz and G.Hilmas and D.Ellerby (2005). “Oxidation of ZrB2-SiC ceramics under atmospheric and reentry conditions”. *Refractories Applications Transactions*.
5. Frédéric Monteverde, Luigi Scatteia (2007). “Resistance to thermal shock and to oxidation of metal diborides-SiC ceramics for aerospace application”. *Journal of American Ceramic Society*.
6. Paolo Colombo, Gabriela Mera and Ralf Riedel (2010). “Polymer-derived ceramics: 40 years of research and innovation in advanced ceramics”. *Journal of American Ceramic Society*.
7. Vlasov, A.S. (1991). *Refractories and Industrial Ceramics* .
8. Harris, Gary Lynn (1995). “Properties of silicon carbide”.
9. Byrappa, K.; Ohachi, T. (2003). “Crystal growth technology”. *Springer*..
10. Bakin, Andrey S. (2006). SiC materials and devices, vol. 1, edited by M. Shur, S. Rumyantsev, M. Levinshtein - Chap.:"SiC Homoepitaxy and Heteroepitaxy". World Scientific.
11. Pitcher, M. W.; Joray, S. J.; Bianconi, P. A. (2004). "Smooth Continuous Films of Stoichiometric Silicon Carbide from Poly(methylsilyne)". *Advanced Materials* .
12. Bunsell, A. R.; Piant, A. (2006). "A review of the development of three generations of small diameter silicon carbide fibres". *Journal of Materials Science.*
13. Laine, Richard M.; Babonneau, Florence (1993). "Preceramic polymer routes to silicon carbide". *Chemistry of Materials*.
14. Sung S. Hwang, Alexander L Vasiliev, Nitin P.Padture (2007). “Improved processing and oxidation-resistance of ZrB_2 ultra-high temperature ceramics containing SiC nanodispersoids”. *Materials Science and Engineering*.

15. Changming Xie, Mingwei Chen, Xi Wei, Min Ge and Weigang Zhang (2011). “Synthesis and microsture of zirconium diboride formed from polymeric precursor pyrolysis”. *Journal of American Ceramic Society*.
16. Yanli Xie, Thomas H. Sanders Jr. and Robert F. Speyer. (2008) “Solution-based of submicrometer ZrB_2 and ZrB_2-TaB_2”. *Journal of American Ceramic Society*.
17. Frederic Monteverde, Stefano Gucciardi, Alida Bellosia. (2003) “Advances in microstructure and mechanical properties of zirconium diboride based ceramics”. *Materials Science&Engineering*.
18. Shu-Qi Guo, Jenn-Ming Yang, Hidehiko Tanaka, Yutaka Kagawa (2008). “Effect of thermal exposure on strength of ZrB_2-based composites with nano-sized SiC particles”. *Composites Science and Technology*.
19. G.Russo, G.Marino (2002). “The USV program &UHTC development”. *4th*, *European Workshop, Hot Structures and thermal protection systems for space vehicles*.
20. J.K.Sonber and A.K.Suri (2010).“Synthesis and consolidation of zirconium diboride: review”. *Institute of Materials, Minerals and Mining.*
21. Sonber, J. K., and A. K. Suri. (2011). "Synthesis and consolidation of zirconium diboride: review". *Advances in Applied Ceramics* **.**
22. Kaufman, Larry, and Edward V. Clougherty. (1963). "Investigation of Boride Compounds for Very High-Temperature Applications". *ManLabs. Inc., Cambridge, Mass*.
23. Guron, Marta M., Myung Jong Kim, and Larry G. Sneddon. (2008). "A Simple Polymeric Precursor Strategy for the Syntheses of Complex Zirconium and Hafnium-Based Ultra High-Temperature Silicon-Carbide Composite Ceramics". *Journal of the American Ceramic Society*.
24. Zhou, Shanbao, et al. (2010). "Microstructure, mechanical properties and thermal shock resistance of zirconium diboride containing silicon carbide ceramic toughened by carbon black". *Materials Chemistry and Physics*.
25. Zhu, Tao, et al. (2009). "Densification, microstructure and mechanical properties of ZrB_2–SiCw ceramic composites". *Journal of the European Ceramic Society* .
26. Zhang, Xinghong, et al. (2008). "Effects of Y2O3 on microstructure and mechanical properties of ZrB2- SiC ceramics". *Journal of Alloys and Compounds* .
27. Chamberlain, Adam L., William G. Fahrenholtz, and Gregory E. Hilmas. (2005). "Pressureless sintering of zirconium diboride". *Journal of the American Ceramic Society* .

28. Wang, Xin-Gang, Wei-Ming Guo, and Guo-Jun Zhang. (2009). "Pressureless sintering mechanism and microstructure of ZrB_2–SiC ceramics doped with boron". *Scripta Materialia*.
29. Khanra, A. K., and M. M. Godkhindi. (2005). "Effect of Ni additives on pressureless sintering of SHS ZrB_2". *Advances in applied ceramics* .
30. Venkateswaran, T., et al. (2006). "Densification and properties of transition metal borides-based cermets via spark plasma sintering". *Journal of the European Ceramic Society*.
31. Zhao, Yuan, et al. (2009). "Effect of holding time and pressure on properties of ZrB_2-SiC composite fabricated by the spark plasma sintering reactive synthesis method".*International Journal of Refractory Metals and Hard Materials* .
32. Dong Gao, Yue Zhang, Chunlai Xu, Yang Song, Xiaobin Shi. (2011) “Atominc oxygen adsorption and its effect on the oxidation behavior of ZrB_2 – ZrC –SiC in air”. *Materials Chemistry and physics*.
33. C. Monticelli, F. Zucchi, A. Pagnoni, M. Dal Colle. (2005) “Corrosion of a zirconium diboride/silicon carbide composite in aqueous solutions”. *Electrochimica acta*.
34. Z. Shen, M. Nygren, U. Halnius. (1997) “Absorption spectra of rare-earth doped α-SiAlON ceramics”, J*ournal of Materials Science.*
35. J. Q. Hu, Q. Y. Lu, K. B. Tang, B. Deng, R. R. Jiang, Y. T. Qian, W. C. Yu, G. E. Zhou, X. M. Liu, and J. X. Wu. (2000) “Synthesis and Characterization of SiC Nanowires through a Reduction-Carburization”, *Journal of Physics and Chemistry*.
36. J. Schulte-Fischedick, A. Zern, J. Mayer, M. Ruhle, M. Frieß, W. Krenkel, R. Kochendorfer. (2002). “The morphology of silicon carbide in C/C–SiC composites”, *Materials Science and Engineering.*